2017

Dynamic Response and Active Control of Flexible Cylindrical Structures Undergoing Vortex-Induced Vibrations

Ersegun Deniz Gedikli
University of Rhode Island, ersegundeniz@gmail.com

DYNAMIC RESPONSE AND ACTIVE CONTROL OF FLEXIBLE CYLINDRICAL STRUCTURES UNDERGOING VORTEX-INDUCED VIBRATIONS

BY

ERSEGUN DENIZ GEDIKLI

A DISSERTATION SUBMITTED IN PARTIAL FULFILLMENT OF THE REQUIREMENTS FOR THE DEGREE OF

DOCTOR OF PHILOSOPHY

IN

OCEAN ENGINEERING

UNIVERSITY OF RHODE ISLAND

2017

DOCTOR OF PHILOSOPHY DISSERTATION

OF

ERSEGUN DENIZ GEDIKLI

APPROVED:

Dissertation Committee:

Major Professor Jason Dahl

James Hu

David Chelidze

Nasser H. Zawia

DEAN OF THE GRADUATE SCHOOL

UNIVERSITY OF RHODE ISLAND

2017

ABSTRACT

This dissertation primarily focuses on understanding the canonical problem of vortex-induced vibration (VIV), a self-excited vibration of bluff bodies caused by the instability of the bluff-body wake. In this work, dynamic response and active control of low mode number flexible cylinders undergoing vortex-induced vibrations are addressed which has potential to significantly impact the development of predictive models for flow-induced-vibrations, a topic of critical importance to the offshore oil and gas industry and important to the cost-effective development of new ocean structures, such as floating offshore wind platforms and offshore wind energy systems.

In the tests, first, dynamic response of a tensioned flexible cylinder is investigated in a recirculating flow channel. Different than hysteresis in the amplitude response, the idea of mode hysteresis is introduced. A transition in the amplitude of the response of a flexible cylinder undergoing vortex-induced vibrations is shown to be related to the transition between fluid coupled structural modes excited by the flow. Also, due to the symmetric drag loading across cylinder's span, the hypothesis of being unable to sustain a asymmetric excitation (even mode excitation) in in-line is discussed. To understand more about this fluid-structure interactions, tensioned flexible cylinder data is used for multivariate analysis. It is shown that traditional reduced order models such as proper orthogonal decomposition and recently introduced smooth orthogonal decomposition methods help to identify nonlinear mode interactions in the flexible cylinder's response. Later, mode shape effect in VIV and the idea of being unable to sustain asymmetric modes in a uniform flow is considered. In the tests, three bending-dominated cylinders are tested with varying stiffness in the cross-flow and in-line directions of the cylinder in order to produce varying structural mode shapes associated with a fixed 2:1

(in-line:cross-flow) natural frequency ratio. Then, the structural mode excitation of bending-dominated flexible cylinders undergoing vortex-induced vibrations is investigated using multivariate analysis of excited empirical modes. Both the analytic and experimental results show that for excitation of low mode numbers, the cylinder is unlikely to oscillate with an even mode shape in the in-line direction due to symmetric drag loading, even when the system is tuned to have an even mode at the expected frequency of vortex shedding. Later, to understand the effect of three-dimensional wake on an oscillating flexible cylinder in VIV, a novel experimental method is introduced. Finally, the idea of active control of flexible cylinders in VIV using piezo stripe actuators is discussed. Piezo stripe actuators are bonded at the anti-nodes of a flexible cylinder in the in-line direction to control low vibration modes (i.e. first, second and third). Experiments show that upto 75% of amplitude reduction is possible in cross-flow where large vibrations occur. In addition to vibration suppression, vibration enhancement is also possible if piezos are activated before an apparent amplitude jump.

ACKNOWLEDGMENTS

First and foremost, I would like to express my deepest gratitude to my advisor Dr. Jason Dahl for his guidance and continuous support of my doctoral studies. His guidance helped me a lot throughout my time at the University of Rhode Island. Jason has provided a supportive environment that has allowed me to explore my interests, and I am grateful for his patience and optimism about my work. His attention to detail and dedication to exceptional scientific writing have made each of our manuscripts a work of art. It has been an honor to work with Jason and a pleasure to be his student.

A special thanks to Dr. David Chelidze. David has been like a second advisor and role model to me and I would like to thank him for his countless hours of discussing my research, for his encouragement and for allowing me to grow as a research scientist. His advice on both research as well as on my career have been invaluable.

I wish to thank my committee members, Dr. James Hu, Dr. Gopu Poty and Dr. Orlando Merino, who were more than generous with their expertise and precious time. I thank my colleagues, Jack, Erdem, Amin, and JJ for a pleasant working environment.

Most importantly, I must acknowledge my wife Hazel for supporting me through my research, providing moral support during my experiments. Also, I would like to extend my greatest appreciation to my parents who have always supported me in my academic pursuits.

I gratefully acknowledge the support of this work by the Ministry of National Education scholarship of Turkey, and the Office of Naval Research (grant no: N00014-16-1-2968, PM Kelly Cooper).

DEDICATION

I dedicate this dissertation work to my wife, Hazel, and my parents, who offered unconditional love and support and have always been there for me. Thank you so much.

PREFACE

This dissertation, *Dynamic response and active control of flexible cylindrical structures undergoing vortex-induced vibrations*, is constructed in the manuscript format and consists of four manuscripts.

The first manuscript (chapter 2), *Mode excitation hysteresis of a flexible cylinder undergoing vortex-induced vibrations* was published in Journal of Fluids and Structures, 69 (2017) 308-322.

The second manuscript (chapter 3), *Multivariate analysis of vortex-induced vibrations in a tensioned cylinder reveal nonlinear modal interactions*, is accepted to be published as a conference proceeding in the proceedings of 10^{th} International Conference on Structural Dynamics, EURODYN 2017.

The third manuscript (chapter 4) is *Structural mode effects on bending dominated flexible cylinders undergoing vortex-induced vibrations.* This work will be submitted to Journal of Fluids and Structures.

The fourth manuscript (chapter 5), *Underwater vibration control of flexible cylinders using piezo stripe actuators*, will be submitted to Journal of Sound and Vibration.

TABLE OF CONTENTS

Page

LIST OF FIGURES

Figure **Page**

Figure **Page**

LIST OF TABLES

CHAPTER 1

Introduction

Vortex-induced vibration (VIV) is an inherent problem seen in many engineered structures such as offshore risers, electric cables, transmission lines, bridges, stacks, engines, heat exchangers and many more hydrodynamic applications. It occurs due to the asymmetric vortex formation behind a bluff body where wake formation depends on the body motion and body motion depends on the formation of the wake. Due to this complex time varying fluid-structure interaction, VIV is a significant issue in offshore structures where it can give fatigue related damages and may cause a catastrophic failure if neglected in design.

Many real life long offshore structures behave similar to flexible cylinders underwater. Therefore, in this dissertation, the effect of vortex-induced vibration on flexible cylinders are extensively studied. A short review of the each manuscript is given below:

In Chapter 2, dynamic response of a tensioned flexible cylinder is investigated in a recirculating flow channel. Cylinder is attached horizontal to incoming fluid flow, and response analysis is done using high speed cameras and motion tracking. Different than hysteresis in the amplitude response, the idea of mode hysteresis is introduced. A transition in the amplitude of the response of a flexible cylinder undergoing vortex-induced vibrations is shown to be related to the transition between fluid coupled structural modes excited by the flow. Estimates of the hydrodynamic forces based on a simple modal system equation show that transitions in the sign of the effective added mass of the system and distribution of excitation forces are consistent with phasing changes in the force associated with transitions in phasing of the relative motion of the body and vortices in the wake. Also, due to

the symmetric drag loading across cylinder's span, the hypothesis of being unable to sustain a asymmetric excitation (even mode excitation) in in-line is introduced.

Chapter 3 focuses on multivariate analysis based on the tensioned flexible cylinder data. Detailed explanation of different multivariate analysis methods are described and focus is given to smooth orthogonal decomposition method for vibration mode identification. It is shown that traditional reduced order models such as proper orthogonal decomposition and recently introduced smooth orthogonal decomposition methods help to identify nonlinear mode interactions in the flexible cylinder's response. In addition, smooth orthogonal mode decomposition is found to be more accurate identifying bifurcations and the hysteretic region associated with those bifurcations. Being able to clearly identify unstable regions and the corresponding bifurcations is of utmost importance to the development of the reduced-order models capable of predicting non-linear fluid-structure interactions.

The idea of being unable to sustain asymmetric modes in a uniform flow and mode shape effect in VIV are considered in Chapter 4. An experiment is designed to understand the modal interactions in the cylinder's response. Three bending-dominated cylinders are tested with varying stiffness in the cross-flow and in-line directions of the cylinder in order to produce varying structural mode shapes associated with a fixed 2:1 (in-line:cross-flow) natural frequency ratio. Then, the structural mode excitation of bending-dominated flexible cylinders undergoing vortex-induced vibrations is investigated using multivariate analysis of excited empirical modes. Measured responses are compared with the analytic response of a beam subjected to a uniform loading. Both the analytic and experimental results show that for excitation of low mode numbers, the cylinder is unlikely to oscillate with an even mode shape in the in-line direction due to symmetric drag loading, even when the system is tuned to have an even mode at the expected frequency of

vortex shedding. Results confirm the observations from previous field and laboratory experiments while demonstrating how structural mode shape is affected by vortex-induced vibrations.

In chapter 5, the idea of active control of flexible cylinders using piezo stripe actuators is discussed. Piezo stripe actuators are bonded at the anti-nodes of a flexible cylinder in the in-line direction to control low vibration modes (i.e. first, second and third). To suppress the VIV motion, piezo stripes are actuated before a mode change, thus tripping the frequency and forcing cylinder to excite with a higher vibration mode. Experiments show that upto 75% of amplitude reduction is possible in cross-flow where large vibrations occur. In addition to vibration suppression, vibration enhancement is also possible if piezos are activated before an apparent amplitude jump. In this case, piezo actuators provides additional energy input and forces cylinder to oscillate with a larger amplitude response earlier than the natural response. As a result, this study successfully demonstrates the ability to suppress and/or enhance VIV motion through the use of piezo stripe actuators.

Finally, conclusions and some possible future research ideas are given in Chapter 6.

CHAPTER 2

Mode excitation hysteresis of a flexible cylinder undergoing vortex-induced vibrations

by

Ersegun Deniz Gedikli and Jason Dahl

Department of Ocean Engineering, University of Rhode Island, Narragansett, RI 02881, USA

Published in Journal of Fluids and Structures, 69 (2017) 308-322

Abstract

A series of experiments was performed to investigate the modal excitation of a tensioned flexible cylinder in a uniform flow due to flow-induced vibrations. Experiments were conducted in a recirculating flow channel using a flexible cylinder with relatively low aspect ratio such that low structural mode numbers were excited. The spanwise motion of the cylinder was measured using standard motion tracking techniques with high-speed cameras. Hysteresis is observed in the response of the cylinder dependent on whether the flow speed is increased or decreased from the previous experiment. This observation differs from predictions in the literature regarding hysteresis and is attributed to hysteresis in the transition between excited structural modes coupled with the cylinder wake. It is also found that the flexible cylinder is unable to sustain excitation of asymmetric modes in the in-line direction unless the fluid-structure interaction excites a 1:1 frequency response between the in-line (IL) and cross-flow (CF) directions, resulting in a pedaling mode response. The inability to excite asymmetric modes is consistent with the response of linear systems undergoing a symmetric drag load and is consistent with the cylinder undergoing a preferred figure eight shape motion when excited. Distributed fluid forces are derived from the structural characteristics and body motions illustrating the transition of the distribution of added mass and excitation forces on the body.

2.1 Introduction

Vortex-induced vibrations (VIV) are a fundamental fluid-structure interaction problem in many engineered systems (e.g. offshore structures, mooring systems, heat exchangers, etc.). The non-linear interaction between a circular cylinder in a uniform current and the vortex shedding in the wake of the cylinder is dependent on a large number of variables [1]. In order to study the phenomenon of VIV, simplifications are often made when conducting experiments in order to limit the

number of variables that may affect the observed response. This often leads to observed differences between the responses of different systems undergoing VIV. For example, an elastically mounted, rigid cylinder undergoing VIV in an experimental water channel [2] will inherently display different response features than the multi-mode excitation of a flexible pipe in a sheared current in the ocean [3, 4]. Differences may simply occur based on the experimental setup due to differences in surface roughness, free stream turbulence, or blockage effects. One of the observed non-linear behaviors of VIV, particularly for experiments conducted in confined channels, is hysteresis.

In the context of vortex-induced vibrations, hysteresis is typically associated with the amplitude response of the structure as a function of reduced velocity. For example, if one conducts an experiment with an elastically mounted circular cylinder in a water channel with a uniform current, one may observe different responses of the structure by varying the flow speed. The variation in flow speed is related to a change in both the reduced velocity of the system and a change in the Reynolds number. As one increases the flow speed, one may observe a transition from a large amplitude response to a lower amplitude response. In contrast, if the flow speed is reduced, one may observe a transition from low amplitude response to high amplitude response, however this transition may not occur at the same reduced velocity, hence a hysteretic response. This type of response is common in non-linear systems and has been observed in vortex-induced vibrations under a variety of experimental and simulation conditions.

Hysteresis in vortex-induced vibrations is known to be related to blockage and Reynolds number effects, often being observed in experiments and simulations with high blockage ratios and low Reynolds numbers. It has been observed in both free vibration conditions and forced vibration conditions, where transitions between

wake modes become dependent on whether flow speed is increased or decreased from the previous experimental condition. Bishop and Hassan [5] observed hysteresis in a series of forced vibration experiments, where the cylinder was forced to oscillate in the cross-flow direction with a prescribed frequency. In these experiments, Reynolds numbers ranged from 4×10^3 to 11×10^4 and the blockage ratio was 8.3. In order to understand the parameters which affect hysteresis in VIV, Stansby [6] conducted a systematic series of forced cylinder experiments in air in which blockage ratio was varied, demonstrating hysteresis for higher blockage ratios. Khalak and Williamson [7] reported hysteresis in freely-vibrating rigid cylinder experiments where the cylinder was allowed to oscillate only in the cross-flow direction for low mass ratio and damping and relatively low Reynolds numbers between $2 \times 10^3 - 13 \times 10^3$. Klamo et al. [8] conducted a systematic set of rigid cylinder experiments in order to examine the effects of damping on the response of the cylinder, where the cylinder was only allowed to oscillate in the cross-flow direction. In these experiments, a hysteretic region was observed for low Reynolds numbers between 525 and 2600.

Prasanth et al. [9] developed a general characterization map for hysteresis, defining a critical blockage ratio region as a function of mass ratio. The map, based on a comprehensive set of low Reynolds number simulations with varying blockage ratio and mass ratio, shows that for a freely vibrating rigid circular cylinder, at low mass ratios and low blockage ratios, a region exists where hysteresis will not be observed. The map is compared with a number of experiments and simulations to demonstrate that it holds for a variety of conditions. Although the simulations are performed at very low Reynolds number, in the laminar boundary layer and laminar wake region, the map still compares well with experiments performed at Reynolds numbers with turbulent wakes. In addition, Prasanth et al. [9] shows

good prediction of hysteresis conditions for rigid cylinder experiments [7, 8] and flexible cylinder experiments [10, 11].

Although the experiments of Brika and Laneville [10] and Triantafyllou et al. [11] were performed with flexible cylinders in a wind tunnel and water tunnel respectively, these experiments still demonstrate many response features similar to the vibration of an elastically mounted rigid cylinder, since neither experiment observed a multi-modal response of the cylinder. For example, the pinned locations of the flexible cylinder in Brika and Laneville [10] required a characterization of the excited structural mode such that the peak response at the center of the test section could be reconstructed from measurements of vibrations of the flexible cylinder outside of the wind tunnel. This center point measurement only gives information about the response of the cylinder at a single point and the resulting hysteresis of the response at that single point. Similarly, the response of the flexible cylinder in Triantafyllou et al. [11] is only measured at the center point and the cylinder only displays a first mode response at the center point.

A significant number of experiments have been performed to characterize the multi-mode responses of long, flexible cylinders, particularly with interest in modeling the characteristics of ocean structures. Often, these experiments are performed in the field to capture characteristics typical of operating conditions for offshore structures [4, 12, 13, 3], however field experiments introduce many additional experimental parameters that are difficult to control. This introduces a need for conducting controlled laboratory experiments to help limit variables in the experiment. Recent controlled laboratory experiments have characterized the response of flexible structures undergoing VIV with low mode number and high mode number excitations [14, 15, 16, 17], where the response of the structure follows excitation of distinct modes or combinations of modes. However, conducting laboratory experi-

ments with flexible structures introduces questions about hysteresis, as laboratory experiments are typically conducted in confined water channels or towing tanks. In the above mentioned flexible cylinder experiments, hysteresis was not observed.

In this paper, results are reported for the observed vortex-induced vibration of a low mode number, tensioned flexible cylinder. In contrast to previous studies, a hysteretic effect on the dynamic response of the body is observed. In contrast to rigid cylinder experiments, this hysteretic effect is observed to be related to the transition between mode excitation, rather than a transition between upper and lower branch responses. When compared with the critical blockage map predicted by Prasanth et al. [9], the structural characteristics and blockage characteristics place the cylinder directly in the middle of the "no hysteresis" region. The fundamental difference in the present experiment from the requirements of the critical blockage map in Prasanth et al. [9] is the possibility of multi-mode excitation of the structure.

2.2 Experimental Description

Experiments were conducted in a uniform recirculating water channel located on the Narragansett Bay Campus of the University of Rhode Island. The flow channel has a test section with dimensions 38 cm wide by 48 cm tall. The test section of the flow channel consists of three glass walls on the sides and bottom, with the top of the channel open. The flow channel can be operated at speeds between 0.1 to 1.3 m/s, although the present experiments were limited to speeds between 0.1 and 0.6 m/s. Figure 1 shows a schematic drawing of the experimental set-up inside the flow channel. A flexible cylinder made of rubber was stretched horizontally across the width of the tunnel and submerged at half the depth of the tunnel (30 diameters above the tunnel floor). The cylinder was cut to be slightly shorter than the width of the tunnel, such that when stretched, the cylinder was

under tension with an initial tension of 0.15 N. The ends of the cylinder were attached to two universal joints to allow a simply supported end condition at the end of the cylinder. The universal joints were then connected to suction cups that adhered to the glass tank walls. Circular end plates with a diameter ten times larger than the test cylinder diameter were connected to the universal joints at the wall side and positioned to align with the pivot point on the universal joint in order to avoid end effects due to the joint and suction cups.

As illustrated in Figure 1, two high speed cameras (Phantom V10) were used to capture the motion of the cylinder. One of the cameras was placed underneath the flow channel in order to capture the cylinder displacement in the direction of the fluid flow and the second camera was placed behind the flow channel, looking through a streamwise facing viewing window, in order to capture the cross-flow displacement of the cylinder. The cameras used a frame rate of 250 Hz with a viewing window size of 2400×560 $pixels$. The cylinder was marked with 25 white dots with a regular spacing of 1 cm along the span of the cylinder and motion tracking software (Pro Analyst) was used to track the location of the cylinder markings, giving a spatially resolved measurement of the in-line and cross-flow body motions. Figure 2 shows the cross-wise view of the test cylinder to illustrate the marking pattern on the cylinder. Specific structural characteristics of the test cylinder and camera specifications are given in Table 1, where D is the cylinder diameter, L is the cylinder length, E is the modulus of elasticity, T is the initial tension of the cylinder, H is the water tunnel height, m is the cylinder mass, ρ is the water density, and f_n is the fundamental natural frequency in air.

To perform motion tracking on the cylinder, the cameras were aligned and calibrated in a orthogonal reference frame. A laser level was used to orient the cylinder in a horizontal position with respect to gravity. Camera's 1 and 2 were

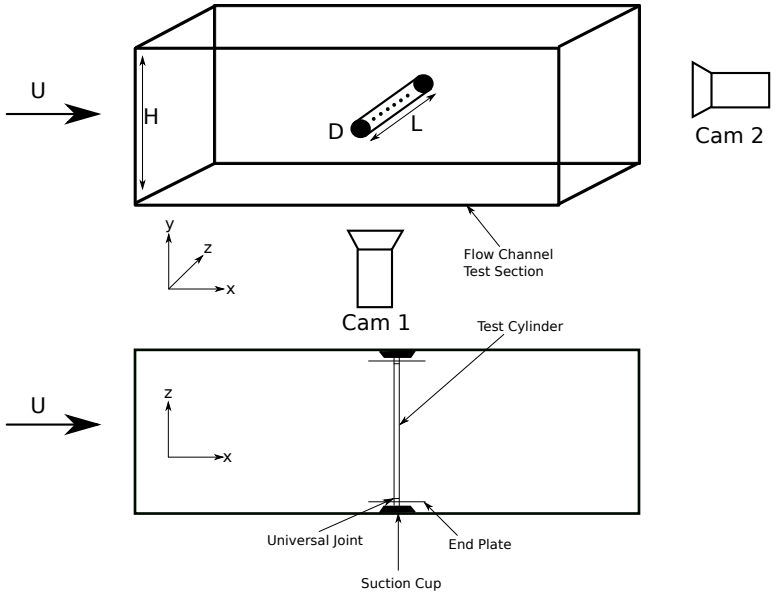

Figure 1: Experimental test setup showing isometric view at the top and top view at the bottom. Flow is coming from left to right.

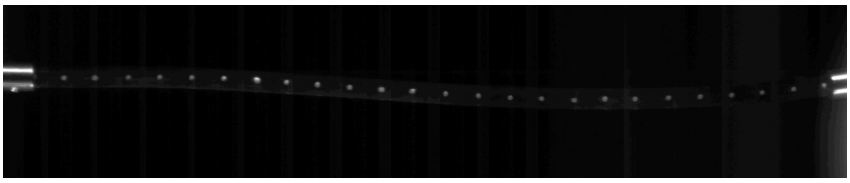

Figure 2: Example image of test cylinder with markings for motion tracking.

Table 1: Test cylinder structural characteristics and fixed experimental parameters

Test Cylinder Material	Urethane Rubber
Cylinder Diameter	$D = 6.35\ mm$
Modulus of Elasticity	$E = 1.146\ MPa$
Initial Tension	$T = 0.15N$
Fundamental Natural Frequency in Air	$f_n = 3\ Hz$
Aspect Ratio	$AR = \frac{L}{D} = 41$
Blockage Ratio	$B = \frac{D}{H} = 1.66$
Mass Ratio	$m^* = \frac{4m}{\rho\pi LD^2} = 3.76$
Damping Ratio	$\zeta = 0.04$

oriented under and behind the flow channel using levels to keep the camera views close to orthogonal. A calibration plate with regular circular markings located at known distances was used to take a reference picture from each camera, where the calibration plate was mounted to a fixture to ensure orthogonality in each camera frame. A pinhole camera assumption, where all light rays are traced back through a single point at the cameras lens, was used to calibrate the resulting images and correct for slight misalignment of the cameras and lens distortion, such that the resulting calibrated images were planar and orthogonal to one another.

The motion tracking algorithm follows white dots marked on the black background of the test cylinder. Two different lenses were used for each direction in order to maximize the resolved motion of the cylinder from the two different camera locations. For the in-line direction a Nikon Nikkor 50 mm f/1.2 lens was used and for the cross-flow direction, a Nikon Nikkor 105 mm f/2 lens was used.

The motion tracking method requires the identification of an object of interest (in this case, a white dot), which is identified in the first image in a time series. The algorithm then determines the cross-correlation of the reference feature with subsequent images to determine the new location of the feature. With a feature that is spread over multiple pixels, tracking of the cross-correlation enables sub pixel accuracy in tracking the centroid of the feature. In the experiment, each dot was composed of between 6 to 10 pixels (in-line direction features vary between 8 - 10 pixels, and cross-flow direction features vary between 6 - 8 pixels) depending on the specific feature along the span. Through statistical analysis of the feature pixel dimensions over the different flow speeds tested, it was found that the characteristics of the pixel size was not dependent on the flow speed in this setup, indicating that the relative error in determining feature location is similar at different flow speeds. It was observed that there was little to no variation in feature intensity or

size as a function of time as well, due to the small amplitude of motion and consistent light conditions. Using the calibrated resolution and observed variation in dot size, the dots on the cylinder could be tracked to within an error of 0.035 ± 0.005 cylinder diameters in the cross-flow direction and 0.027 ± 0.004 cylinder diameters in the in-line direction. With sub-pixel interpolation of the determined centroid of features, this error is significantly lower. Even using the mean estimated error based on the pixel resolution of the images, 0.035 diameters is significantly smaller than the observed vibration amplitudes (on the order of 1 diameter), giving good confidence in this technique for motion tracking.

For the experimental test matrix, the cylinder's motion was measured at 25 different flow speeds ranging from 0.1 to 0.6 m/s under two separate conditions. In the first set of experiments, the flow speed was increased by small increments throughout the test matrix range, maintaining a constant tunnel speed for at least 5 minutes before collecting images at the speed. The same procedure was repeated for decreasing flow speeds with small decrements between each flow speed. At each flow speed, motion tracking of the markings on the cylinder give a time dependent measurement of the cylinder at the 25 marked locations along the span of the cylinder, in both the cross-flow direction and in-line direction. Although the measured motions are generally periodic, the motion of the cylinder was treated as a random process, such that the amplitude of the response is reported as an average of the top ten percent of measured peak values. In the reported results, the amplitude of motion in the cross-flow direction, A_y, and amplitude of motion in the in-line direction, A_x, are normalized by the cylinder diameter, D. Details of the test matrix and governing non-dimensional parameters are given in Table 2, where U is the flow speed and ν is the kinematic viscosity.

Table 2: Test matrix dimensional and non-dimensional parameters

Flow Speed	$U = 0.1 - 0.6\ m/s$
Reynolds Number	$Re = \frac{UD}{\nu} = 650 - 3500$
Nominal Reduced Velocity	$V_{rn} = \frac{U}{f_n D} = 5 - 27$

2.3 Results

2.3.1 Averaged Maximum Amplitude Response

The maximum amplitude response of the cylinder along the span is shown in Figure 3 as a function of the nominal reduced velocity for both in-line (IL) and cross-flow (CF) directions. The local maximum at each tracking point is determined as the average of the top ten percent of the local maxima. The spanwise maximum amplitude is then determined as the largest local maximum over the span. At first inspection, the response appears to demonstrate a super upper branch response transitioning to a lower branch response, similar to what might be seen in a rigid cylinder experiment [18]. This is not the case, however, since the present test cylinder undergoes multi-mode excitation. Huera-Huarte [19] shows that in the multi-mode excitation of a flexible cylinder, when structural mode frequencies are close to one another, as with a tensioned string, the structure will display an initial upper branch excitation that then transitions to a new upper branch excitation at the next mode. The transitions in the measured maximum amplitude response in Figure 3 at $V_{rn} = 14.4$ and $V_{rn} = 21$ come from excitation of additional higher modes, as shown later through modal decomposition.

A second observation can be made from Figure 3, where there is a distinct difference between the response of the structure when the flow speed is increased and when the flow speed is decreased. In Figure 3, the response measured for increasing flow speeds is distinguished from the response measured for decreasing flow speeds. The transition point between the low amplitude response and high

amplitude response is indicated by arrows, showing that the transition occurs at different nominal reduced velocities, dependent on whether the speed is increasing or decreasing. As the flow speed is increased, the response amplitude grows to a maximum of $1.22D$ at $V_{rn} = 13.3$ before transitioning to a lower amplitude of 0.7 at $V_{rn} = 14.4$. For decreasing flow speeds, this transition is delayed, where the transition from low amplitude to high amplitude motion occurs at $V_{rn} = 10.5$. As seen in Figure 3c and 3d, this hysteretic transition is accompanied by a frequency jump in the response. There is also a large IL amplitude response at $Vr_n = 11.5$ for the decreasing flow speed case which is explained further in Sections 2.3.3 and 2.4.2.

2.3.2 Modal Decomposition of the Cylinder Response

The frequency jumps seen in Figure 3 occur consistent with transitions between excited modes in the response of the test cylinder. In order to investigate the modal excitation of the cylinder, the motion of the cylinder is decomposed into modal components. This decomposition is done using the standard Proper Orthogonal Decomposition (POD) method. While in the structural analysis of a simply-supported beam, analytic decomposition of modes may be obtained based on sinusoidal functions, in this system, the presence of the dense fluid with a low mass ratio system, results in coupled dynamics between the fluid and structure. The modal response is then dependent on both the structural characteristics and behavior of the surrounding fluid and it is not possible to define an analytic modal decomposition that includes the fluid's contribution to the mode. POD is therefore used to decompose the modal response of the cylinder based on energy, where the resulting modes do not oscillate at the structural natural frequencies, but rather at effective natural frequencies that incorporate effects of the fluid. The goal in using POD in this context is to identify the dominant modes being excited by the

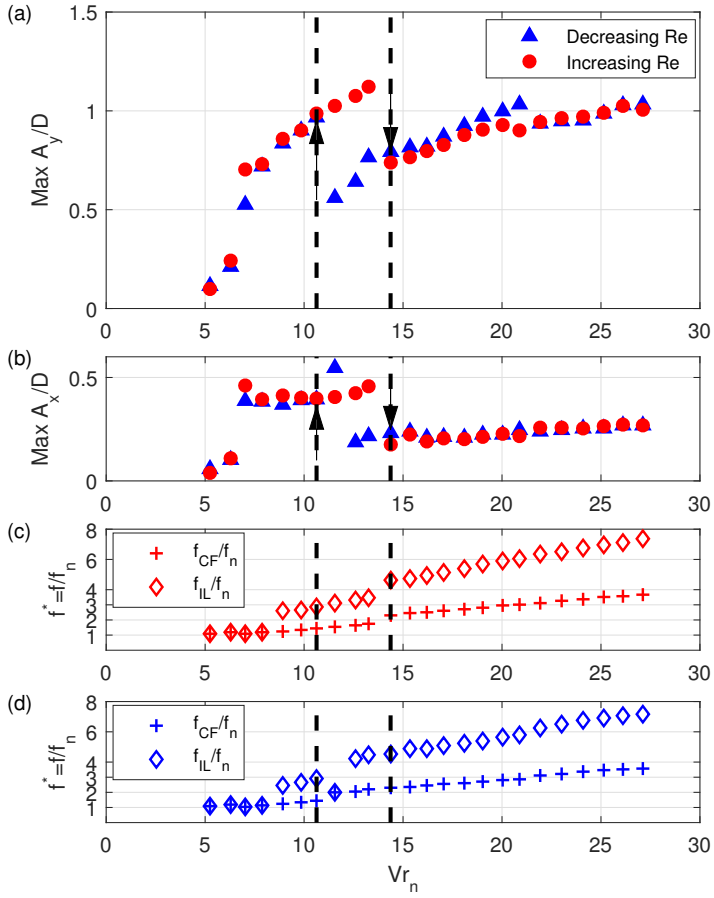

Figure 3: Measured maximum amplitude response of the flexible cylinder along the span. (a) Non-dimensional maximum cross-flow amplitude. (b) Non-dimensional maximum in-line amplitude. (c) Cross-flow and in-line normalized frequencies measured for increasing flow speeds. (d) Cross-flow and in-line normalized frequencies measured for decreasing flow speeds. Hysteretic response region shown with arrows and vertical dotted lines. Transition between large amplitude and small amplitude response is accompanied by a jump in frequency. Blue shows decreasing Reynolds number, red shows increasing Reynolds number.

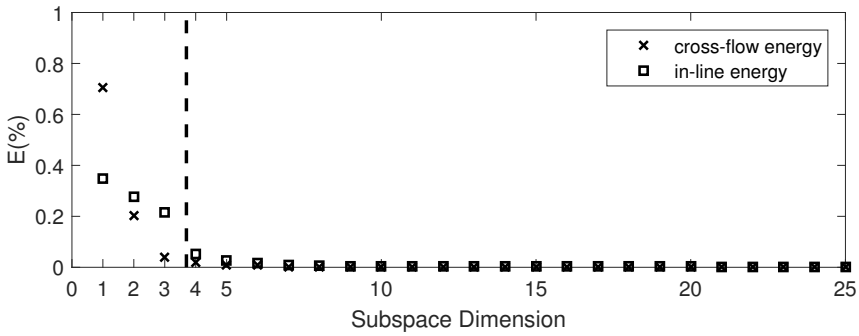

Figure 4: Energy fraction of each possible modes in cross-flow and in in-line directions for $Vr_n = 14.4$. Dashed line separates the first three modes from the higher subspace dimensions.

system and their corresponding energies, not specifically to identify higher order modes of the structure. It is found that this method successfully identifies the dominant modes in the transition region in both IL and CF directions, and shows transitions to second and third mode components. For simplicity in discussing the POD modes, the mode shapes are analogized with the structural mode shapes that occur in a vacuum, but the POD modes do not perfectly match sinusoidal mode shapes. A description of the POD method used for decomposing the cylinder motion is given in 4.9.

Figure 4 shows the energy fraction of the identified dominant modes using POD for an example reduced velocity. The decomposition shows that the overwhelming majority of energy in this particular example is contained within the first three modes and these three modes are sufficient to describe the total motion of the structure with very small error as illustrated in Table 3. As shown in Figure 4, the energy associated with the first Proper Orthogonal Mode (POM) in both in-line and cross-flow directions is higher than the other POMs, representing the most dominant mode. The contribution of the energy decreases as the subspace dimension increases. The root mean square error (RMSE) between reconstructed motion based on the POD and the observed oscillations are shown in Table 3 show-

ing that as the sum of the contribution of the POMs increase, relative error in the convergence decreases. RMSE IL 1 is the RMSE value between the original IL signal and first POM in the IL direction, RMSE IL 2 is the RMSE value between the original IL signal and sum of first two POMs in IL, and RMSE IL 3 indicate RMSE value between the original IL signal and sum of first three POMs in IL. The analogy is the same for the cross-flow RMSE calculations.

Table 3: Root mean square error (RMSE) between the original measured signal and decomposition of the signal using the first, second, and third modes in the cross-flow and in-line directions. Comparisons are made for both increasing and decreasing flow speeds for measurements in the studied hysteresis region.

Root Mean Square Error (RMSE)						
Increase	1 CF	1,2 CF	1,2,3 CF	1 IL	1,2 IL	1,2,3 IL
$Vr_n = 10.5$	0.001	0.0006	0.0001	0.0008	0.0003	5e-05
$Vr_n = 11.5$	0.0013	0.0006	0.0001	0.0012	0.0004	9e-05
$Vr_n = 12.6$	0.001	0.0005	0.0001	0.001	0.0003	7e-05
$Vr_n = 14.4$	0.0057	0.0003	0.0001	0.0015	0.0009	5e-05
Decrease						
$Vr_n = 10.5$	0.0009	0.0004	0.0001	0.0006	0.0003	4e-05
$Vr_n = 11.5$	0.0034	0.0001	0.0001	0.0038	0.0001	5e-05
$Vr_n = 12.6$	0.0036	0.0002	0.0001	0.0012	0.0004	4e-05
$Vr_n = 14.4$	0.0134	0.0003	0.0001	0.0029	0.0012	7e-05

Consider $Y(z,t)$ to be the time dependent motion response data set in the CF direction, where z is the spanwise spatial coordinate. In the experiments, the first three terms of the singular values $(\sigma_1, \sigma_2, \sigma_3)$ are used to give the best three-term approximation to $Y(z,t)$, capturing more than 90 percent of the total oscillation energy . The modal contribution of the first three dominant modes are computed for both increasing and decreasing flow speed cases. Figure 5 shows the contribution of first, second and third POMs in the CF and IL directions computed from the measured response time histories.

Figure 5 shows that as the flow speed increases, the first mode in the CF direction is dominant for nominal reduced velocities up to 14 with a contribution

of approximately 85% of the total response. The second mode becomes dominant above a nominal reduced velocity of 14 with approximately 75% contribution to the total response. With decreasing flow speeds, the CF response displays a dominant second mode for nominal reduced velocities greater than 10.5, with the first mode only becoming dominant for nominal reduced velocities lower than 10.5. The nominal reduced velocity at which the dominant mode transitions from first mode to second mode is the same as the transition point observed between a large amplitude response and small amplitude response in Figure 3. In this case, the third mode in the CF direction is not excited for the region of flow speeds tested.

Figure 5 also shows the modal contributions from the IL response. In contrast to the CF response, the IL response indicates a prominent excitation of the first mode with almost equal contributions of the second and third modes. For increasing flow speeds, when the CF response transitions from first mode to second mode, the IL response decreases with the first mode contribution and the second and third mode contributions becomes stronger. The second mode contribution is slightly stronger than the third mode in the hysteresis region, while the third mode becomes stronger after the hysteresis region. As the flow speed is decreased, hysteresis is seen in the first and third mode contributions to the response, however the second mode follows roughly the same contribution except at one point, where $V_{rn} = 11.5$. In this case, a very different time-dependent response of the cylinder is observed. This different response is highlighted in the discussion of the cylinder's orbital response, demonstrating an unusual condition where the response has a dominant second mode in both CF and IL directions.

2.3.3 Response in the Hysteresis Region

Four reduced velocities are chosen in order to further characterize the response of the flexible cylinder in the hysteresis region. Specifically, $V_{rn} = 10.5$ and

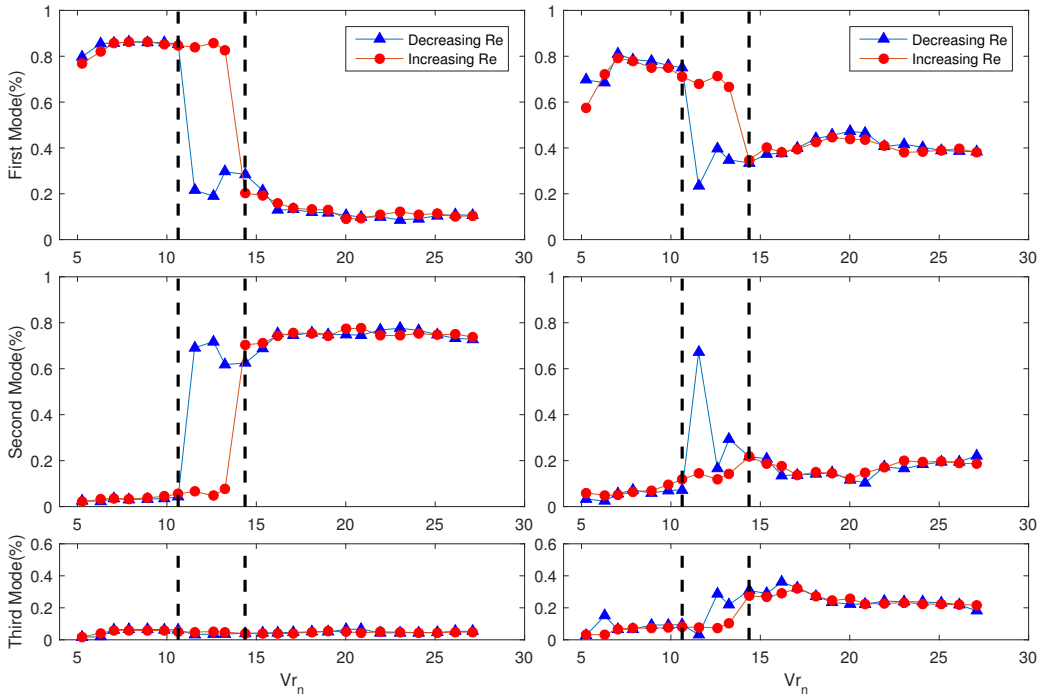

Figure 5: Contribution of First Three POMs. Left Column: Cross-flow Direction; Right Column: In-line Direction. Top row - first mode, second row - second mode, bottom row - third mode contribution. Red circles indicate increasing flow speed. Blue triangles indicate decreasing flow speed. Hysteresis region is indicated by the vertical dashed lines.

14.4 are on the edge of the hysteresis region, just outside the hysteresis region, while $V_{rn} = 11.5$ and 12.6 are in the hysteresis region. These reduced velocities are chosen as representative points lying across the region over which hysteresis occurs. Comparisons are made for responses at each reduced velocity for both the increasing and decreasing flow conditions.

Figure 6 shows the maximum spanwise amplitude response in IL and CF directions for the chosen reduced velocities in the hysteretic region. One can see the dominant mode shape of the response, where a dominant first mode shows a single peak over the span, while a dominant second mode shows two peaks over the span of the cylinder. For increasing flow speeds, the spanwise response initially shows a dominant first mode spatial excitation of the cylinder in both IL and CF

directions. Although the spatial mode resembles the first structural mode, it is important to note that the frequency response in the IL direction is twice the frequency as in the CF direction. This is demonstrated with the Lissajous figures, which show the orbital response of the cylinder at three span locations along the cylinder. A figure eight orbital response is seen in these cases with the cylinder moving upstream at the top and bottom of its motion. This response is sometimes referred to as a counterclockwise orbit [20] since the motion of the top of the figure eight is clockwise in a left to right flowing current.

When the cylinder response in the CF direction transitions from a dominant first mode excitation to a dominant second mode excitation, the IL motion transitions from a first mode excitation with twice the CF frequency to a multi-mode excitation with a prominent third mode component. This can be seen by three slight bumps in the IL spanwise amplitude response in Figure 6 at the highest shown reduced velocity. This multi-mode combination, however leads to very small, irregular motions in the IL direction.

For decreasing flow speeds, an additional response type is observed for the single reduced velocity of $V_{rn} = 11.5$. At higher flow speeds, the CF spanwise mode shape is primarily second mode while the IL mode shape is multi-mode. The dominant frequencies, however, have a ratio of 2:1 (in-line:cross-flow), although additional frequency content exists in the IL direction. At the reduced velocity $V_{rn} = 11.5$, a transition occurs in the IL direction, where the system takes on a second mode shape in the IL direction and maintains a second mode shape excitation in the CF direction. When this occurs, the frequency of oscillation in both directions becomes equal, with a value 1.5 times the fundamental natural frequency of the structure. In contrast to the typical figure eight or crescent shaped motions of a structure undergoing VIV, this response resembles a pedaling

mode (similar to rotating bicycle pedals), where the anti-nodes of the structure are rotating with an oval motion and the motion at the anti-nodes has a 180 degree phase difference.

Figure 6 also shows the phase between in-line and cross-flow motion, θ_{xy}. This phase is illustrative of the orbit shape observed for the cylinder motions over the span of the cylinder. Consider sinusoidal in-line and cross-flow motions with a phase shift in the in-line direction:

$$y = A_y \sin(\omega_y t) \tag{1}$$

$$x = A_x \sin(\omega_x t + \theta_{xy}) \tag{2}$$

The phase angle θ_{xy} between the in-line (x) and cross-flow (y) can be computed using the inner product [21] as long as x and y are synchronized:

$$\theta_{xy} = \cos^{-1}\left(\frac{\langle x, y\rangle}{\|x\|\|y\|}\right) \tag{3}$$

The phase between IL and CF motion shows that when a dominant first mode is excited in both directions, the phase is nearly constant over the span of the cylinder. When asymmetric modes are excited, however, the asymmetry requires that the phase between in-line and cross-flow motion changes over the span, as can be seen at the highest reduced velocities shown. In the case of the pedaling mode, a significant change in phase occurs since a node exists at the center of the span.

Figures 7, 8, 9, and 10 show the time history of the spanwise response for the four example test cases in the hysteresis region, for both increasing and decreasing flow speeds. The frequency content of the spanwise response is also shown. Figure 7 shows the responses for $V_{rn} = 10.5$. When the flow speed is increased, the spanwise response exhibits a standing wave with predominant first mode shape in

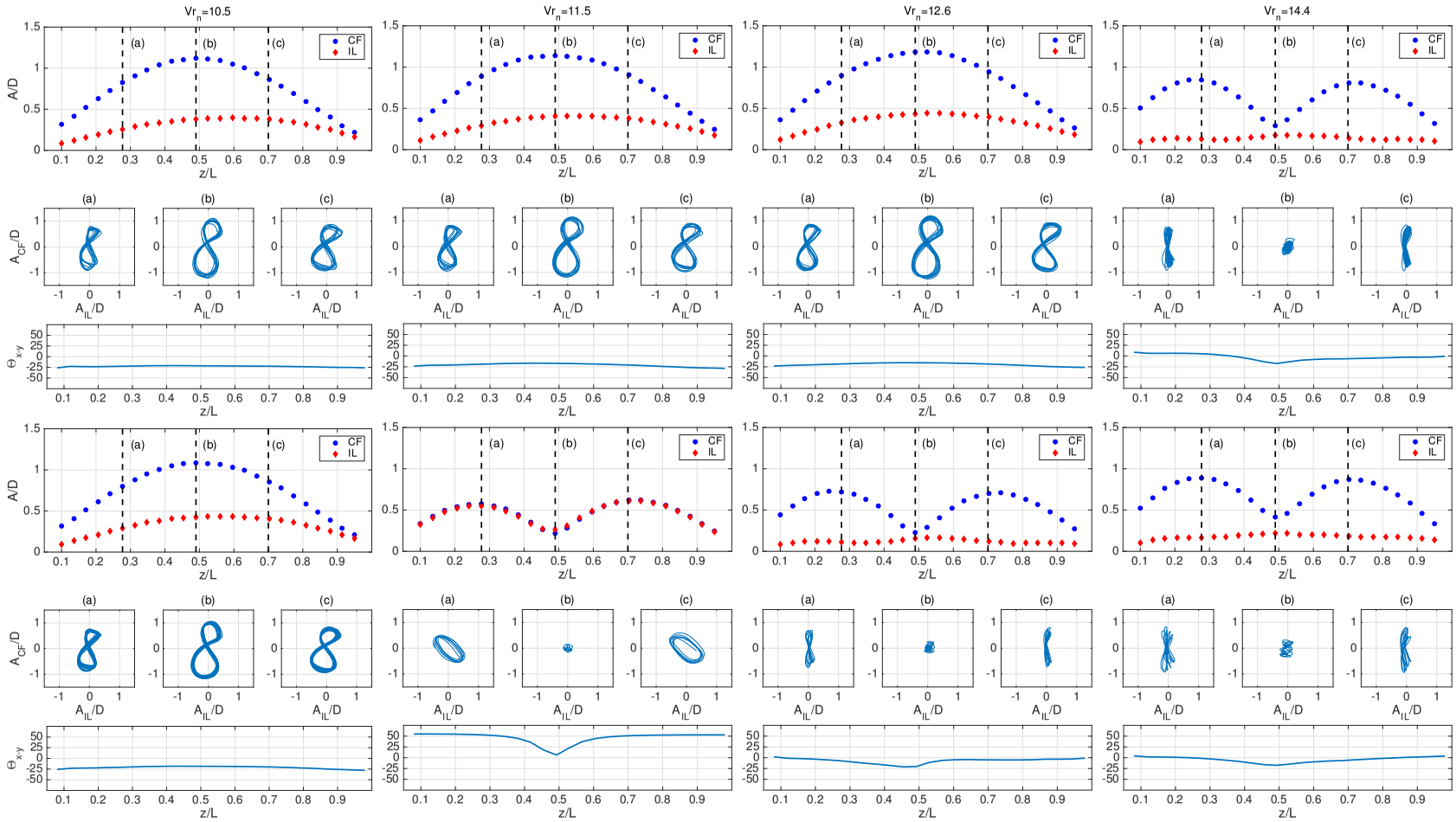

Figure 6: Maximum spanwise response and Lissajous figures of cylinder response at various spanwise locations. From left to right, top row shows the response at $V_{rn} = \{10.5, 11.5, 12.6, 14.4\}$ for increasing flow speeds. Bottom row shows responses for the same reduced velocities and decreasing flow speeds. For increasing flow speeds, one sees a transition from a dominant first mode shape in both in-line and cross-flow directions to a dominant second mode shape cross-flow and a nearly dominant third mode shape in-line. The Lissajous figures transition from figure eights to almost purely cross-flow motion as the third mode response is very small. For decreasing flow speeds, this transition is delayed due to hysteresis, but an intermediate condition is also observed for $V_{rn} = 11.5$, where a dominant second mode is observed both in-line and cross-flow. The frequency characteristics in this case are 1:1 instead of 2:1, leading to oval Lissajous figures. Lissajous figures are shown for spanwise locations $z/L = \{0.28, 0.49, 0.7\}$.

both IL and CF directions. The frequency in the IL direction is observed to be twice the frequency in the CF direction with some first mode frequency content. The case for decreasing flow speed shows a similar response. Figure 8 shows the time history of the spanwise response for $V_{rn} = 11.5$. In this case, the increasing flow speed response is similar to the previous speed, however the decreasing flow speed demonstrates the pedaling mode, where the IL and CF directions have the same frequency and both demonstrate a second mode shape. For $V_{rn} = 12.6$ (see Figure 9), the increasing flow speed response is still similar to the previous speeds, while the decreasing flow speed response demonstrates a second mode excitation in the CF direction and a multi-mode excitation in the IL direction. The frequency in the IL direction is closest to the third structural natural frequency. At the fourth speed of interest, $V_{rn} = 14.4$, the increasing and decreasing conditions both demonstrate similar responses with a dominant second mode excitation in CF and a multi-mode excitation in IL.

2.3.4 Fluid Force Estimates

Although forces were not directly measured in the experiments, if one assumes an equation of motion for the body with known structural characteristics, tension, and body motions, the hydrodynamic forces may be estimated through the equation of motion [22]. Assuming small body motions, one can treat the cylinder as a tensioned beam with cross-flow forces described as:

$$m\frac{\partial^2 y}{\partial t^2} + b\frac{\partial y}{\partial t} - \frac{\partial}{\partial z}\left(T\frac{\partial y}{\partial z}\right) + \frac{\partial^2}{\partial z^2}\left(EI\frac{\partial^2 y}{\partial z^2}\right) = f_y\left(z,t\right) \tag{4}$$

where y is the cross-flow displacement with respect to time, m is cylinder mass per length, b is the structural damping, E is the modulus of elasticity, I is the area moment of inertia, t is time, and z is the spanwise spatial dimension. This equation can only give an approximation of the spanwise hydrodynamic forcing since in

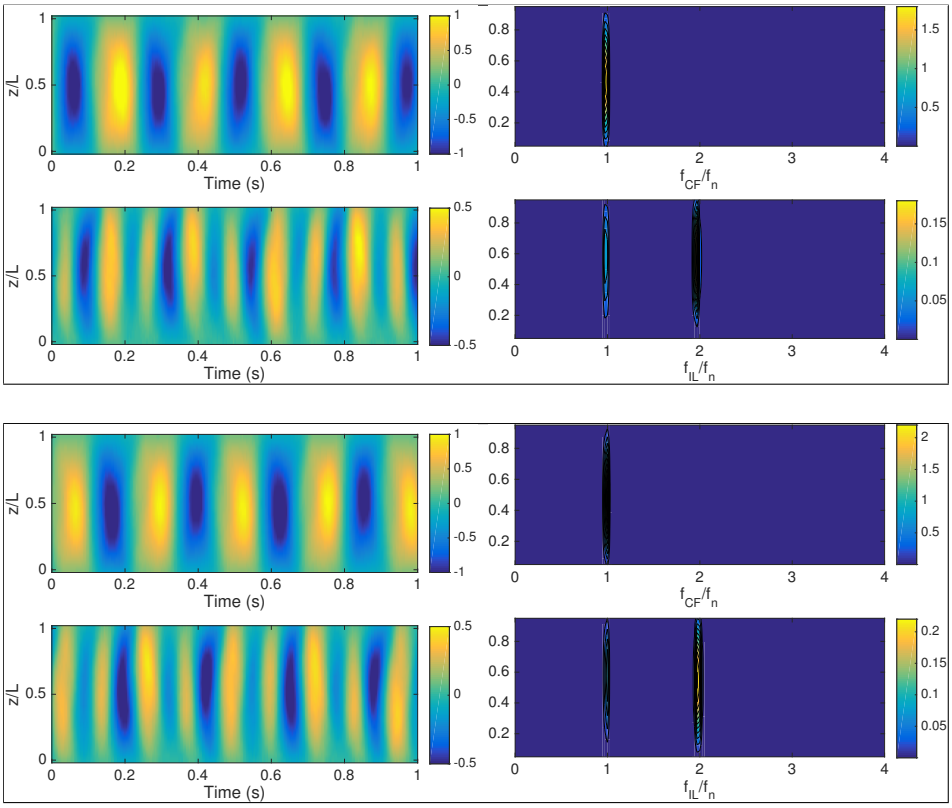

Figure 7: Time history and frequency content of spanwise response for increasing and decreasing flow speeds at $V_{rn} = 10.5$. First row: Increasing flow speed, CF spanwise response (left) and CF frequency response (right). Second row: Increasing flow speed, IL spanwise response (left) and IL frequency response (right). Third row: Decreasing flow speed, CF spanwise response (left) and CF frequency response (right). Fourth row: Decreasing flow speed, IL spanwise response (left) and IL frequency response (right).

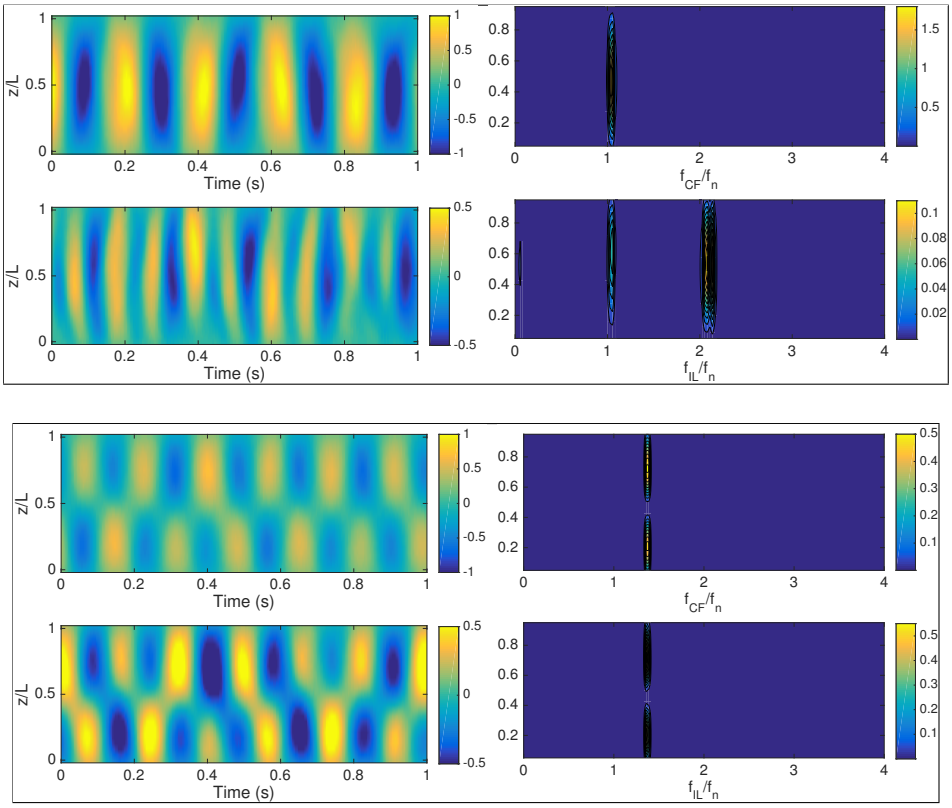

Figure 8: Time history and frequency content of spanwise response for increasing and decreasing flow speeds at $V_{rn} = 11.5$. First row: Increasing flow speed, CF spanwise response (left) and CF frequency response (right). Second row: Increasing flow speed, IL spanwise response (left) and IL frequency response (right). Third row: Decreasing flow speed, CF spanwise response (left) and CF frequency response (right). Fourth row: Decreasing flow speed, IL spanwise response (left) and IL frequency response (right).

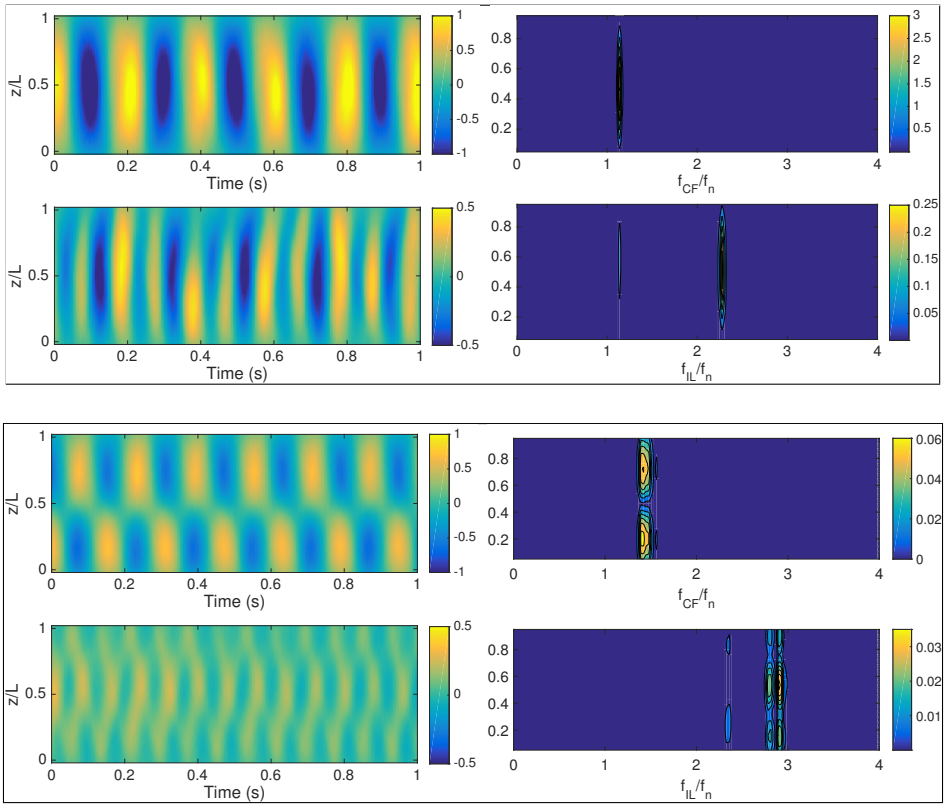

Figure 9: Time history and frequency content of spanwise response for increasing and decreasing flow speeds at $V_{rn} = 12.6$. First row: Increasing flow speed, CF spanwise response (left) and CF frequency response (right). Second row: Increasing flow speed, IL spanwise response (left) and IL frequency response (right). Third row: Decreasing flow speed, CF spanwise response (left) and CF frequency response (right). Fourth row: Decreasing flow speed, IL spanwise response (left) and IL frequency response (right).

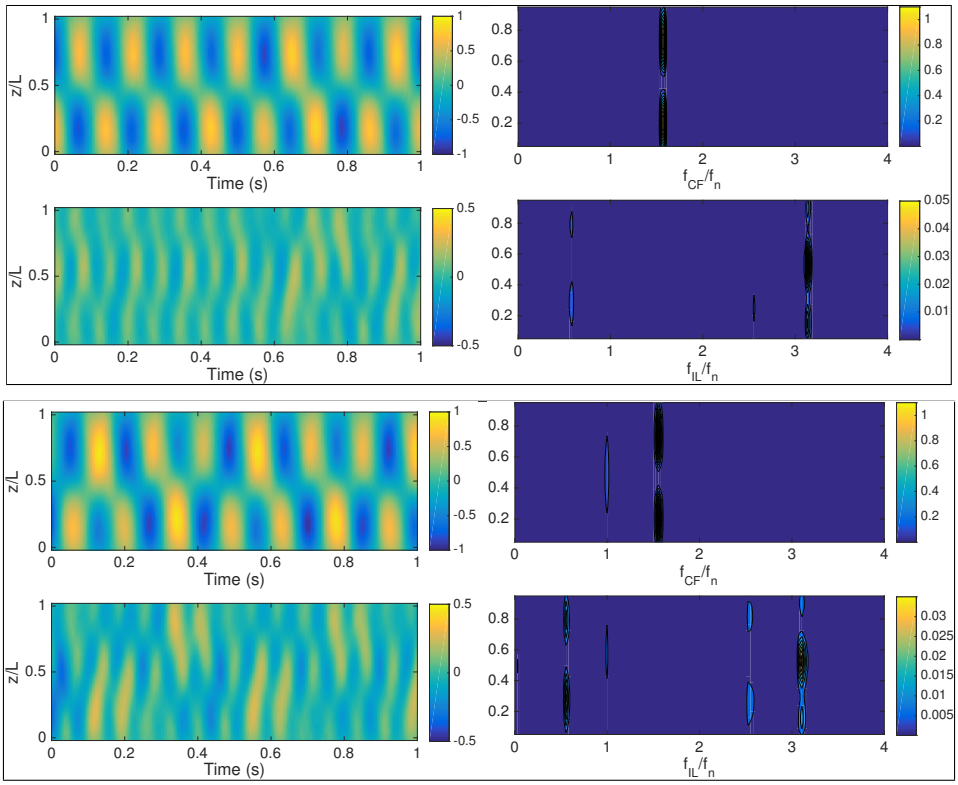

Figure 10: Time history and frequency content of spanwise response for increasing and decreasing flow speeds with $V_{rn} = 14.4$. First row: Increasing flow speed, CF spanwise response (left) and CF frequency response (right). Second row: Increasing flow speed, IL spanwise response (left) and IL frequency response (right). Third row: Decreasing flow speed, CF spanwise response (left) and CF frequency response (right). Fourth row: Decreasing flow speed, IL spanwise response (left) and IL frequency response (right).

the real non-linear structure, deformation of the body can affect the tension and structural characteristics of the body. Since the tension is not measured directly, the tension is assumed to be constant based on the initial tension. This analysis is not intended to provide accurate force estimates over the span, but rather to estimate the sign, order of magnitude, and distribution of the excitation/damping force and added mass.

Assuming the hydrodynamic force acting on the cylinder is a phase shifted sinusoid and that the body undergoes periodic motion, the linear portion of the fluid force may be decomposed into the non-dimensional force in phase with velocity, C_{lv}, that governs the excitation of the structure, and the non-dimensional force in phase with acceleration, C_{la} that governs the effective mass of the system. When C_{lv} is positive, there is a positive energy transfer from fluid to the structure (excitation) whereas when C_{lv} is negative, energy is transferred from structure to the fluid (damping). Knowing the motion of the body and spanwise non dimensional force C_l, as determined from Equation 4 and 5, the forces in phase with acceleration and velocity may be computed according to the inner product [23]:

$$Cl(z) = \frac{f_y(z,t)}{\frac{1}{2}\rho U^2 LD} \tag{5}$$

$$C_{lv} = \sqrt{\frac{2}{T}} \frac{C_l(t) \cdot \dot{y}(t)}{\sqrt{\dot{y}(t) \cdot \dot{y}(t)}} \tag{6}$$

$$C_{la} = \sqrt{\frac{2}{T}} \frac{C_l(t) \cdot \ddot{y}(t)}{\sqrt{\ddot{y}(t) \cdot \ddot{y}(t)}} \tag{7}$$

where T is the window length of the inner product and C_l is the non-dimensional lift coefficient. The same form of equations may be applied for determining force coefficients associated with IL motions using the fluctuating force

component in the IL direction to determine C_{dv}. The added mass coefficient for each point along the length of the cylinder is computed by equating the force in phase with acceleration to an effective added mass times acceleration of the body, which gives Equation 8. Again, a similar formulation may be applied to compute the added mass coefficient in the IL direction, C_{mx}.

$$C_{my} = \frac{-C_{la} V r^2 D}{2\pi^3 A_y} \tag{8}$$

Figure 11 shows the variation of computed force and added mass coefficients along the length of the cylinder for the same reduced velocities in the hysteresis region. For the lowest reduced velocity, the lift and fluctuating drag in phase with velocity are symmetric over the length of the cylinder, consistent with the symmetric excitation at the first mode shape. When the cylinder transitions to a second mode excitation in the cross-flow direction, the lift in phase with velocity shifts to being negative at one end of the cylinder and positive at the other end. This indicates that the power in region for the cylinder shifts with the change in mode. The fluctuating drag in phase with velocity shifts from a first mode shape to a symmetric shape similar to a third mode.

The added mass in both the in-line and cross-flow directions show relatively large magnitudes, which may not be realistic due to an under resolved calculation of the spatial derivatives of the cylinder, however the signs of the added mass and relative distribution of the added mass seem reasonable and are consistent with the observed dynamic behavior of the system. It should be noted that in the in-line direction, the added mass is always negative, except for the single case of $V_{rn} = 11.5$ for decreasing flow speeds, when the system undergoes the pedaling mode. For this case, since the in-line response is very similar to the cross-flow response, the distribution and magnitude of the in-line added mass is similar to

the cross-flow added mass distribution. In contrast, when the structure undergoes first mode excitation in both directions, the added mass is observed to be nearly constant over the length of the cylinder.

2.4 Discussion

Two significant observations may be made from the present experiments: 1) a strong hysteretic effect is observed in the response of the flexible cylinder and 2) a limited asymmetric response of the structure is seen in the in-line direction. These two behaviors are unusual based on observations from previous experiments, however an understanding of the differences between the present experiments and previously observed systems are crucial in understanding the observed excitation of a flexible cylinder in a uniform free-stream.

2.4.1 Hysteretic Effect

Prasanth et al. [9] gives a systematic characterization of hysteresis based on blockage ratio for a rigid cylinder in a uniform free stream. The study shows how hysteresis is affected by Reynolds number, blockage ratio, and mass ratio, demonstrating regions where hysteresis will or will not occur for different combinations of parameters. In the present experiments, the structural characteristics of the test cylinder were chosen such that the cylinder lies in the middle of the "no-hystersis" region identified by Prasanth et al. [9], however hysteresis still occurs. Additionally, Prasanth et al. [9] compares this systematic study with several flexible cylinder experiments that show consistent hysteresis effects with the mapped hysteresis regions. The question then remains as to why the present experiments demonstrate hysteresis while the mapped response regions from Prasanth et al. [9] predict that no hysteresis should occur.

The simulations performed by Prasanth et al. [9] were for an elastically

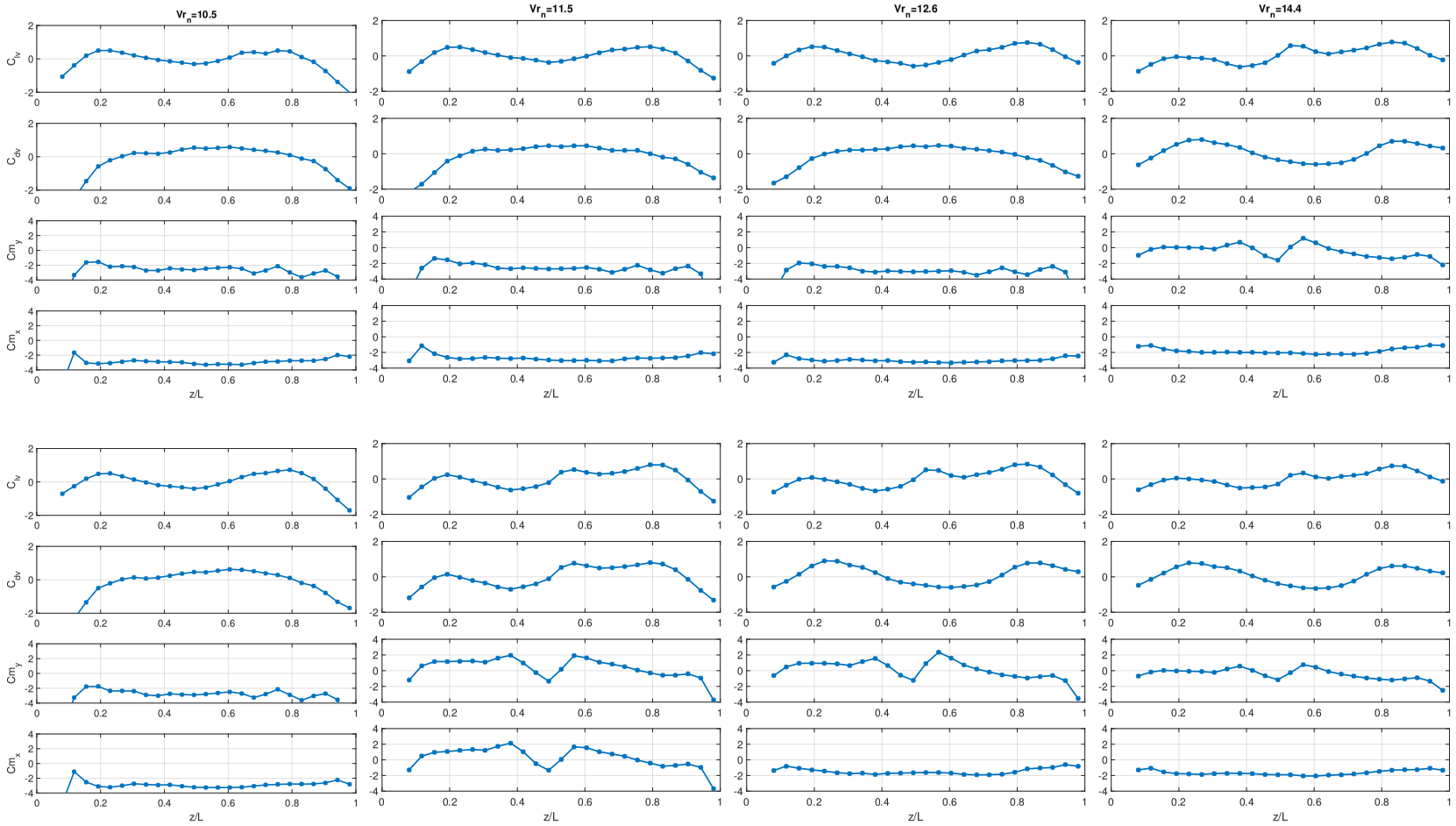

Figure 11: Estimated force distribution in hysteresis region for $V_{rn} = 10.5, 11.5, 12.6, 14.4$ (from left to right). Top fours rows show force distributions for increasing flow speeds, bottom four rows show force distributions for decreasing flow speeds. Figure shows lift in phase with velocity (C_{lv}), fluctuating drag in phase with velocity (C_{dv}), cross-flow effective added mass (C_{my}), and in-line effective added mass (C_{mx}).

mounted rigid cylinder. In the case of a rigid cylinder, the observation of hysteresis is related to the transition of the wake, as the wake switches from '2S' to 'C(2S)' modes such that the phasing between the motion of the structure and the wake-induced force changes. Delay of this mode transition results in a delay in the change of the amplitude response as flow speed is changed, and Prasanth et al. [9] demonstrates how this response is related to blockage and mass ratio. When the cylinder is flexible, however, mode transitions may occur for the structure in addition to mode transitions in the wake. In the case of Brika and Laneville [10], the flexible structure is pinned in such a way that only the first mode of the structure is excited in the experiment. The experiment very closely resembles the response of a rigid cylinder and follows the hysteretic behavior predicted by Prasanth et al. [9].

In contrast, the present study shows a hysteretic response that is related to the transition of the fluid coupled structural mode that is being excited, which could not previously be observed in the response of a rigid cylinder. As shown in Figure 5, hysteresis in the present study is related to the transition between the first and second modes in the cross-flow direction. This is fundamentally different than the hysteresis observed in Prasanth et al. [9], since the transition is not only related to a change in the wake or the phasing of forcing on the structure. It must be noted that flow visualization was not performed in the present study, and since this study shows the response of a fluid-structure coupling, there is likely some resulting change to the wake associated with the observed hysteresis that could not be observed. Additional parametric studies like the comprehensive study of Prasanth et al. [9] may be necessary to fully characterize hysteretic behavior in flexible structures undergoing vortex-induced vibrations.

2.4.2 Limited Asymmetric Response

The second main observation from the present experiments is that in uniform flow conditions, asymmetric modes, such as the second mode, are not observed to be easily excited, and a strong asymmetric mode in the in-line direction is only observed to exist in very limited conditions, dependent on the response in the cross-flow direction. Vandiver and Jong [4] observed an interesting behavior in field experiments on a taut cable undergoing vortex-induced vibration in a uniform current, where when the cross-flow motion of the test cylinder was excited at the second mode, the in-line motion was observed to have a third mode shape excited at the fourth mode frequency, rather than excitation of the fourth mode shape. This is attributed to an inertia controlled response and is explained based on the distribution of loading in the drag direction. Since the distribution of the drag load in a uniform current is symmetric over the structure, it will not excite an asymmetric mode and instead a forced motion at the next lower symmetric mode occurs. The same behavior is observed in the present experiments for nearly all cases, however the hysteretic region displays one flow condition that differs from this behavior.

For decreasing flow speeds in the hysteresis region, Figure 6 shows one condition where both the cross-flow and in-line modes are excited with a second mode shape at a frequency directly in between the first and second structural mode natural frequency. This case is likely a marginally stable dynamic condition, where the added mass in each direction drives the excitation frequency to have a value of $f^* = 2$. Since this condition is only observed for a single experimental test case and flow visualization was not performed for the test case, it is unclear exactly how this particular mode excitation is chosen by the system, although slight changes to the flow speed, result in a dramatically different system response. The resulting

"pedaling" mode was only observed to be present for decreasing flow speeds in the hysteresis region, however it was observed to be repeatable by repeating the experiment four times at this speed, and it may be possible that this response is a result of the non-linear system transition that occurs from a low amplitude response to a high amplitude response as the flow speed decreases. Further detailed analysis of the full dynamic system would be necessary to demonstrate this.

Although an asymmetric response is observed to be limited in the present experiments, other experiments on flexible cylinders have noted significant asymmetric mode excitation when undergoing a uniform current. Sanaati and Kato [24] shows significant excitation of the fourth mode in the in-line direction with a second mode cross-flow excitation for a horizontally towed flexible cylinder in a uniform current. In this case, the aspect ratio of 200 is much larger than the present experiments. Additionally, small asymmetries to the experimental setup may lead to excitation of even modes as well. For example, orienting the same cylinder as in the present experiment vertically in the flow channel, such that the cylinder intersects the free surface would induce a slight asymmetry to the loading. It is expected that such an orientation would result in a different system response that may include more contribution from even modes. Similarly, loading of the flexible structure in a sheared flow would introduce asymmetry to the excitation force, leading to excitation of even modes.

The presence of different mode combinations also appears to have a significant effect on the structural response, at least for the low mode number experiments in the present experiment. For example, as the second mode is excited in the cross-flow direction, the response becomes much smaller with significantly less excitation in the IL direction. This is significant, since large figure eight type responses are connected with significantly larger high harmonic forces acting of the body

[20], which have the potential for increasing fatigue damage on structures [25]. This would imply that some mode excitations may be more susceptible to higher harmonic forcing than others.

Finally, although the presented force estimations have error due to calculation of derivatives based on limited spatial measurements over the length of the cylinder, the sign and relative distribution of forces are consistent with the observed motions of the body. For example, as the second mode in the cross-flow direction becomes excited, it is necessary for an asymmetry to exist in C_{lv}, since one side of the cylinder must act as an energy source and the other side must act as a sink to balance excitation and damping over the span [26]. This behavior is observed where for first mode excitation, C_{lv} is only negative for the large peak motions at the center of the cylinder, taking on a symmetric distribution, while for second mode excitation, C_{lv} varies from negative to positive over the length of the cylinder, taking on an asymmetric distribution.

2.5 Conclusion

For the present experiments, a transition in the amplitude of the response of a flexible cylinder undergoing vortex-induced vibrations is shown to be related to the transition between fluid coupled structural modes excited by the flow. For increasing or decreasing flow speeds in a recirculating water channel, the transition is observed to occur at different flow speeds, indicating hysteresis in the response. It is shown that the hysteretic response associated with the modal excitation of the tensioned flexible cylinder undergoing vortex-induced vibrations is a function of the spanwise mode transition of the structure as opposed to a pure mode transition in the wake. A mode transition in the wake likely occurs in concert with the observed structural transition, however wake measurements were not made in the present experiments, so mode transitions in the wake were not quantified. Estimates of

the hydrodynamic forces based on a simple model system equation show that transitions in the sign of the effective added mass of the system and distribution of excitation forces are consistent with phasing changes in the force associated with transitions in phasing of the relative motion of the body and vortices in the wake.

Additionally, it is observed that the cylinder does not demonstrate excitation of even modes in the in-line direction when undergoing a uniformly distributed drag loading. This is consistent with previously published observations, indicating that asymmetric modes are not typically excited under symmetric loading of the structure. In the hysteresis region, a single instance is observed where the asymmetric second mode is excited in the in-line direction in combination with the asymmetric second mode being excited in the cross-flow direction. This results in a "pedaling" mode, where both directions are excited at the same frequency and the anti-nodes oscillated with a slanted oval motion 180 degrees out of phase with one another. This single instance is hypothesized to be an intermediate response condition within the transition of the non-linear dynamic system from low amplitude response to higher amplitude response in the hysteresis region.

2.6 Appendix A. Proper Orthogonal Decomposition (POD)

This appendix explains how the POD method is applied in the current study.

Consider $Y(z,t)$ to be the time dependent motion response data set in the CF direction, where z is the spanwise spatial coordinate. The motion response can be approximated as a modal sum as follows:

$$Y(z,t) \approx \sum_{k=1}^{N} a_k(t)\Phi_k(z) \tag{9}$$

where,$a_k(t)$ is the modal contribution matrix (weights of the spatial modes), $\Phi_k(z)$ is the spatial modal shape matrix, k is the mode number and N is the total number of modes.

Equation 9 is a discrete approximation of the modal decomposition of the signal Y. This discrete approximation can be computed using singular value decomposition (SVD). The signal Y can be decomposed as:

$$Y(z,t) = U\Sigma V^T \tag{10}$$

where U is an $M \times M$ orthogonal matrix representing the proper orthogonal modes (POM), V is an $N \times N$ orthogonal matrix representing the time evaluation of the signal, and Σ is an $M \times N$ diagonal matrix of the singular values of Y representing the energy captured in each POM.

Using the POD, one can approximate the full rank N data matrix using the singular values Σ $(\sigma_1, \sigma_2, ..., \sigma_k)$ and find a low dimensional rank k matrix (where $k \ll N$) of the original matrix to represent the total motion with a certain accuracy.

The accuracy of the approximation depends on the matrix of Σ. This matrix is representative of the energy captured by the k^{th} singular vector and can be used to compute the contribution of each mode to total motion, where E_k is the percentage of energy associated with the k^{th} mode.

$$E_k = \frac{{\sigma_k}^2}{\sum_{i=1}^{N} {\sigma_i}^2} \tag{11}$$

List of References

[1] T. Sarpkaya, "A critical review of the intrinsic nature of vortex-induced vibrations," *Journal of Fluids and Structures*, vol. 19, no. 4, pp. 389–447, 2004.

[2] C. Williamson and R. Govardhan, "Vortex-induced vibrations," *Annu. Rev. Fluid Mech.*, vol. 36, pp. 413–455, 2004.

[3] J. K. Vandiver, V. Jaiswal, and V. Jhingran, "Insights on vortex-induced, traveling waves on long risers," *Journal of Fluids and Structures*, vol. 25, no. 4, pp. 641–653, 2009.

[4] J. Vandiver and J.-Y. Jong, "The relationship between in-line and cross-flow vortex-induced vibration of cylinders," *Journal of Fluids and Structures*, vol. 1, no. 4, pp. 381–399, 1987.

[5] R. Bishop and A. Hassan, "The lift and drag forces on a circular cylinder oscillating in a flowing fluid," *Proceedings of the Royal Society of London A*, vol. 277, pp. 51–75, 1964.

[6] P. K. Stansby, "The locking-on of vortex shedding due to the cross-stream vibration of circular cylinders in uniform and shear flows," *Journal of Fluid Mechanics*, vol. 74, pp. 641–665, 1976.

[7] A. Khalak and C. Williamson, "Motions, forces and mode transitions in vortex-induced vibrations at low mass-damping," *Journal of fluids and Structures*, vol. 13, no. 7, pp. 813–851, 1999.

[8] J. Klamo, A. Leonard, and A. Roshko, "The effects of damping on the amplitude and frequency response of a freely vibrating cylinder in cross-flow," *Journal of Fluids and Structures*, vol. 22, pp. 845–856, 2006.

[9] T. Prasanth, V. Premchandran, and S. Mittal, "Hysteresis in vortex-induced vibrations: critical blockage and effect of m*," *Journal of Fluid Mechanics*, vol. 671, pp. 207–225, 2011.

[10] D. Brika and A. Laneville, "Vortex-induced vibrations of a long flexible circular cylinder," *Journal of Fluid Mechanics*, vol. 250, pp. 481–508, 1993.

[11] M. Triantafyllou, A. Techet, F. Hover, and D.-P. Yue, "Viv of slender structures in shear flow," in *IUTAM Symposium on Flow-Structure Interaction*, Rutgers State University, New Brunswick, NJ, 2003.

[12] H. Lie and K. Kaasen, "Modal analysis of measurements from a large-scale {VIV} model test of a riser in linearly sheared flow," *Journal of Fluids and Structures*, vol. 22, no. 4, pp. 557 – 575, 2006. [Online]. Available: http://www.sciencedirect.com/science/article/pii/S0889974606000077

[13] J. Vandiver, H. Marcollo, S. Swithenbank, V. Jhingran, *et al.*, "High mode number vortex-induced vibration field experiments," in *Offshore Technology Conference*. Offshore Technology Conference, 2005.

[14] E. D. Gedikli and J. M. Dahl, "Mode shape variation for a low-mode number flexible cylinder subject to vortex-induced vibrations," in *ASME 2014 33rd International Conference on Ocean, Offshore and Arctic Engineering*. American Society of Mechanical Engineers, 2014, pp. V002T08A071–V002T08A071.

[15] F. Huera-Huarte and P. Bearman, "Wake structures and vortex-induced vibrations of a long flexible cylinderâ"part 1: Dynamic response," *Journal of Fluids and Structures*, vol. 25, no. 6, pp. 969 – 990, 2009. [Online]. Available: http://www.sciencedirect.com/science/article/pii/S0889974609000449

[16] E. Passano, C. M. Larsen, and J. Wu, "Viv of free spanning pipelines: Comparison of response from semi-empirical code to model tests," in *ASME 2010 29th International Conference on Ocean, Offshore and Arctic Engineering*. American Society of Mechanical Engineers, 2010, pp. 567–577.

[17] A. Trim, H. Braaten, H. Lie, and M. Tognarelli, "Experimental investigation of vortex-induced vibration of long marine risers," *Journal of fluids and structures*, vol. 21, no. 3, pp. 335–361, 2005.

[18] N. Jauvtis and C. Williamson, "The effect of two degrees of freedom on vortex-induced vibration at low mass and damping," *Journal of Fluid Mechanics*, vol. 509, pp. 23–62, 2004.

[19] F. Huera-Huarte, "Multi-mode vortex-induced vibrations of a flexible circular cylinder," PhD, Imperial College London, London, April 2006.

[20] J. Dahl, F. Hover, M. Triantafyllou, S. Dong, and G. Karniadakis, "Resonant vibrations of bluff bodies cause multi-vortex shedding," *Physical Review Letters*, vol. 99, no. 144503, 2007.

[21] G. Strang, *Introduction to applied mathematics*. Wellesley-Cambridge Press Wellesley, MA, 1986.

[22] B. Seyed-Aghazadeh and Y. Modarres-Sadeghi, "Reconstructing the vortex-induced-vibration response of flexible cylinders using limited localized measurement points," *Journal of Fluids and Structures*, vol. 65, pp. 433–446, 2016.

[23] O. N. Smogeli, F. S. Hover, and M. S. Triantafyllou, "Force-feedback control in viv experiments," in *ASME 2003 22nd International Conference on Offshore Mechanics and Arctic Engineering*. American Society of Mechanical Engineers, 2003, pp. 685–695.

[24] B. Sanaati and N. Kato, "Vortex-induced vibration (viv) dynamics of a tensioned flexible cylinder subjected to uniform cross-flow," *Journal of Marine Science and Technology*, vol. 18, pp. 247–261, 2013.

[25] H. Zheng, R. Price, Y. Modarres-Sadeghi, and M. Triantafyllou, "On fatigue damage of long flexible cylinders due to higher harmonic force components and chaotic vortex-induced vibrations," *Ocean Engineering*, vol. 49, pp. 318–329, 2014.

[26] S. Swithenbank and J. Vandiver, "Identifying the power-in region for vortex-induced vibrations of long flexible cylinders," in *26th International Conference on Offshore Mechanics and Arctic Engineering (OMAE 2007)*, vol. 3, 2007, pp. 723–730.

CHAPTER 3

Multivariate analysis of vortex-induced vibrations in a tensioned cylinder reveal nonlinear modal interactions

by

Ersegun Deniz Gedikli*, Jason Dahl*, and David Chelidze**

*Department of Ocean Engineering, University of Rhode Island, Narragansett, RI 02882, USA

**Department of Mechanical, Industrial and Systems Engineering, University of Rhode Island, Kingston, RI, 02881, USA

Accepted to be published in EURODYN2017 conference

Abstract

The modal structure of a tension-dominated flexible cylinder undergoing vortex-induced vibrations in a uniform current is investigated through multivariate analysis. Experiments are performed in a recirculating flow channel where a flexible cylinder is mounted across the flow channel and subjected to a uniform current. The cylinder response is measured using motion tracking with two high speed cameras, allowing for the measurement of both in-line and cross-flow motions of the cylinder. The recorded motion of the cylinder is analyzed in its measured phase space using smooth orthogonal decomposition (SOD) and proper orthogonal decomposition (POD). Both decompositions show that most of the motion energy is captured in a six-dimensional subspace; however, the corresponding modal structures are different between the decompositions. While SOD-based modes are persistent regardless of whether the flow speed is increasing or decreasing, the POD modes do not maintain this consistency. For example, the dominant (i.e., most energetic) POD mode appears to be dependent on the hysteric response, leading to a different mode shape depending on whether the flow speed is undergoing an increase or decrease. This inconsistency leads to a variability in the modal energy that is affected by hysteresis if the POD method is used. Modal frequency response curves show the corresponding variance of the modal response versus the reduced flow velocity. SOD-based plots show hardening spring behavior in the first mode oscillations, which are dominant at low reduced velocities and have negligible amplitude at high reduced velocities. Second mode oscillations are negligible at low reduced velocities but undergo subcritical Hopf bifurcation at higher reduced velocities. The associated hysteresis behaviors are observed over the same range of reduced velocity values for both modes. POD analysis also detects this behavior, but it is less pronounced and leaks into higher-order modes.

3.1 Introduction

Vortex-induced vibrations (VIV) are a self-limiting fluid-structure interaction caused by vortex shedding in the wake of a flexible structure. The coupling of the flexible structure's wake with the motion of the structure can lead to a wide band motion response and large amplitude motions that can contribute to fatigue damage in many engineering applications (e.g. bridges, marine cables, risers, transmission lines, heat exchangers, etc.). A significant volume of work has been devoted to understanding this problem, particularly through simplifications studying the interaction of single-degree-of-freedom, elastically-mounted rigid cylinder subjected to a cross-flow as discussed in a variety of reviews [1, 2, 3]. Sarpkaya [1] discusses the significant complexities of the problem in continuous systems, highlighting the large number of factors that contribute to this fluid-structure interaction in a continuous system.

Recent studies have illustrated the significance of studying combined IL and CF motion of continuous structures, due to the presence of large high-harmonic forces associated with figure eight type motion of a continuous structure's cross-section [4, 5], which can significantly contribute to fatigue damage in structures. While a large number of studies on continuous, flexible structures have characterized the multimode response of flexible structures undergoing VIV in field experiments [6, 7, 8, 9] and laboratory scale experiments [10, 11, 12, 13], the analysis of the structural mode response has often been limited to a linear Fourier analysis of the system. While a Fourier analysis of structural modes in this highly nonlinear phenomenon can give a base estimate of the dominant response shapes and a characterization of the multiple frequency response of the system, these methods are not capable of characterizing the general underlying nonlinear behavior of the system. This is particularly important where the interaction of specific modes in

the IL and CF direction may result in a different overall nonlinear behavior of the structure.

The present study aims to characterize the nonlinear response of a low-mode and low-mass ratio flexible cylinder, particularly when highly nonlinear behaviors (e.g., hysteresis) appear in the overall response of the system. A tensioned, flexible cylinder placed in a uniform free stream is used as the test apparatus, while multivariate analysis is used to characterize the underlying nonlinear behavior of the continuous system. The multi-mode dynamic response of the cylinder is analyzed in its phase space using smooth orthogonal decomposition (SOD) as described in [14] and compared with traditional proper orthogonal decomposition (POD) to illustrate the importance of using empirical modes in characterizing the nonlinear response of the system. Since the fluid-structure interaction in VIV is inherently nonlinear, there is no physical basis to argue that the modal response of the cylinder must consist of sinusoidal Fourier modes. These multivariate data analysis methods allow for the determination of the empirical spatial mode shapes associated with the energy in the system, with the first mode being the most energetic and so on. Applying both decomposition methods reveals that most of the motion energy is captured in a six-dimensional subspace of the phase space. More interestingly, SOD-based decomposition clearly identifies the hardening spring type behavior and subcritical Hopf bifurcation in first and second mode oscillations, respectively; whereas POD analysis also detects this behavior, but it is less pronounced and leaks into higher-order modes.

3.2 Experiments in Flow Channel

Experiments were carried out in a re-circulating flow channel at the University of Rhode Island. The flow channel has a cross section of $38 \times 48\,\text{cm}$ and generates uniform flows up to $1\,\text{m/s}$. Fig. 12 shows a schematic of the experimental

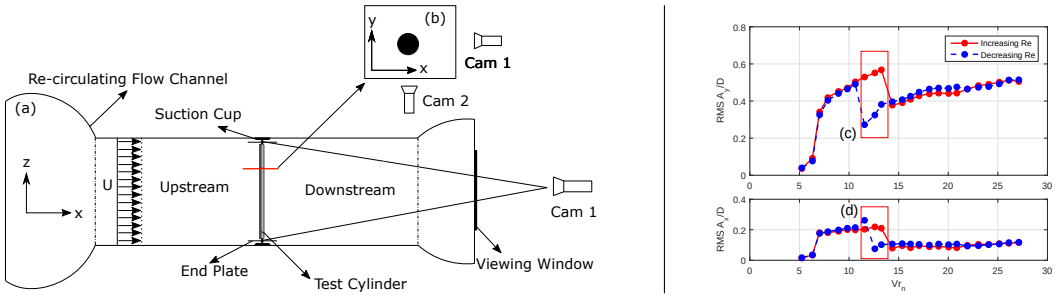

Figure 12: Left image: Schematic of the experimental setup; (a) Top view. Camera 1 is located in front of the flow channel; (b) Side view of cylinder cross-section. Camera 2 is located underneath the flow channel. Flow is from left the right. Right image: Priori RMSE Amplitude response for increasing and decreasing Reynolds number values. Red boxes show different amplitude responses obtained (c) in CF and (d) in IL respectively.

setup. The cylinder was placed horizontal to the incoming flow, and marked with 25 evenly spaced white dots to capture the motion response of the cylinder over the entire length. Two Vision Research Phantom V-10 high speed cameras were used to capture high speed video of the vibrating cylinder at a frame rate of 250 frames per second. One of the cameras was placed behind the flow channel to measure CF motion of the cylinder and the second camera was placed underneath the flow channel to measure IL motion of the cylinder as shown in Fig. 12.

ProAnalyst motion tracking software was used to track the dot features in the video using the cross-correlation of subsequent images to track the markings on the test cylinder. The flow speed in the water channel was varied between 0.1–0.54 m/s. Separate measurements were made for increasing and decreasing flow speeds in the flow channel to observe potential hysteric behavior of the system. The right

Table 4: Test cylinder and experimental parameters

Variable	Values	Units
D	6.35	mm
T	0.15	N
f_n	3	Hz
U	0.1–0.54	m/s
Re	650–3500	–
m^*	3.76	–
AR	41	–

image in Fig. 12 shows the RMSE amplitude response for increasing and decreasing nominal reduced velocity, $V_{rn} = U/f_n D$. This plot shows there is a region where the system undergoes different oscillation amplitudes and a different modal response depending on whether the speed is increasing or decreasing, indicating hysteresis. Physical characteristics of the test cylinder are shown in Table 1 and a more detailed description of the experimental system can be found in Gedikli and Dahl [15].

3.3 VIV Modes and Multivariate Analysis

In linear modal analysis, a simply supported flexible beam can be shown to have sinusoidal spatial mode shapes corresponding to the natural frequencies of the continuous system, with a first mode shape appearing as a half sine, a second mode shape as a full sine, and so on. These mode shapes satisfy the structural equation of motion for the linearized structural systems; however, in fluid-structure interaction problems where a dense fluid surrounds a light structure (i.e. low mass ratio systems), the interaction of the fluid wake with the vibration of the structure leads to large variability of the mass, damping/excitation, and stiffness properties of the total fluid-structure system, such that the effective resonant properties of the system may change with the excitation provided by the fluid wake [15]. This highly nonlinear behavior alters the resonant behavior of the system as the linear Fourier modes of the system only account for the structural properties of the system and do not account for fluid effects on the system response frequencies and modes. If the system is nonlinear, as in VIV, the modal response of the system will be altered by the interaction with the fluid wake and characterization of the modal response will require an analysis of the empirical modes of the system. These empirical modes do not follow a sinusoidal function shape, however they may resemble to the linear modes, for example, taking on a shape similar to a half sine or full sine

wave over the length of the cylinder.

3.3.1 POD and SOD Analysis

For multivariate analysis, the IL and CF motion tracking (ie., displacement) data $X \in \mathbb{R}^{M\times 2N}$ (M indicates the number of total time samples, and N indicate the number of measurement points) is used to estimate the corresponding IL and CF velocities $V = \mathcal{D}X \in \mathbb{R}^{M\times 2N}$ using the forward difference method. The data is then arranged into a matrix $Y = [X, V] \in \mathbb{R}^{M\times 4N}$ describing the measured phase space trajectory. The corresponding time derivatives are assembled into an additional matrix $\mathcal{D}^k Y = [\mathcal{D}^k X, \mathcal{D}^k V] \in \mathbb{R}^{M\times 4N}$, where k is the order of the differentiation.

POD, at each k-dimensional realization, provides the best possible approximation to the original matrix Y in the least squares sense. POD of Y can be solved by its economical singular value decomposition $Y = P\Sigma X^T$, where superscript T indicates matrix transpose. Columns of $P\Sigma \in \mathbb{R}^{M\times 4N}$ are proper orthogonal coordinates (POCs), the diagonal matrix $\Sigma \in \mathbb{R}^{4N\times 4N}$ contains singular values or square roots of proper orthogonal values (POVs), and columns of orthogonal matrix $X \in \mathbb{R}^{4N\times 4N}$ are proper orthogonal modes (POMs).

Geometrically, points in the matrix Y can be pictured as a cloud of points in a $4N$-dimensional space. POD fits the best ellipsoid to this cloud of points in the least square sense. The directions of the semi-principal axes of this ellipsoid give the POMs. The squared magnitudes of the semi-principal axes correspond to the variance of the projected points on the subspace span by the corresponding axes and represent POVs, which are square of the corresponding singular values of the matrix Y. Therefore, POD provides an energy optimal order reduction.

SOD identifies projective vectors ψ, such that the corresponding projections $q = Y\psi$ have minimal roughness and maximal variance. The roughness of the

projection can be expressed as:

$$h(\psi; k) = M^{-1}(\mathcal{D}^k Y\psi)^T \mathcal{D}^k Y\psi\,, \tag{12}$$

where $\mathcal{D}^k$ is the k^{th} order derivative matrix based on forward difference. The choice of k is application dependent, and in the present analysis, $k = 3$ was used. The SOD then translates into the following optimization problem:

$$\max_{\psi} q^T q = \max_{\psi} (Y\psi)^T Y\psi, \tag{13}$$

subject to

$$\min_{\psi} \left(\mathcal{D}^k q\right)^T \mathcal{D}^k q = \min_{\psi} \left(\mathcal{D}^k Y\psi\right)^T \mathcal{D}^k Y\psi \tag{14}$$

This optimization problem is solved by the economical generalized singular value decomposition:

$$Y = UC\Phi^T = Q\Phi^T, \quad \mathcal{D}^k Y = VS\Phi^T = \mathcal{D}^k Q\Phi^T\,, \tag{15}$$

where U and V are unitary, and C and S are diagonal matrices; columns of the square matrix Φ contain smooth orthogonal modes (SOMs), columns of $Q = UC$ are smooth orthogonal coordinates (SOCs), $\lambda_i = C_{ii}/S_{ii}$ are smooth orthogonal values (SOVs), and $\Psi = \Phi^{-T}$ are smooth projective modes (SPMs) , which are bi-orthogonal to SOMs.

In summary, SOD identifies the SOM subspaces where the scalar field projections are maximally smooth. SOMs are linearly independent but not orthogonal to each other. They span smooth modal subspaces ($Y = Q\Phi$). SPMs form a bi-orthonormal set with SOMs and are used to obtain SOCs ($Q = Y\Psi$). These SOCs are orthogonal to each other (i.e., their covariance matrix is diagonal) and invariant under invertible linear coordinate transform of data matrices.

3.4 Results

Gedikli and Dahl [15] initially used POD analysis of the present data set on the individual CF and IL observed motions, where data recorded at each reduced velocity value were analyzed individually. It was observed that the dominant first two empirical modes in CF and dominant first three empirical modes in IL correspond to $\sim 90\,\%$ of the total oscillation. This analysis showed that a hysteresis is observed in the response of the system that appears in the transition between dominant POD modes of the system.

Here, global POD and SOD analysis is applied to the displacement-time matrix over all experiments and all reduced velocities such that multivariate response analysis is performed for the total response. POD and SOD are applied to the whole data record for the entire range of flow speeds, only separating the data by whether the flow speed was increasing or decreasing. The IL and CF displacements of each data point along the cylinder's span were concatenated into one large data matrix $Y_{M\times 4N}$ where M now represents the total time samples and N represents the total displacement points.

Energy fraction is calculated using both POD and SOD methods and shown in the left plot in Fig. 13 as a function of subspace dimension for increasing and decreasing flow speeds. Calculated motion energy shows that the sum of the first six modes corresponds to more than 95% of the total system response.

The subfigures on the right in Fig. 13 show the first six global POMs and SOMs. POD decomposition shows that the first dominant POM in CF resembles a full sinusoidal shape (corresponding to the second structural mode) and the second dominant POM in CF resembles a half sinusoidal shape (corresponding to the first structural mode) for both increasing and decreasing flow speeds. This is unusual, since a frequency analysis of the response indicates that the system

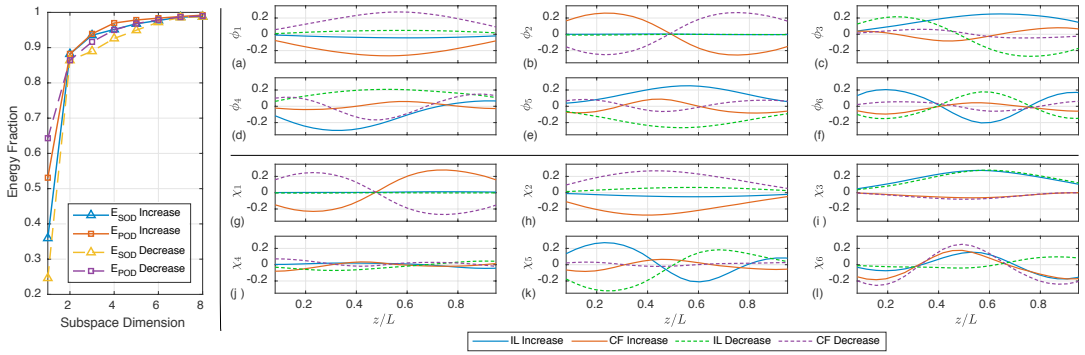

Figure 13: Left Plot: Motion energy fraction versus subspace dimension. Right Plots: First six dominant global SOMs and POMs for all tested reduced velocities: (a)–(f) show the SOMs, and (g)–(l) show the POMs.

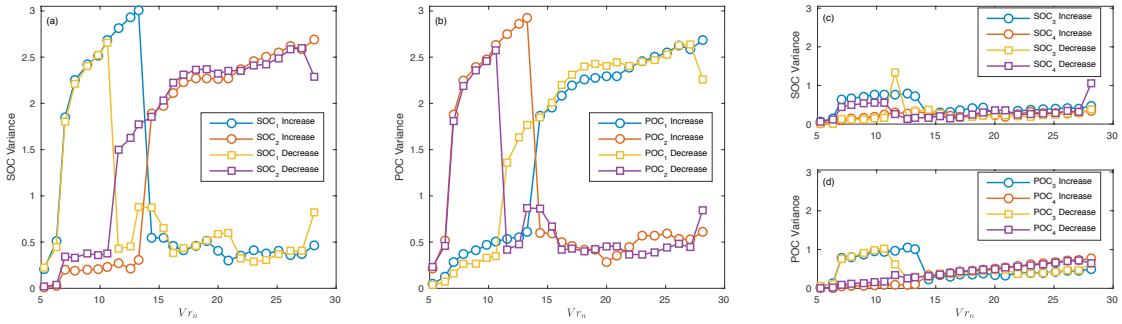

Figure 14: Frequency response function of first four dominant components as a function of nominal reduced velocity using SOD (a,c) and POD (b,d). (a-b) First two dominant components using SOD and POD. (c-d) Third and fourth dominant components using SOD and POD, respectively.

oscillates at a frequency near the fundamental natural frequency in the CF direction for low reduced velocities and transitions to a frequency near the second structural natural frequency as reduced velocity increases. In contrast, the order of the decomposed modes in SOD are more consistent with the order of the structural natural modes. For example, the first and second CF SOMs resemble the first and second structural natural modes, respectively. In both cases, the relative contribution of the IL motion is very small, and higher order POMs and SOMs demonstrate higher frequency components or asymmetrical structures that have significantly less energy content.

Figure 14 illustrates the decomposed frequency response functions as a func-

tion of nominal reduced velocity for the first four dominant modes using SOD (a,c) and POD (b,d). From SOD, as the nominal reduced velocity increases, the dominant first mode (Fig. 3(a), blue circles) variance increases until the reduced velocity of $Vr_n = 14$, where it suddenly drops below 0.5. When the flow velocity decreases, the first SOC amplitude stays near 0.5 until $Vr_n = 11$ (see Fig. 3(a); yellow squares), before jumping to a larger amplitude. This hysteresis loop associated with the first SOC mode reproduces a typical hardening spring frequency response behavior. In contrast, with increasing flow speed, the second dominant SOC amplitude (see Fig. 3(a); red circles) stays close to zero until the jump in amplitude at $Vr_n = 14$. For decreasing flow speeds a drop in amplitude of the second SOC (see Fig. 3(a); purple squares) is observed at $Vr_n = 11$. This hysteric behavior in the second SOC corresponds to a subcritical Hopf bifurcation type of structural response, where the system transitions from a stable point to a limit cycle. For both first and second modes, there is an unstable region in between the reduced velocities of 11 and 14, where depending on the increasing or decreasing flow speed, the system can experience two different responses. This is significant since this hysteresis is observed in the first two empirical modes of the system, but the type of nonlinear response is different depending on which mode is dominant. For the third and fourth SOCs (see Fig.14c), the amplitudes stay low and do not exhibit any hysteric behavior. However, there is small energy leakage from the first SOC to the third SOC when the flow speed is increased. In the present experiments, limitations of the experimental apparatus prevented observations of similar bifurcations that may occur for higher mode transitions since the flow speed did not reach high enough velocities to generate vortex shedding frequencies near the third structural mode in CF.

The POCs are also shown in Fig. 14(b,d) for both increasing and decreasing

flow speeds. The POD results are similar to SOD, however the ordering of the dominant modes are switched as mentioned previously. POD does still capture the same hysteric behavior of the first two modes; however, there is significant energy leakage from the second POC to the third for both increasing and decreasing speeds, leading to increased magnitude of the third mode. This energy leakage is also apparent in Fig. 13 where second and third POMs both resemble to a half sinusoidal shape, whereas second and third SOMs are distinctly different. This leakage is observed in the fourth mode as well, indicating that the POD method is not independently separating the physical CF response in the second mode from the other lower modes, which leads to the reordering of modes as compared with the SOD method. In addition, all the POD modes show gradual increase in the amplitude, while SOD modes do not for the third and higher modes. As a final remark, SOD method surprisingly captures a real physical characteristic of pedaling motion [15], which is the single peak in Fig.14(c); however, POD method is not able to capture this particular case. In this particular case, cylinder in IL and CF directions have the same frequency and both demonstrate a second mode shape.

3.5 Summary and Conclusion

The multivariate methods such as POD and SOD identify underlying nonlinear response behavior that is present in the tensioned flexible cylinder undergoing VIV. Different than local POD analysis, global multivariate analysis provides more insight into the physical dynamics underlying the overall response behavior as a function of frequency. For example, global SOD analysis clearly identifies bifurcations and the hysteretic region associated with those bifurcations in the first two modes, whereas global POD analysis cannot limit the corresponding bifurcation curves to just the first two dominant vibration modes, due to energy leakage into

high mode components. SOD is more suitable to define the hysteresis loops and the corresponding bifurcations in the current problem. In the present experimental study, where multiple structural modes are present, it was found that with increasing and decreasing flow speed, there is a significant bifurcation region which causes system to have different responses, dependent on which mode is excited, that may not be predicted using a standard structural modal analysis of the system. Being able to clearly identify unstable regions and the corresponding bifurcations is of utmost importance to the development of the reduced-order models capable of predicting these types of fluid-structure interactions.

List of References

[1] T. Sarpkaya, "A critical review of the intrinsic nature of vortex-induced vibrations," *Journal of Fluids and Structures*, vol. 19, no. 4, pp. 389–447, 2004.

[2] C. Williamson and R. Govardhan, "Vortex-induced vibrations," *Annu. Rev. Fluid Mech.*, vol. 36, pp. 413–455, 2004.

[3] P. Bearman, "Circular cylinder wakes and vortex-induced vibrations," *Journal of Fluids and Structures*, vol. 27, no. 5, pp. 648–658, 2011.

[4] J. Dahl, F. Hover, M. Triantafyllou, S. Dong, and G. Karniadakis, "Resonant vibrations of bluff bodies cause multi-vortex shedding," *Physical Review Letters*, vol. 99, no. 144503, 2007.

[5] R. Bourguet, G. Karniadakis, and M. Triantafyllou, "Vortex-induced vibrations of a long flexible cylinder in shear flow," *Journal of Fluid Mechanics*, vol. 677, pp. 342–382, 2011.

[6] J. Vandiver and J.-Y. Jong, "The relationship between in-line and cross-flow vortex-induced vibration of cylinders," *Journal of Fluids and Structures*, vol. 1, no. 4, pp. 381–399, 1987.

[7] H. Lie and K. Kaasen, "Modal analysis of measurements from a large-scale {VIV} model test of a riser in linearly sheared flow," *Journal of Fluids and Structures*, vol. 22, no. 4, pp. 557 – 575, 2006. [Online]. Available: http://www.sciencedirect.com/science/article/pii/S0889974606000077

[8] J. Vandiver, H. Marcollo, S. Swithenbank, V. Jhingran, *et al.*, "High mode number vortex-induced vibration field experiments," in *Offshore Technology Conference*. Offshore Technology Conference, 2005.

[9] J. K. Vandiver, V. Jaiswal, and V. Jhingran, "Insights on vortex-induced, traveling waves on long risers," *Journal of Fluids and Structures*, vol. 25, no. 4, pp. 641–653, 2009.

[10] F. Huera-Huarte and P. Bearman, "Wake structures and vortex-induced vibrations of a long flexible cylinderâ"part 1: Dynamic response," *Journal of Fluids and Structures*, vol. 25, no. 6, pp. 969 – 990, 2009. [Online]. Available: http://www.sciencedirect.com/science/article/pii/S0889974609000449

[11] E. Passano, C. M. Larsen, and J. Wu, "Viv of free spanning pipelines: Comparison of response from semi-empirical code to model tests," in *ASME 2010 29th International Conference on Ocean, Offshore and Arctic Engineering*. American Society of Mechanical Engineers, 2010, pp. 567–577.

[12] A. Trim, H. Braaten, H. Lie, and M. Tognarelli, "Experimental investigation of vortex-induced vibration of long marine risers," *Journal of fluids and structures*, vol. 21, no. 3, pp. 335–361, 2005.

[13] E. D. Gedikli and J. M. Dahl, "Mode shape variation for a low-mode number flexible cylinder subject to vortex-induced vibrations," in *ASME 2014 33rd International Conference on Ocean, Offshore and Arctic Engineering*. American Society of Mechanical Engineers, 2014, pp. V002T08A071–V002T08A071.

[14] D. Chelidze and W. Zhou, "Smooth orthogonal decomposition-based vibration mode identification," *Journal of Sound and Vibration*, vol. 292, no. 35, pp. 461 – 473, 2006. [Online]. Available: http://www.sciencedirect.com/science/article/pii/S0022460X05005948

[15] E. D. Gedikli and J. M. Dahl, "Mode excitation hysteresis of a flexible cylinder undergoing vortex-induced vibrations," *Journal of Fluids and Structures*, vol. 69, pp. 308 – 322, 2017. [Online]. Available: http://www.sciencedirect.com/science/article/pii/S0889974616303188

CHAPTER 4

Structural mode effects on bending dominated flexible cylinders undergoing vortex-induced vibrations

by

Ersegun Deniz Gedikli*, David Chelidze** and Jason Dahl*

*Department of Ocean Engineering, University of Rhode Island, Narragansett, RI 02882, USA

**Department of Mechanical, Industrial and Systems Engineering, University of Rhode Island, Kingston, RI, 02881, USA

To be submitted to Journal of Fluids and Structures

Abstract

The structural mode excitation of bending-dominated, flexible cylinders undergoing vortex-induced vibrations is investigated using multivariate analysis of the excited empirical modes. The response of the bending-dominated cylinders is compared with the response of a tension-dominated cylinder using the same analysis technique. Experiments were conducted in a recirculating flow channel with a uniform free stream with Reynolds numbers between 650 and 5500. Three bending-dominated cylinders were tested with varying stiffness in the cross-flow and in-line directions of the cylinder in order to produce varying structural mode shapes associated with a fixed 2:1 (in-line:cross-flow) natural frequency ratio. A fourth cylinder with natural frequency characteristics determined through applied axial tension was also tested. The spanwise in-line and cross-flow responses of the flexible cylinders were measured through motion tracking with high-speed cameras. Global smooth-orthogonal decomposition was applied to the spatio-temporal response for mode identification. Measured responses are compared with the analytic response of a beam subjected to a uniform periodic loading. Both the analytic and experimental results show that for excitation of low mode numbers, the cylinder is unlikely to oscillate with an even mode shape in the in-line direction due to the symmetric drag loading, even when the system is tuned to have an even mode at the expected frequency of vortex shedding. In addition, no mode shape changes were observed in the in-line direction unless a mode change occurs in the cross-flow direction, implying that the in-line response is a forced response dependent on the cross-flow response. An even mode oscillation (i.e. second mode) in the in-line direction is observed to be excited in the tensioned cylinder, however this is only observed in a hysteretic response region. The results confirm observations from previous field and laboratory experiments, while demonstrating how

structural mode shape is affected by vortex-induced vibrations.

4.1 Introduction

The vortex-induced vibration (VIV) of long, flexible structures is a complex problem due to the large number of variables that can contribute to the coupled response of the structure with the surrounding fluid [1]. While a significant number of experimental studies have been devoted to characterizing the fundamental fluid-structure interaction for an elastically mounted rigid circular cylinder undergoing vortex-induced vibrations [2, 1, 3, 4], the spanwise effects of flexible structures have been more difficult to quantify due to the complexity of additional variables associated with flexible, continuous systems that are capable of multi-modal responses.

In the single degree of freedom spring-mass-dashpot model for vortex-induced vibrations, the forcing function resulting from vortex shedding may be represented as a phase shifted harmonic function to the first order approximation [1]. Assuming a sinusoidal response to the system, one can show that the amplitude and frequency of a cylinder undergoing vortex-induced vibrations in purely cross-flow excitation are functions of the motion of the cylinder and the resulting forces acting on the cylinder in phase with the acceleration and velocity of the body. The force in phase with acceleration alters the effective mass of the system, while the fluid force in phase with velocity alters the effective damping of the system. Since these fluid force terms are functions of the motion of the body, the frequency at which the body oscillates may constantly change in time, however this frequency is often fairly constant when observed in laboratory experiments. Using integral quantities of the forces in phase with velocity and acceleration, one can consider the system to have an effective natural frequency that is dependent on the fluid force in phase with acceleration.

In contrast to a single degree of freedom system, the natural frequencies of a continuous system are not only related to the stiffness and mass of the physical structure, but also are dependent on the particular spanwise shape of the oscillating structure. For example, an infinite string contains an infinite number of natural frequencies with each frequency corresponding to a particular spanwise shape. In VIV, the relative motion of vortices shed from the structure in relation to the motion of the body determines the phasing and magnitude of forces exerted on the body, hence for a continuous structure, the particular shape of the structure oscillation must have an effect on the resulting forces exerted on the structure. If we model a continuous system undergoing VIV similar to the 1 DOF system undergoing VIV, this would imply that the mode shapes corresponding to particular natural frequencies of the structure must be excited when that natural frequency is excited (or slightly modified by the added mass). The problem with this assumption is that since the fluid forces are dependent on the body oscillation and vice versa, there is no guarantee that the resulting fluid forces will drive a motion that is consistent with the analytic structural mode shape in a vacuum. This paper attempts to systematically test the effects of vortex-induced vibrations on the expected modal response of a flexible body by tuning several beams to have specific frequency properties for specific structural mode shapes. The purpose of these experiments is to illustrate differences in the response of a flexible structure from an elastically-mounted rigid structure due to the spanwise excitation of the flexible structure. Comparisons are made with a bending-dominated structure and tension dominated structure, with the modal response analyzed empirically through multivariate analysis.

The complexity of the flow-induced vibration of flexible cylinders is evident in the variety in the types of responses that are observed for these types of struc-

tures. For instance, the flow-induced vibration of flexible structures may undergo complex three-dimensional vibrations, experiencing traveling waves [5] and chaotic motions [6]. Sarpkaya [7] discusses such complexities and effects of additional VIV parameters on the dynamic response. A variety of studies on marine risers [8, 9, 10, 11] have shown that long, flexible structures exhibit similar forcing from vortex shedding as that observed for rigid cylinders, where vortex shedding leads to an oscillating drag force with a dominant frequency that is twice the oscillating lift force frequency. The laboratory experiments conducted by Passano et al. [12], Huera-Huarte et al. [13] and field experiments conducted by Vandiver et al. [11], Vandiver and Jong [14] showed that for long flexible structures subjected to vortex-induced vibrations, it is possible to excite different modes in in-line and cross-flow directions separately, as observed from the frequency of the response and reconstructions of the spatial shape of the structure. In particular, Huera-Huarte et al. [13] examined very low mass ratios $\sim$1, where the response frequency can vary significantly due to forcing in phase with the acceleration of the body.

In an effort to model the effects of different modal excitations in flexible cylinders, Dahl et al. [15] investigated the effect of differing natural frequency ratios (in-line to cross-flow) on an elastically mounted rigid cylinder. The cylinder was allowed to oscillate both in cross-flow and in-line directions while the natural frequency in each direction was tuned with different values in an attempt to model a long structure excited with different structural modes in each direction. These experiments demonstrated response behaviors that consisted of preferred figure-eight type motions where the cylinder moves upstream at the top and bottom of its orbital motion, which can contribute to large third harmonic forcing of the structure in the lift direction [16]. Similar studies by Srinil et al. [17] and Kang and Jia [18] have demonstrated similar behaviors and expanded understanding of

frequency ratio effects on a rigid cylinder response for frequency ratios less than one, where tear drop shape motions may be observed with multifrequency excitation of the structure in the in-line direction. Dahl et al. [19] observed similar behaviors for rigid cylinders at supercritical Reynolds numbers.

In the studies of Dahl et al. [15] and Kang and Jia [18], the effect of natural frequency ratio is modeled by tuning natural frequencies on a rigid cylinder, hence the mode shape of the cylinder does not play a role in the excitation of the body. A problem persists; however, for a cylinder that may be excited with an odd mode cross-flow and an even mode in-line. For example, consider a tensioned infinitely long string, where the natural frequencies are multiples of a fundamental frequency. If the first mode of the structure is excited in the cross-flow direction and the second mode with twice the fundamental frequency is excited in the in-line direction, the anti-nodes of the second mode may move with a figure eight orbital pattern under the right flow conditions. However, since the mode shape in the in-line direction is a sine curve, the two anti-nodes must move in opposite directions, with one figure eight moving downstream at the top and bottom of the orbit (referred to as clockwise motion in the literature) and the other moving upstream at the top and bottom of the orbit (counter-clockwise motion). The observations from Dahl et al. [16], indicate that there is a natural preference for the figure eight to move upstream at the top and bottom of the orbit, so if these frequencies of the structure are truly excited, which anti-node, if any, will move with this motion?

In the present study, several low mode number flexible cylinders are designed and tested to understand the dynamic relationship between the cylinder's structural characteristics and the modal response. Assuming that one can control the modal response of a flexible cylinder by controlling the structural characteristics (this is a significant assumption since the fluid-structure interaction will inherently

change these effective properties), it is possible to excite the flexible cylinder with a particular mode shape. For example, in the present experiments, a long rectangular shaped beam (aluminum or plastic) with a particular cross-section and material characteristics is used to tune the structural mode characteristics, encouraging the cylinder to oscillate with a desired mode shape when the frequency of that particular mode shape is reached by anticipating the forcing frequency in the in-line direction to be twice the frequency in the cross-flow direction.

Under these conditions, one may expect a cylinder to oscillate with first mode shape (half sinusoidal) when it is excited with a forcing function at the first mode frequency, and second mode shape (full sinusoid) when it is excited with the second mode frequency; however, if the flow is uniform, can even modes (asymmetric modes) in the direction of fluid flow be truly excited? Vandiver and Jong [14] argues that these modes will not be excited due to the distribution of forcing function. If these even modes cannot be excited, what body motions will be observed and which frequencies will dominate the motion? The present paper aims to systematically understand this behavior through a set of experiments using specifically crafted model cylinders. Three different rectangular shaped plastic beams are designed and molded in the center of a flexible urethane cylinder in order to create three cylinders with specific structural mode shape properties with a fixed 2:1 frequency relation between the in-line and cross-flow directions. The cylinders are placed in a uniform flow to observe the resulting response over a range of reduced velocities. The results are compared with experiments for a tension-dominated system [20] (see Fig. 15a) in which the experimental setup is identical to the current system.

4.2 Methods

Experiments are conducted in a recirculating flow channel that is located at the University of Rhode Island's Narragansett Bay campus. The channel test sec-

tion is glass and also features a downstream viewing window, allowing for visual motion tracking of the test apparatus within the test section. Tests in the present study are conducted for flow speeds between 0.1-0.7 m/s, where free surface disturbances due to the operation of the flow channel are not observed.

Figure 15 shows an idealized schematic the test cylinders that are mounted across the viewing walls of the flow channel. Fig.15(a) shows the tension dominated cylinder and Fig.15(b) shows the second mode excitation of a bending dominated cylinder as an example response. Example cross-section of the beam is also illustrated in the same figure. In the sketch, T represents the applied tension and U represents the flow speed. Flow is uniform and moves from left to right.

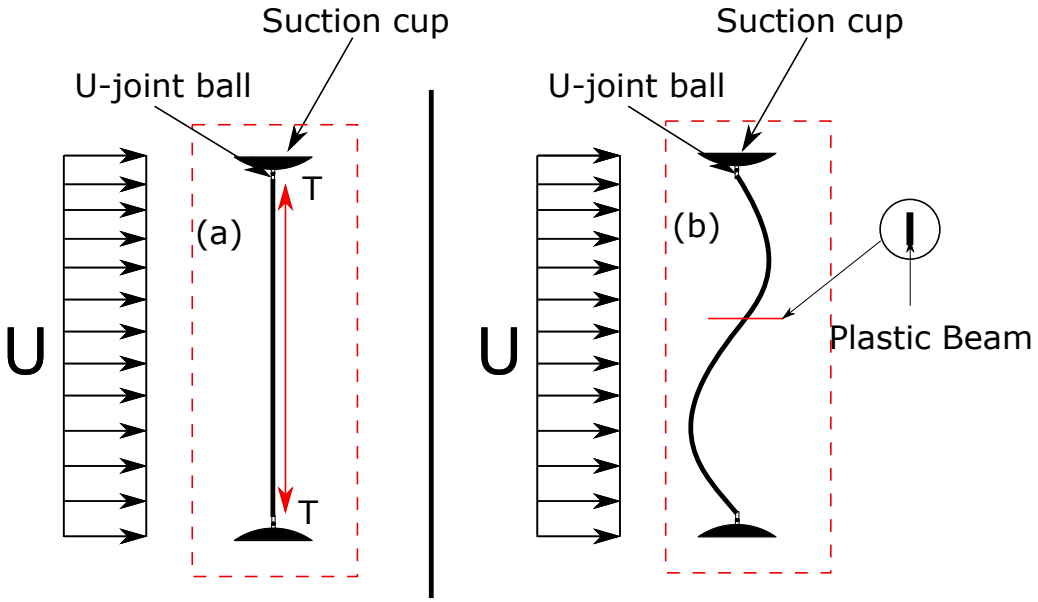

Figure 15: Top view of the flow channel. Idealized in-line even mode excitation for (a) tension [20] and (b) bending dominated cylinder under a symmetric loading. T is the initial tension applied both ends.

4.2.1 Test cylinders and Experimental Setup

Dahl et al. [19] showed that in combined in-line and cross-flow oscillations, in-line frequency of motion naturally adjusts to be twice the cross-flow frequency over a large of non-dimensional flow speeds. The motion of the body can be char-

acterized by a singular frequency in the cross-flow direction while the in-line has twice the cross-flow frequency. The beam characteristics in the present study were chosen so that there would be a 2:1 (in-line to cross-flow) structural natural frequency ratio between the structural mode shapes to be excited. This was achieved by varying the cross-sectional dimensions of a beam that was then molded inside a urethane cylinder. To investigate the effects of the combined in-line and cross-flow spatial modal response, the tuned structure's in-line mode shape is varied while keeping the cross-flow structural mode constant. In this case, cylinder 1 is tuned to have a first mode shape in the in-line direction and first mode shape in the cross-flow direction with an in-line natural frequency twice the cross-flow natural frequency. Cylinder 2 is tuned to have a first mode shape in the cross-flow direction and second mode shape in the in-line direction with the in-line natural frequency twice the cross-flow natural frequency. Similarly, cylinder 3 is tuned to have a first mode shape in cross-flow and a third mode shape in in-line with a 2:1 in-line:cross-flow natural frequency ratio as illustrated in Fig.16. Cylinder 4 is a tensioned rubber cylinder with no beam inside it with characteristics as described in Gedikli and Dahl [20].

Beam dimensions were chosen assuming a simply-supported tensioned beam with natural frequencies as below:

$$f_n = \sqrt{\frac{EI\pi^2 n^4}{4ML^4} + \frac{Tn^2}{4ML^2}} \tag{16}$$

where E is the elasticity modulus, I is the area moment of inertia, n is the mode number, M is the mass per unit length, and T is the initial tension applied. For cylinders 1-3, in the experiments, the applied tension is very small, and the second term in Eq.16 can be neglected such that:

$$f_n = \frac{\pi n^2}{2}\sqrt{\frac{EI}{ML^4}} \tag{17}$$

Beam modeling

In Eq. 17, E, L and M are roughly constant, n varies depending on the desired mode number, and I varies depending on the orientation of the beam with respect to incoming fluid flow. Therefore, the area moment of inertia in the in-line direction and cross-flow direction must be different to achieve the desired frequency characteristics of the beam. Using Eq.18, one can calculate the required beam sizes for a specific combination of modes. The calculated cylinder characteristics and dimensionless parameters are shown in Table 5 for each cylinder.

$$I = \frac{ML^4}{E}\left(\frac{4f_s^2}{\pi^2 n^4}\right), \text{ where } I \rightarrow \ I_x = \frac{bh^3}{12}, I_y = \frac{b^3 h}{12} \tag{18}$$

The ideal structural mode shapes for each cylinder with the corresponding beam orientation are shown in Figure 16.

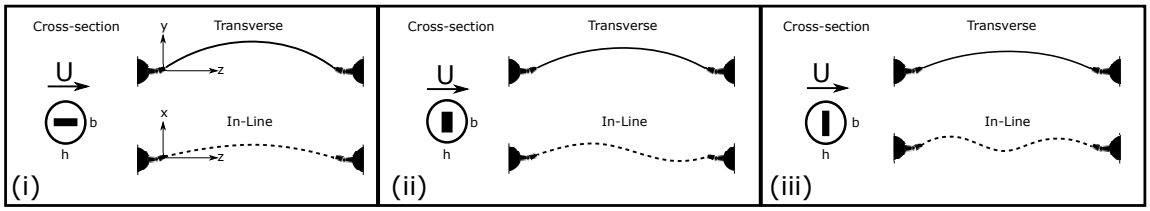

Figure 16: Idealized mode oscillations. (i) First mode in-line, first mode transverse, (ii) Second mode in-line, first mode transverse, (iii) Third mode in-line, first mode transverse. Flow is in the $x-$direction.

To mount the cylinder in the flow channel, a universal ball joint was attached to a suction cup on each end of the test cylinder. End-plates were mounted at the location of the u-joint in order to inhibit flow irregularities at the ends of the cylinder. The suction cups allowed the test cylinder to be mounted horizontally in the flow channel by mounting directly to the glass walls. The test cylinders

Table 5: Cylinder characteristics and dimensionless parameters.

Parameter (Abbrv., Unit)	Equation	Cylinder 1	Cylinder 2	Cylinder 3	Cylinder 4
Cylinder Type	-	Bending	Bending	Bending	Tension
Cylinder Material	-	Urethene	Urethene	Urethene	Neoprene
Beam Material	-	Plastic	Plastic	Plastic	None
Diameter (D, mm)	-	6.35	6.35	6.35	6.35
Cylinder Length (L, mm)	-	250	250	250	250
In-line beam width (h, mm)	-	1.27	2	2.25	None
Cross-flow beam width (b, mm)	-	2.5	0.04	0.508	None
Initial Tension (T, N)	-	-	-	-	0.15
Blockage Ratio (BR)	T/H	1.66	1.66	1.66	1.66
Aspect Ratio (AR)	L/D	41	41	41	41
Mass Ratio (m)	$4m/(\rho\pi LD^2)$	1.1	1.05	1.02	3.7
Reynolds Number (Re)	UD/ν	1500-5500	1700-5400	1600-4700	650-3500
Sampling frequency (f_{samp}, Hz)	-	250	250	250	250
In-line natural frequency (f_{IL}, Hz)	Mode 1	34	7	1.82	3
	Mode 2	136	28	7.3	6
	Mode 3	306	63	16.4	12
Cross-flow natural frequency (f_{CF}, Hz)	Mode 1	17	14	8.2	3
	Mode 2	68	56	32.8	6
	Mode 3	153	126	73.8	12

were aligned with respect to the still water free surface using a laser. Each test cylinder was marked with $23 - 25$ white dots, evenly distributed with spacings of 1 cm along the span. The cylinder motion was captured using two synchronized Phantom V10 high speed cameras at a frame rate of $250Hz$. Motion tracking software (ProAnalyst) was used to determine the displacement of each data point in the in-line and cross-flow directions. The program works based on sub-pixel accuracy where mean position of each data point is tracked with an error margin less than 1% in all directions. A more detailed description of the experimental setup and details of the motion tracking routine are documented in [20].

4.3 Amplitude Response

Fig. 17 shows the maximum RMS amplitude response for each tested cylinder as a function of the reduced velocity. In the figure, top image shows the cross-flow RMS response and the bottom image shows the in-line RMS response.

As seen in Fig.17, the tension dominated cylinder 4 (red diamond) was observed to have the highest cross-flow RMS amplitude response among all the cylinders tested, reaching a maximum amplitude at reduced velocity of 7.6, near the

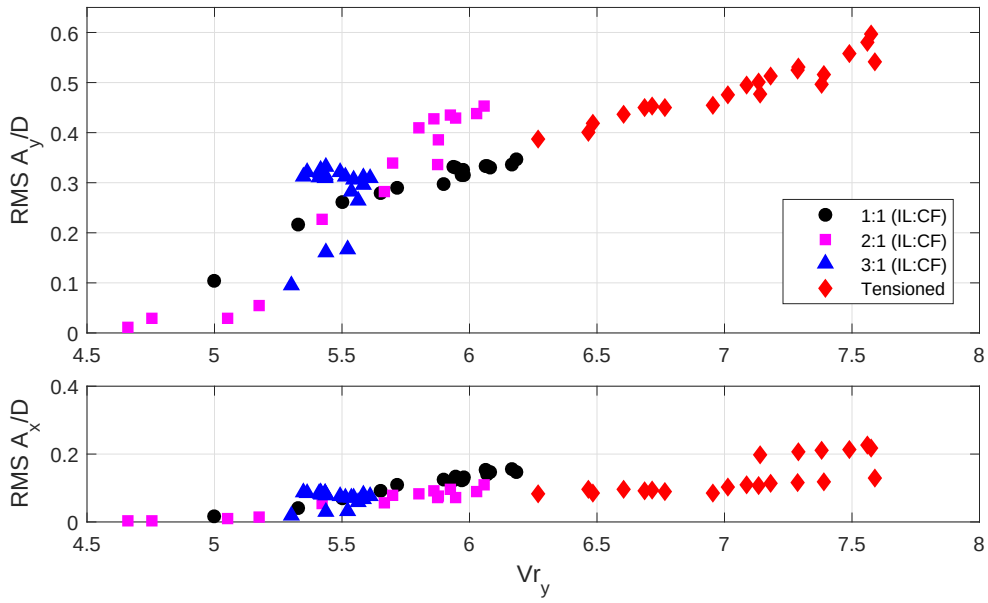

Figure 17: Maximum RMS amplitude response over the span as a function of reduced velocity. Colors indicate separate test cylinders. Black circle shows cylinder 1, purple square shows cylinder 2, blue triangle shows cylinder 3 and red diamond shows the tensioned cylinder (cylinder 4).

highest flow speed tested. Alternately, cylinder 1 (black circle) and cylinder 2 (purple square) reached maximum cross-flow RMS amplitude at reduced velocities of 6.3 and 6, respectively, over the same range of tested flow speeds. Although the tests were performed over a similar range of flow speeds with parameters tuned to achieve similar reduced velocities, cylinder 3 (blue triangle) was observed to oscillate in a very narrow band region between reduced velocity values of 5.3 and 5.65. The observed maxima in the response curves typically occur at the highest flow speeds, where additional tests could not be conducted at higher speeds due to limitations of the flow channel.

The in-line amplitude responses show similar trends to the cross-flow responses where cylinders 1 and 2 have increasing amplitude responses with increasing reduced velocity. However, unlike the cross-flow response, cylinder 1 reaches a higher amplitude response in the in-line direction than cylinder 2, opposite from the ob-

served cross-flow response. This is likely due to changes in phasing between the in-line and cross-flow responses due to the different frequency characteristics of the beams.

The cylinder 3 response consists of two distinct region of clustered points in the cross-flow response, indicating two separate types of response. One region lies in between the RMS amplitudes of 0.25 and 0.35. In this region, the cylinder oscillates with 2:1 (in-line:cross-flow) frequency ratio and has a typical figure eight type of response. The second region is apparent between the RMS amplitudes of 0.1 and 0.2. In this region, the cylinder oscillates with 1:1 (in-line:cross-flow) frequency ratio, and the response motion resembles a tear drop shape. These responses are discussed in more detail in subsequent sections.

The cylinder 4 response also consists of two response regions, with the regions more distinct in the in-line response for reduced velocities in between 7.2 and 7.7. Unlike cylinder 3, the two response regions in the motion of cylinder 4 is due to a mode transition and change in response along the span of the cylinder. Below a nominal reduced velocity of 7.2, the cylinder oscillates with a dominant first mode in both directions, and above the nominal reduced velocity of 7.2, the dominant first mode switches to second mode in cross-flow and to some combination of second and third mode in in-line.

4.4 Frequency Analysis

In this section, the normalized frequency response in the in-line and cross-flow directions are shown as a function of normalized reduced velocity for each cylinder.

The top two images in Fig.18 show frequencies for cylinder 1 and the bottom two images in Fig. 18 show frequencies for cylinder 2 in the cross-flow and in-line directions. In the cross-flow direction, the frequency analysis shows that he dominant frequency increases with flow speed and does not level off at the natural

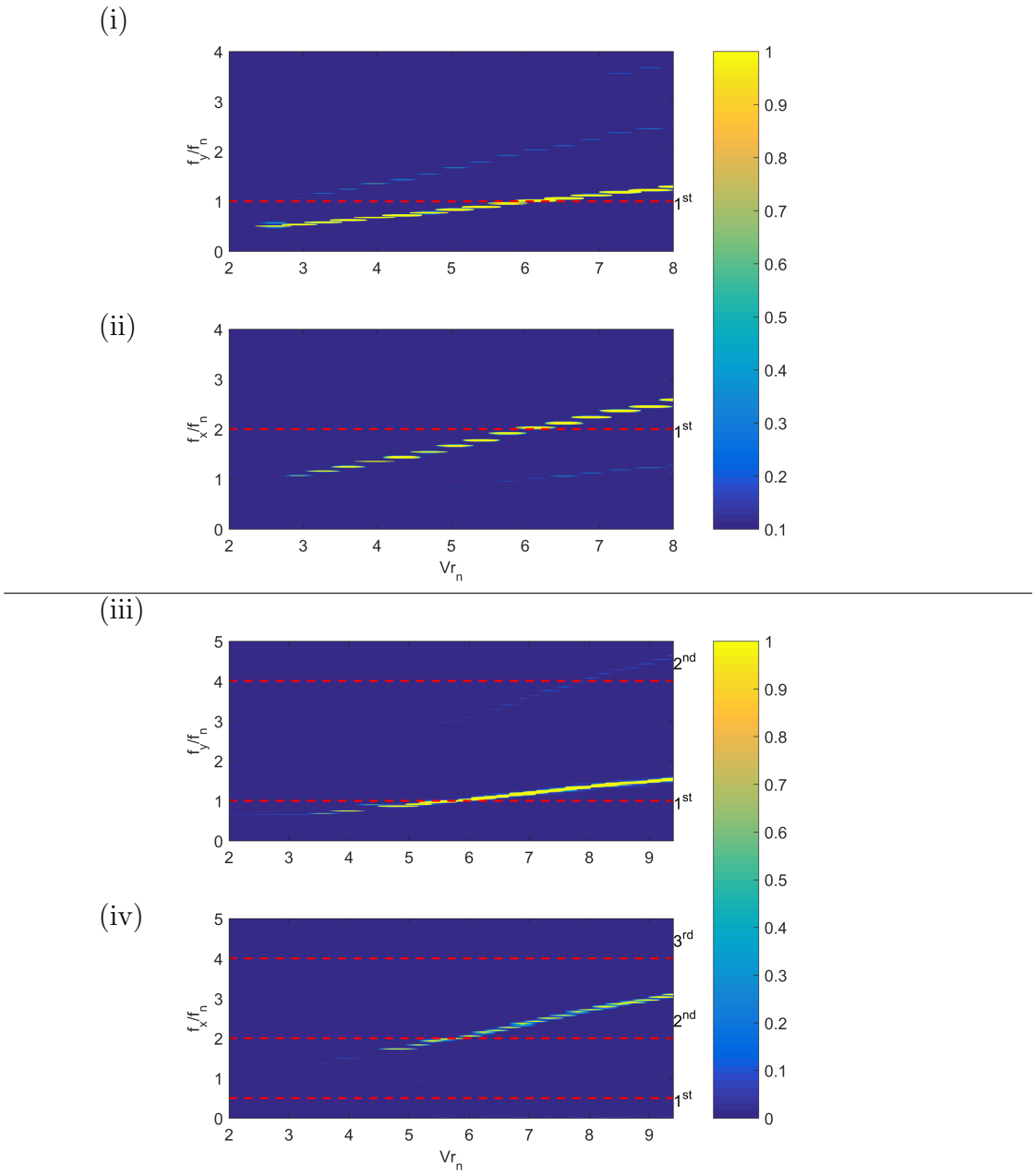

Figure 18: Frequency spectra as a function of nominal reduced velocity for cylinder 1 and cylinder 2. All spectra are normalized by the respective cylinder's fundamental frequency in the cross-flow direction. (i) Frequency response for cylinder 1 in cross-flow. (ii) Frequency response for cylinder 1 in in-line. (iii) Frequency response for cylinder 2 in cross-flow. (iv) Frequency response for cylinder 2 in in-line. Red dashed lines indicate the structural natural frequencies in the respective directions of each individual plot. Number indicator on right side of plot indicates which in-line or cross-flow structural mode is associated with that frequency.

frequency, consistent with observed responses for low mass ratio cylinders. In addition, there are second and third harmonic frequency components present. In the in-line direction, the dominant frequency is twice the frequency in the cross-flow direction for all the flow speeds tested, and there are lower frequency components present in the response at higher reduced velocities, which may come from bleeding of the frequency content from the cross-flow direction.

Similar to cylinder 1, the frequency content for cylinder 2 displays a 2:1 (in-line:cross-flow) dominant frequency ratio that is observed for all flow speeds tested. There is also higher harmonic frequency content present in the cross-flow direction at higher reduced velocity. Additional frequency content in the in-line direction is not observed for cylinder 2. It should be noted that, since all frequencies in Fig. 18 are normalized by the fundamental natural frequency in cross-flow, then frequencies can be compared directly across plots, such that the in-line frequencies are typically observed to be twice the cross-flow frequency. Dotted lines indicate the structural natural frequencies that were tuned for each cylinder in order to achieve desired structural mode shapes with specific frequency combinations. For the cylinder responding with frequency content near a particular dashed line, one may expect the cylinder to take on the particular structural mode shape associated with that frequency; however, multivariate analysis of the spatial response of the cylinders will show that this is not the case, despite the clear presence of a 2:1 frequency relationship between the in-line and cross-flow directions for both of these cylinders.

Figure 19 shows the cylinder 3 (top two images) and cylinder 4 (bottom two images) frequency content in the in-line and cross-flow directions normalized by the cross-flow fundamental natural frequency. Similar to cylinder 1 and cylinder 2, the dominant frequency for cylinder 3 in the cross-flow direction increases as the flow

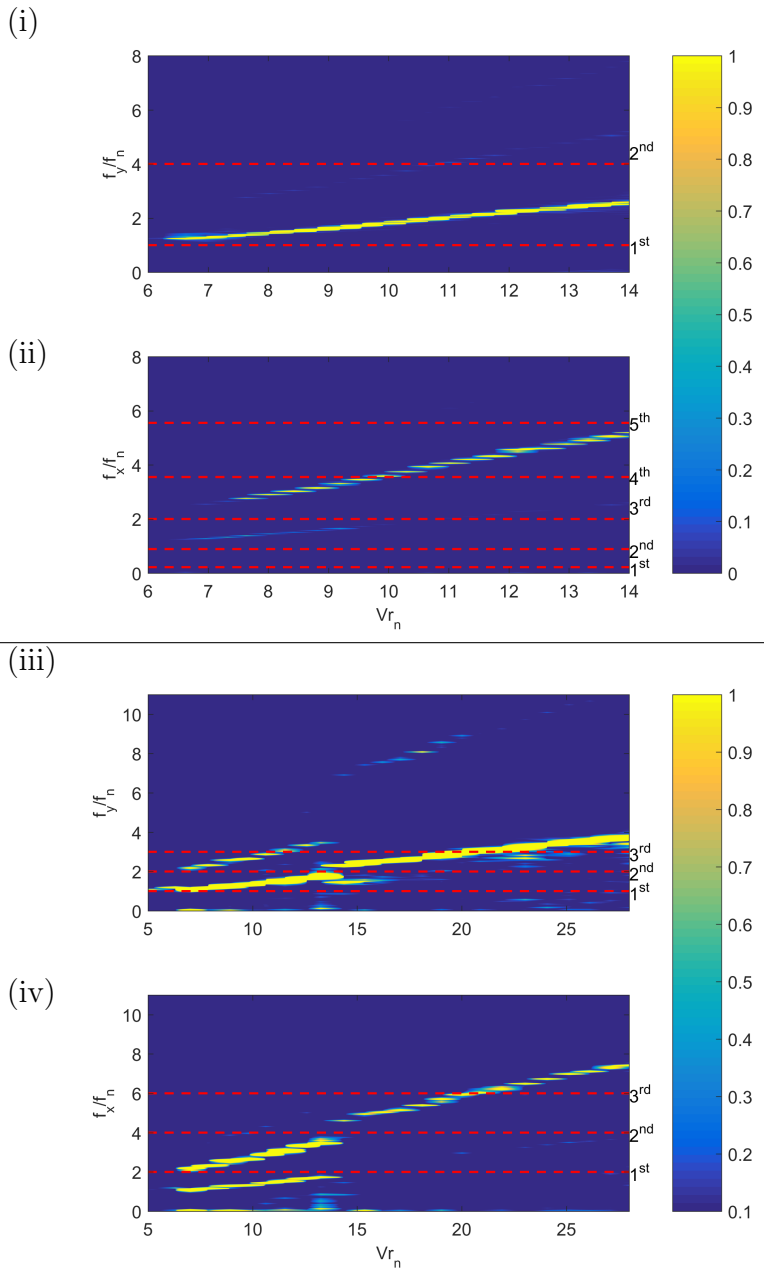

Figure 19: Frequency spectra as a function of nominal reduced velocity for cylinder 3 and cylinder 4. All spectra are normalized by the respective cylinder's fundamental frequency in the cross-flow direction. (i) Frequency response for cylinder 3 in cross-flow. (ii) Frequency response for cylinder 3 in in-line. (iii) Frequency response for cylinder 4 in cross-flow. (iv) Frequency response for cylinder 4 in in-line. Red dashed lines indicate the structural natural frequencies in the respective directions of each individual plot. Number indicator on right side of plot indicates which in-line or cross-flow structural mode is associated with that frequency.

speed increases without leveling at the structural natural frequency due to the low mass ratio. Additionally, there are some higher harmonic frequency components present, although they are not particularly strong in the cross-flow direction. In the in-line direction, at very low reduced velocity, the dominant frequency is equal to the frequency in cross-flow up to the nominal reduced velocity of 7.3. For higher reduced velocities, the dominant in-line frequency becomes twice the cross-flow frequency. It should be noted that cylinder 3 was designed with the intention of exciting the third structural mode shape in the in-line direction and first structural mode in the cross-flow direction. In the in-line direction, the dominant frequency is never observed to take the third -in-line mode value (at two times the cross-flow first mode value) where frequency jumps over third mode as flow speed increased. The system avoids oscillating at this frequency as clearly seen in the frequency jump that occurs at nominal reduced velocity of 7.3. Instead, the system oscillates with a lower frequency in the in-line direction, then switches to a higher frequency, avoiding the third mode altogether. This illustrates the significance of specific in-line and cross-flow mode combinations, as complex interactions between the wake and structure can significantly alter the expected response of the system.

The bottom two images in Fig.19 show the frequency spectra for cylinder 4 (tensioned cylinder) which is based on the displacement data from [20]. In contrast to the three bending dominated cylinders, cylinder 4 shows significant regions with multi-frequency content. Additionally, it should be noted that the tested range of reduced velocities for this cylinder was much larger due to the lower natural frequencies, hence a larger region of the frequency response is shown. In particular, cylinder 4 displays first and second mode frequency components at the same time up to the nominal reduced velocity of 14, where the in-line and cross-flow excitation frequencies start to get close to the second structural mode frequencies. Above a

reduced velocity value of 14, the cylinder displays different response characteristics due to a mode change in the cross-flow direction, this is accompanied by a distinct change in the excitation frequencies, where a jump occurs in the in-line direction.

4.4.1 Dynamic response relationship between in-line and cross-flow

To gain a more complete understanding of the total cylinder response, the in-line and cross-flow spanwise response, phase angle between in-line and cross-flow along the span, center point frequencies, and center point Lissajous figures are given for selected reduced velocities of each cylinder. Phase angle distribution was calculated using the inner product method as described in Gedikli and Dahl [20].

Cylinder 1

In this case, the test cylinder was tuned to attempt to excite the first structural mode in both directions (in-line and cross-flow) under a 2:1 (in-line:cross-flow) excitation frequency.

The frequency response in Fig.18 showed that cylinder 1 vibrates near the frequency associated with the fundamental modes in both directions. Two separate flow speed cases are selected to expand on characterizing the dynamic response of the cylinder. $Vr_n = 4.6$ is chosen as the observed response frequencies lie below the structural first mode frequency and $Vr_n = 6.8$ is chosen as the observed response frequencies lie above the structural first mode frequency, as indicated with the dotted line in Fig. 18. The spanwise response and Lissajous figures for the center points are shown in Fig. 20 for both of these cases.

As expected, the cylinder oscillates with a shape similar to a dominant first mode in both in-line and cross-flow directions. In these cases, the Lissajous figure at the center point is similar to a figure eight shape with a phase angle close to zero at the center point of the cylinder, with slight changes to the phase as one

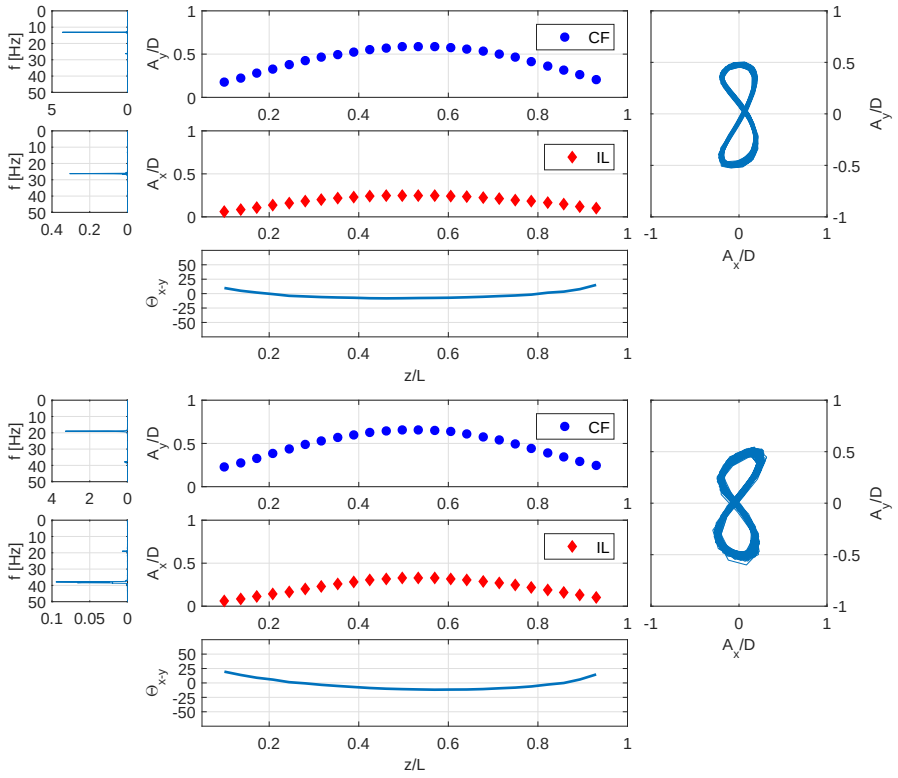

Figure 20: Spanwise response of cylinder 1, showing the frequency spectrum for the center point in cross-flow and in-line directions, the maximum spanwise response in the cross-flow and in-line directions, the computed phase between in-line and cross-flow motions, and the Lissajous figure of the center point. Top image: $Vr_n = 4.6$. Bottom image:$Vr_n = 6.8$.

moves outwards from the center. The figure eight orbital motion of the cylinder is consistent with the type of motion observed for rigid elastically mounted cylinders [15]. This is an expected observation, since the excited spanwise mode shape in the in-line direction was tuned to be the same as in the cross-flow direction in this case.

Cylinder 2

In this case, cylinder 2 was tuned to attempt to excite the first structural mode shape in the cross-flow direction and the second structural mode shape in the in-line direction under a 2:1 (in-line:cross-flow) excitation frequency. Based on Fig.18, the frequencies of the cylinder response lie very close to the structural mode

frequencies that the system was tuned to oscillate near. It was expected that the system would therefore oscillate with a first mode shape in the cross-flow direction and a second mode shape in the in-line direction. $Vr_n = 5.6$ and $Vr_n = 8.6$ are chosen as example points in Fig. 21 to demonstrate the spanwise response when the oscillation frequency was below or above the tuned structural frequency.

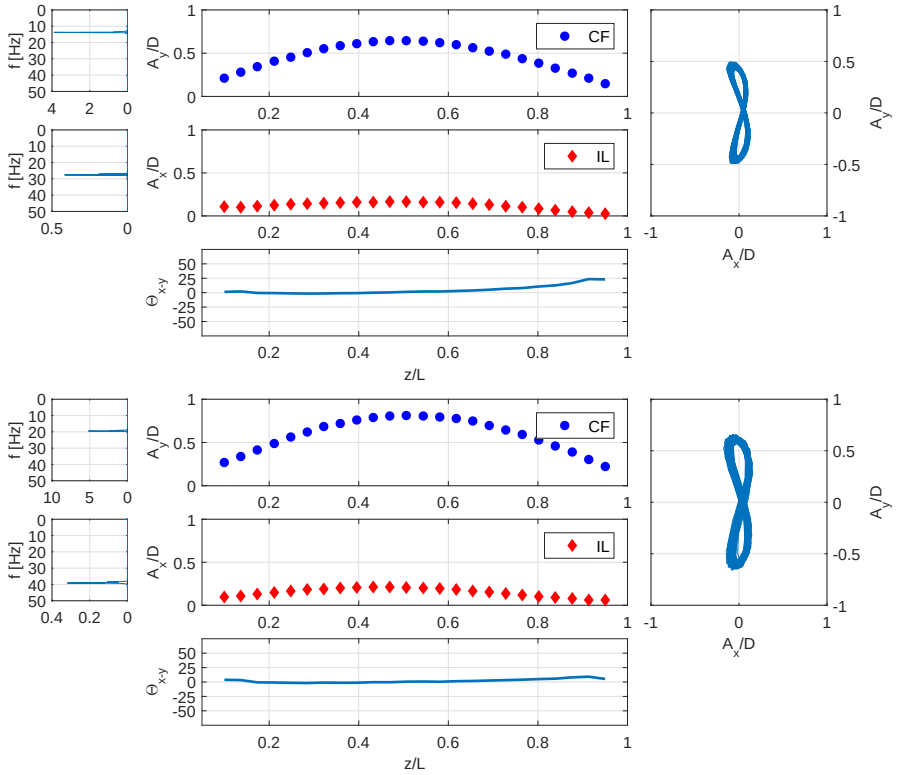

Figure 21: Spanwise response of cylinder 1, showing the frequency spectrum for the center point in cross-flow and in-line directions, the maximum spanwise response in the cross-flow and in-line directions, the computed phase between in-line and cross-flow motions, and the Lissajous figure of the center point. Top image: $Vr_n = 5.6$. Bottom image:$Vr_n = 8.6$.

The sets of images in Fig. 21 show the spanwise response of cylinder 2 at $Vr_n = 5.6$ and $Vr_n = 8.6$ along with the Lissajous figures at the center point. At these flow speeds, a 2:1 oscillation frequency ratio is observed between in-line and cross-flow motion, as evident in the curved figure eight Lissajous figures. The phase between in-line and cross-flow motion is observed to be near zero in both cases.

Of note, is that although the cylinder is excited with a first mode in the cross-flow direction as expected, the response in the in-line direction is different than anticipated. Although the frequency of the response in the in-line direction is twice the frequency of the cross-flow direction, the spanwise shape of the response in the in-line direction is primarily a first mode type shape, with only slight asymmetries near the end points. In these cases, the mean deflection of the cylinder due to drag has been removed, such that these responses only show the magnitude of the oscillation in the in-line direction.

This behavior was observed to be consistent for all reduced velocities tested, such that the in-line response of cylinder 2 was never observed to take on a second mode shape. Since higher speeds could not be tested, it is unclear if this behavior would hold at speeds where the second mode in the cross-flow direction begins to be excited. It is important to not, however that based on this case, representing vortex-induced vibrations as a resonant vibration occurring separately in the in-line and cross-flow directions would be incorrect, since the second structural mode shape is not excited. Instead, it appears the the cylinder undergoes a forced in-line motion, which happens to occur near the second mode natural frequency, but due to the spanwise uniform loading of the cylinder in drag, the second mode shape is not excited. This observation is consistent with observations by Vandiver and Jong [14] where a similar behavior was observed in the field testing of a long cable in a uniform current.

Cylinder 3

In this case, cylinder 3 was tuned to attempt to excite the first structural mode shape in the cross-flow direction and the third structural mode shape in the in-line direction under a 2:1 (in-line:cross-flow) excitation frequency. Since it was found with cylinder 2 that an asymmetric second mode could not be excited

under the experimental conditions, it was hypothesized that by tuning the in-line direction to be excited with a higher odd mode shape, the system may respond with an excitation resembling the structure natural modes. Analytic modeling of the structural characteristics for cylinder 3 indicated that the cylinder may pass through modes up to the fourth structural mode in-line while still exciting the cross-flow direction with frequencies close to the first mode frequency.

Figure 22 shows the spanwise response of cylinder 3 at three different normalized reduced velocity values, $Vr_n = 7.3$, $Vr_n = 8.4$, and $Vr_n = 14.1$. The lowest reduced velocity is in a region, as indicated by Fig. 22, where the response frequency in the in-line direction is equal to the frequency in the cross-flow direction. The other two cases show the response just after the dominant frequency in the in-line direction switches and the response at the highest reduced velocity tested.

The top image for Fig. 22 shows the response at $Vr_n = 7.32$ where the in-line and cross-flow response frequencies are equal. The Lissajous figure in this case shows a squished tear drop shape response, where the in-line motion is slightly larger at the bottom of the orbit than at the top. This type of asymmetric response has been observed previously in experiments on elastically mounted rigid cylinders, where the in-line natural frequency is tuned to have a frequency lower than the cross-flow natural frequency [18]. Based on the relation between the natural frequencies of the cylinder in the in-line direction, the frequency of oscillation for this case ends up being closest to the second mode frequency in the in-line direction, which is equal to the first mode frequency in the cross-flow direction. This results in a response with frequencies being the same in both directions, although the second spanwise mode shape is not excited in the in-line direction.

The middle image in Fig. 22 shows the spanwise response of cylinder 3 at nominal reduced velocity of 8.43 where the cylinder has transitioned to oscillate

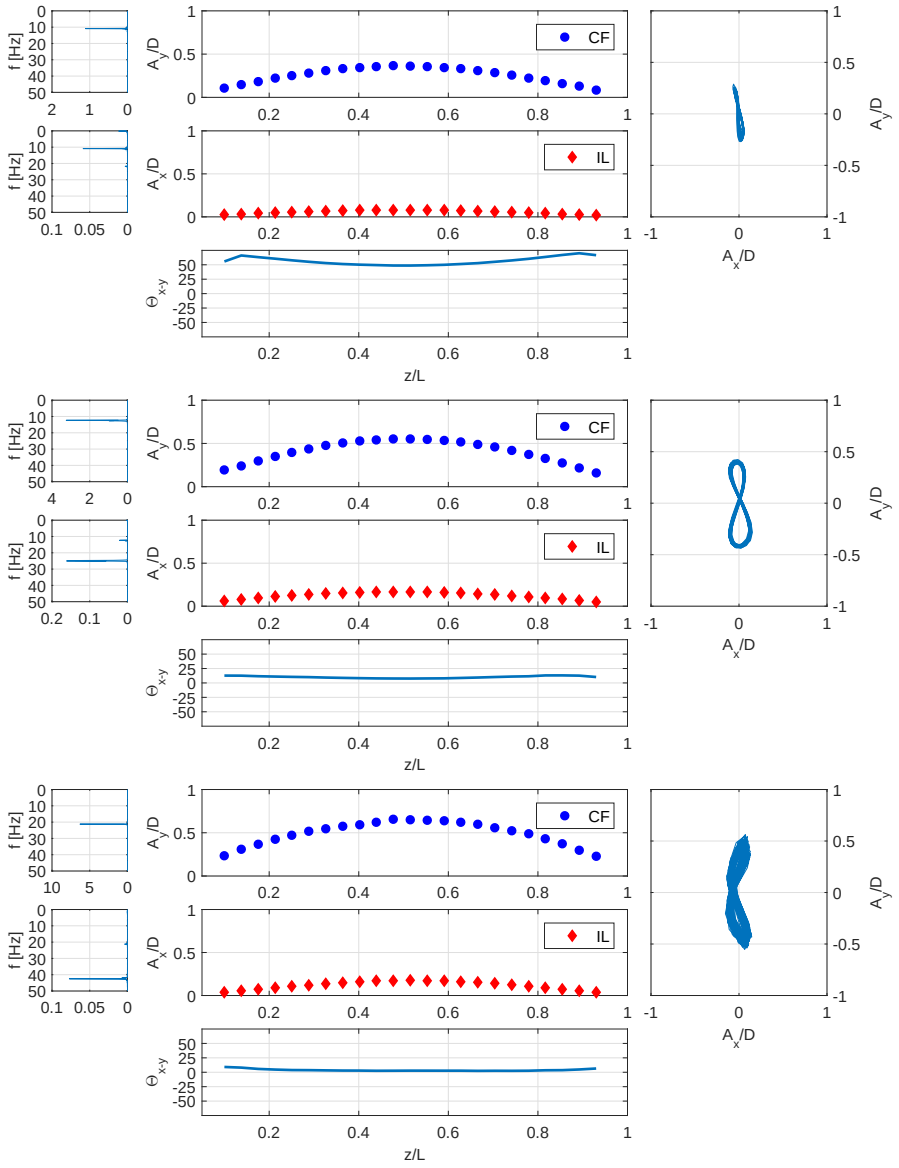

Figure 22: Spanwise response of cylinder 3, showing the frequency spectrum for the center point in cross-flow and in-line directions, the maximum spanwise response in the cross-flow and in-line directions, the computed phase between in-line and cross-flow motions, and the Lissajous figure of the center point. Top image: $Vr_n = 7.3$. Middle image: $Vr_n = 8.4$. Bottom image:$Vr_n = 14.1$.

with a 2:1(in-line:cross-flow) frequency relation. Figure 19 shows that cylinder oscillates with a frequency closest to the third mode in the in-line direction and a frequency closest to the first mode in the cross-flow direction at this reduced velocity. Similar to cylinder 2, the expected frequency relation is achieved in exciting

the response of the cylinder, but again, the spanwise response of the cylinder does not follow the structural mode shape if the system were undergoing resonance at these frequencies. The cylinder again displays a spanwise shape similar to a half sine in both the in-line and cross-flow directions, rather than having a third mode shape in the in-line direction.

The bottom image in Fig.22 shows the spanwise response of cylinder 3 at nominal reduced velocity of 14.1. This case is similar to the previous case, demonstrating a 2:1 frequency relation between the in-line and cross-flow motion, but a half sinusoid spanwise shape. The resulting cross-flow frequency for this reduced velocity is directly between the first and second mode frequencies of the structure. If higher flow speed tests were possible with this setup, it is anticipated that the second mode of the structure in the cross-flow direction would be excited with the fifth mode in-line being the closest structural mode to the in-line excitation frequency. With the relatively short span cylinder tested and optical motion tracking techniques, higher mode excitation of the cylinder is not observed based on observation, so multivariate analysis techniques are employed to quantify the empirical mode excitation of the structure.

Cylinder 4 - Tensioned cylinder

Figure 23 shows the spanwise response of cylinder 4 for the increased flow speed experiments that are the same as in [20]. The top image in Fig.23 shows the response at $Vr_n = 10.65$ and bottom image shows the response at $Vr_n = 18.1$. These two reduced velocity values were selected based on the frequency response shown in Fig.19 where at $Vr_n = 10.65$, the test cylinder oscillates with two dominant frequencies in both the in-line and cross-flow directions. The multiple dominant frequencies observed for this case are the same in both the in-line and cross-flow directions and are partly a function of the slight asymmetry in the

response of the cylinder, as evident in the Lissajous figure. The spanwise response in both in-line and cross-flow directions demonstrate a first mode shape based on simple observation of the magnitude fo the spanwise response, although some asymmetry does exist over the span. Since the dominant frequencies at these flow speeds lie closest to the first mode of the structure in the cross-flow direction, it is expected that the spanwise shape in the cross-flow direction resembles a first mode, however, similar to cylinder 2, the frequency in the in-line direction lies closest to the second mode, yet the spanwise shape does not strongly demonstrate a second mode shape.

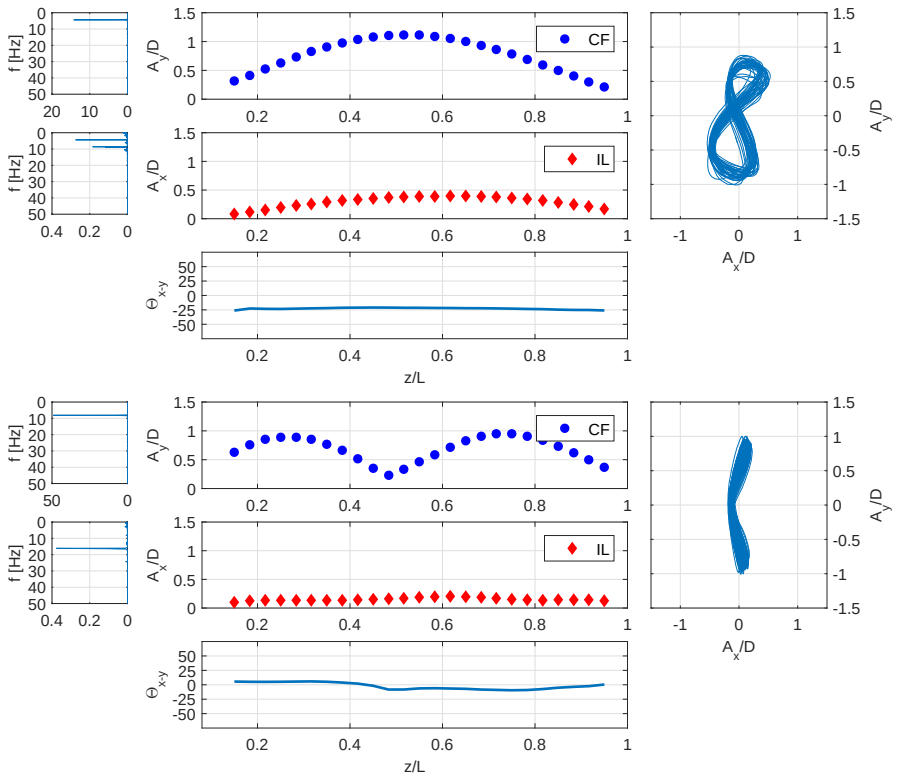

Figure 23: Dynamic response of cylinder 4. Top image: Dynamic response at $Vr_n = 10.65$. Bottom image: Dynamic response at $Vr_n = 18.11$

The bottom image from Fig.23 shows the spanwise response for cylinder 4 at $Vr_n = 18.1$. At this flow speed, the excitation frequency in the cross-flow direction is close to the second mode structural natural frequency and the response

in the cross-flow direction has changed to resembling a second mode shape in the cross-flow direction. The response in the in-line direction appears to have second and third mode components based on the shape of the response, despite a single dominant frequency for the response. Multivariate analysis is used to further elucidate the modal excitation of the structure based on empirical modes.

One important observation from all the cylinders tested, is that even though cylinder has a frequency that may correspond to a higher structural mode in the in-line direction (second mode for example), if there is no change in the cross-flow spanwise mode as flow speed is increased or if the response of the structure is at a frequency that is closest to the first mode frequency, there is no observed spanwise mode shape change in the in-line direction. For example, as with cylinder 4, a change in the shape of the in-line direction response is only observed after the cross-flow motion has undergone a spanwise mode shape change due to excitation of a higher structural mode. These results are only observed for the low mode number flexible cylinders that are tested in the current experiments, however care has been taken to maintain a uniform current and uniform loading of the structure in the flow channel by performing the experiments horizontally in the flow channel. Vertical orientation of the cylinder could introduce asymmetries to the loading through gravitational effects or effects of the free surface.

In addition to higher modes in the in-line direction being delayed based on the mode excitation in the cross-flow direction, the present experiments show that it is difficult to excite asymmetric mode shapes in the in-line direction under a uniform current loading, although asymmetric mode shapes can be excited in the cross-flow direction. It is not possible to claim that this observation is true under all flow conditions, especially since slight asymmetries to an experiment or typical asymmetries that may exist in a field experiment could possibly excite asymmetric

modes.

These findings are based primarily on analysis of the observed maximum response over the span. In order to further understand which dominant modes are excited, particularly in the in-line direction, it is necessary to decompose the observed responses into dominant empirical modes hence one may clearly see the contribution of each mode in the total response. Empirical modes are chosen to characterize the spanwise response of the cylinders in order to avoid requiring particular mode shapes for a phenomenon that is well known to be nonlinear. For this purpose, the recently developed smooth orthogonal decomposition (SOD) is used to characterize the modal response of the different cylinders.

4.5 Multivariate analysis - SOD based VIV mode analysis

Proper orthogonal decomposition (POD) has been widely used in structural vibration modal identification and is shown to converge to the actual vibration modes if the mass distribution in the linear dynamical systems is uniform (i.e., when structural modes form an orthogonal basis for the linear system's phase space) as shown by Feeny and Kappagantu [21]. Alternatively, if the actual mass matrix is known, POD can identify the true vibration modes by premultiplying the motion data by the mass matrix. Due to the uniform distribution of the measurement dots along the beam, the mass distribution of the corresponding discrete system is expected to be uniform in the air (i.e., one expects a uniform diagonal mass matrix). However, when placed in a fluid, the mass matrix is no longer uniform or constant due to the spanwise added mass effect, and the structural modes are no longer expected to form an orthogonal basis. In contrast, Chelidze and Zhou [22] showed that smooth orthogonal decomposition (SOD) does not require the knowledge of mass distribution to converge to the actual vibration modes and is expected to be better at resolving structural modes responsible for the fluid

structure interaction.

The main difference of such multivariate methods than traditional Fourier based mode decomposition is that Fourier based mode decomposition assumes a base modal shape. The empirical multivariate methods used in the present paper do not require any prior knowledge of the mode shape as an input parameter. The resulting empirically determined mode shapes may be similar to a sinusoidal mode shape depending on the loading of the cylinder and for highly non-linear systems, such as low mode number flexible cylinders with multiple excited modes, these methods can be advantageous for identifying the dominant empirical modes.

Previously, Gedikli and Dahl [20] applied local POD analysis and Gedikli et al. [23] applied global POD and SOD to a similar VIV dataset, comparing the results of these two techniques on the analysis of a flexible cylinder undergoing VIV. In the local analysis [20], the POD method was applied to individual cylinder responses to obtain empirical mode shapes for each individual reduced velocity values. In the global analysis [23], the method is applied to all cylinder time histories over all reduced velocities, creating one large input data matrix, to obtain a single global response describing the system modes. In both studies, the methods identified the cylinder's most dominant empirically determined mode shapes; however, Gedikli et al. [23] showed that by applying the global SOD method, the proper ordering of empirical modes based on energy content could be achieved. Therefore, this study applies the global SOD method for empirical modal analysis of the cylinders.

4.5.1 Description of smooth orthogonal decomposition (SOD)

In the SOD method, the displacement data matrix, X, is constructed from all the experimentally measured time histories from the cross-flow and in-line measurements. $X \in R^{m \times 2n}$, where X is the combined in-line and cross-flow data matrix, m is the number of total time samples, and n is the number of points recorded

along the span of the cylinder. Using the forward difference method, one can construct a new data matrix $V = DX \in R^{m\times 2n}$ which includes in-line and cross-flow velocities. With the new velocity data matrix, the phase space representation of the total response can be obtained as $Y = [X, V] \in R^{n\times 4n}$.

SOD identifies the subspaces (ψ) where the scalar field projection $q = Y\psi$ is maximally smooth, while having maximal variance. As explained in Gedikli et al. [23], if one defines the smoothness of the projection as

$$h(\psi; k) = \frac{1}{M}(D^k Y\psi)^T D^k Y\psi \tag{19}$$

where D^k is the k^{th} order derivative matrix based on forward difference ($k = 3$ for this application), SOD translates into the following optimization problem:

$$\max_{\psi} q(\psi)^T q(\psi) = \max_{\psi} (Y\psi)^T Y\psi, \tag{20}$$

subject to

$$\min_{\psi} \left(D^k q(\psi)\right)^T D^k q(\psi) = \min_{\psi} \left(D^k Y\psi\right)^T D^k Y\psi\,. \tag{21}$$

The corresponding SOD problem can be solved by generalized singular value decomposition:

$$Y = UC\Phi^T = Q\Phi^T, \quad D^k Y = ZS\Phi^T = D^k Q\Phi^T\,, \tag{22}$$

where U and Z are unitary matrices; C and S are diagonal matrices; columns of the square matrix Φ contain smooth orthogonal modes (SOMs); columns of $Q = UC$ are smooth orthogonal coordinates (SOCs); $\lambda_i = C_{ii}/S_{ii}$ are smooth orthogonal values (SOVs); and $\Psi = \Phi^{-T}$ are smooth projective modes (SPMs) that form a bi-orthogonal set with SOMs.

4.5.2 Energy contribution and empirical VIV modes

In section 4.4, Fig.18 and Fig.19 showed the frequency responses of the test cylinders and frequency values for the desired mode shapes. Later in section 4.4.1, it is shown that, for test cylinder 1, designed mode shape and frequency value matches very well. However, preliminary results showed that same is not true for the other test cylinders.

In order to see the contribution of each VIV modes to total response and identify the higher order empirical modes which may correspond to higher order frequencies, we use SOD method. The main question here is: Is it possible that a multivariate analysis method such as SOD can capture the desired modal responses in a higher dimension? To understand this, the following procedure is followed: First, designed mode change in in-line is identified for each test cylinder (red dashed lines in Figures 18 and 19) except cylinder 1 because no mode change was predicted for cylinder 1. For cylinder 2,3 and 4, the mode change should occur at $Vr_n = 5.5$, $Vr_n = 9.5$, and $Vr_n = 15$, respectively. So, to see if the SOD method is going to capture these desired mode responses in a higher dimension for these cylinders, we need to separate each of the frequency response plots (in-line and cross-flow) into two parts: part (a) and part (b) so that part (a) will include the response before the mode change, and part (b) will include the response after the mode change. As an example, part (a) for cylinder 2 will include all the reduced velocities up to 5.5 where first mode shape is expected and part (b) will include the remaining reduced velocities, 5.5 and above where second mode in the in-line and first mode in cross-flow is expected. Frequency response plots show that there is also higher order frequency content which leaks to the second mode (see Fig.18). So, when SOD method is applied to these two separate parts, we can obtain so-called smooth orthogonal modes (SOMs) and match them with the required frequencies. Here,

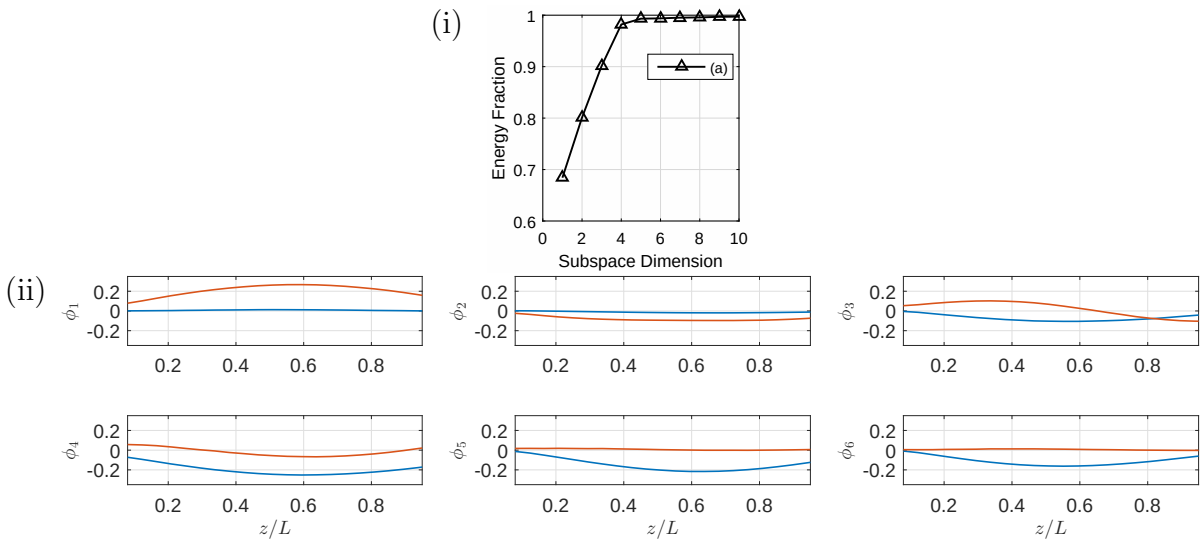

Figure 24: (i) Energy fraction in first 10 subspace dimensions, (ii) First 6 SOMs for cylinder 1 where input data matrix includes the dataset for all the reduced velocities tested. Red is cross-flow, blue is in-line.

the only remaining question would be at which subspace dimension we can achieve this goal. These SOMs are different than the vibration mode shapes where it is traditionally defined using sinusoidal shapes, but due to the nature of the system, the resulting SOMs should have a sinusoidal shape as well.

Figure 24 shows the energy fraction and first 6 subspace dimension of cylinder 1's modal response after SOD method is applied. Fig.24 (i) shows that first four modes make 99 % of the total oscillation and Fig.24 (ii) shows first 6 SOMs. First two dominant SOMs in cross-flow is similar to first mode shape and there is almost no in-line motion. Also, combination of first two modes constitute around 80% of the total oscillation. Third dominant mode consists of second mode in cross-flow and first mode in in-line, and contribution of combined in-line and cross-flow mode is around 10%. Fourth dominant mode is similar to first mode in both directions with %9 of the total energy. Fifth and sixth mode make less than 1% of the total oscillation, therefore modes higher than fourth mode have very little effect on the motion in terms of reconstructing the total motion with lower dimensions.

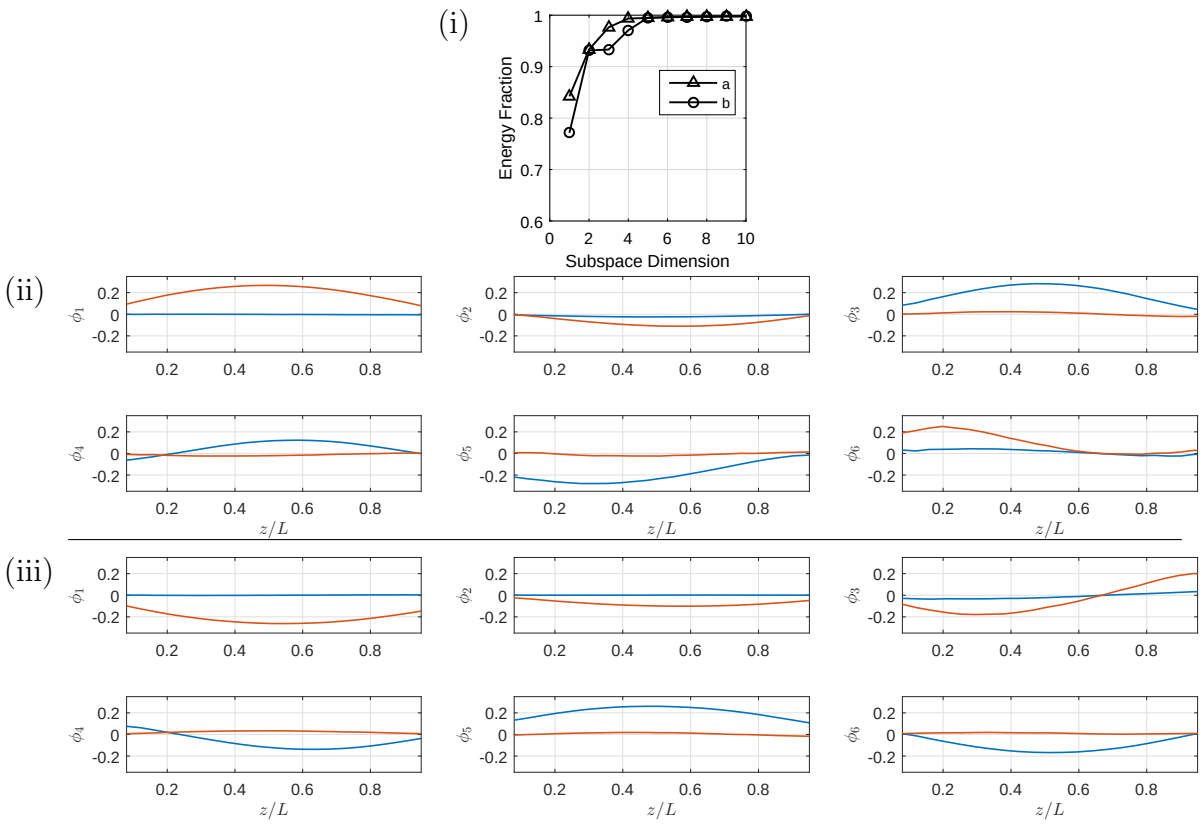

Figure 25: (i) Energy fraction in first 10 subspace dimension, (ii) First 6 SOMs for cylinder 2 where input data matrix includes the dataset up to $Vr_n = 5.5$. (iii) First 6 SOMs for cylinder 2 where input data matrix includes dataset after $Vr_n = 5.5$. Red is cross-flow, blue is in-line.

Figure 25 shows energy fraction and first 6 dominant SOMs of cylinder 2. Different than cylinder 1 response, SOD is applied to two different regions: to the motion response dataset below $Vr_n = 5.5$ and to the motion response dataset above $Vr_n = 5.5$. Figure 25 (i) shows the energy fraction of these two regions where a within the Fig. 25 (i) represents the energy contribution of the motion up to the reduced velocity of 5.5 and b represents the energy contribution after this reduced velocity. SOD analysis of the first half ($Vr_n < 5.5$) shows that first three modes constitutes 99 percent of the total oscillation, but when the same method is applied to the second half ($Vr_n > 5.5$), first 5 modes constitute 99% of the total oscillation. SOD of the first half shows that first four dominant modes

make up to 99% of the total oscillation and SOD of the second half shows that first five modes make up to 99% of the total oscillation. So, there is an extra mode that contributes the motion in the second half. Figures 25 (b) and (c) illustrate the first 6 SOMs of cylinder 2 when the method is applied to these two regions separately. Figure 25 (ii) indicates that first mode is the most dominant mode in cross-flow upto the fifth mode, and there is very small contribution of the second mode in the sixth mode. In the second half of the analysis as shown in Fig. 25, first mode is still the most dominant mode in both directions, but second mode in the cross-flow starts to appear in the third subspace dimension. In this particular case, contribution of the second mode is still very small with a contribution rate less than 1%. Ignoring this motion, there is no existing second mode contribution in the cross-flow direction within the first 6 SOMs which normally constitutes 99.9% of the total motion. It should be remembered that second mode oscillation was expected as a natural response for cylinder 2 due to beam characteristics in the in-line; however, first three dominant SOMs do not show any in-line contribution (or show little first mode contribution) but then second mode starts to appear at the fourth mode in in-line skipping the first mode shape. This means that second mode is the most dominant mode in in-line, and second dominant mode is the first mode which appears at fifth and sixth mode levels. Since the contribution of the fifth and sixth modes are significantly low ($< 0.5\%$), we can conclude that global in-line response resembles to the second mode for cylinder 2 after the reduced velocity of 5.5. However, since the contribution of this response (second SOM in in-line) is very small (making upto only 5%), global in-line response becomes insignificant.

Figure 26 shows the energy fraction and first 6 SOMs of test cylinder 3. SOD is applied to the response dataset before (abbreviated as a) and after (abbreviated as b) the reduced velocity of 9.5. Figure 26 (i) illustrates the contribution of first 10

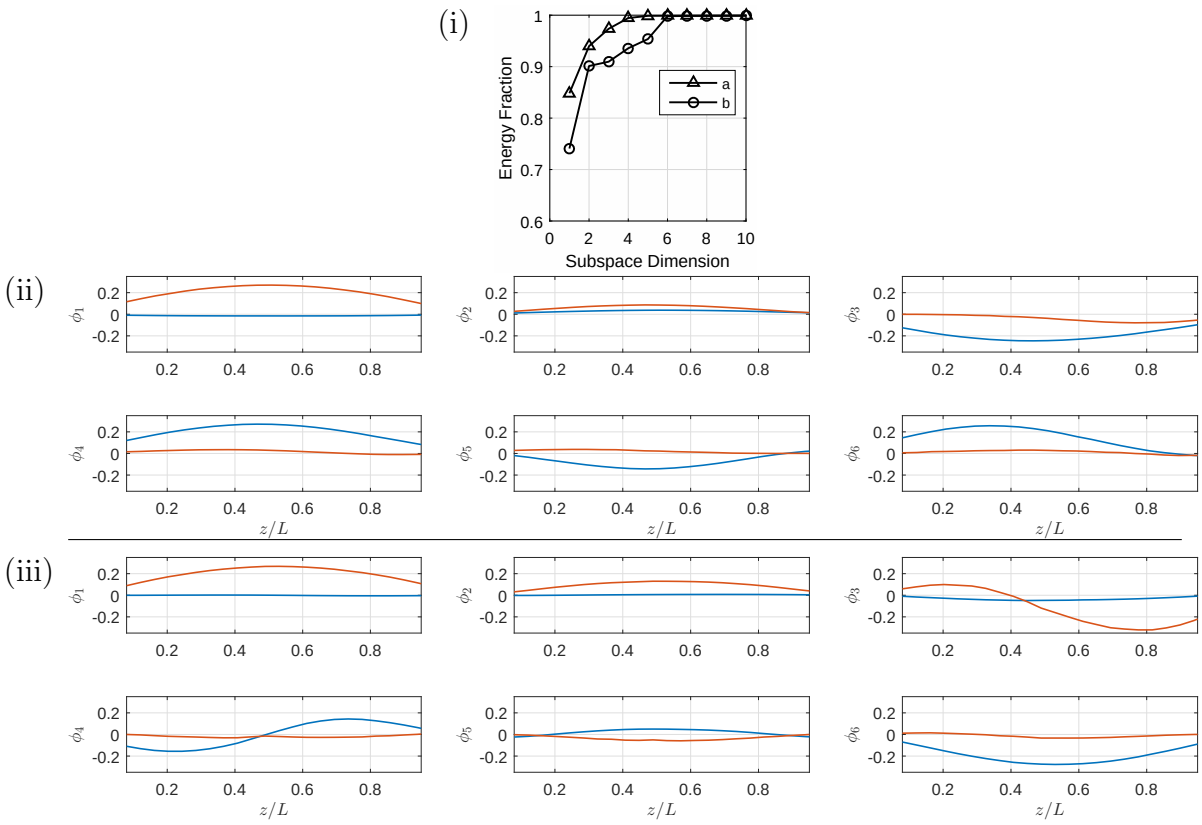

Figure 26: (i) Energy fraction in first 10 subspace dimension, (ii) First 6 SOMs for cylinder 3 where input data matrix includes the dataset up to $Vr_n = 9.5$. (iii) First 6 SOMs for cylinder 3 where input data matrix includes dataset after $Vr_n = 9.5$. Red is cross-flow, blue is in-line.

SOMs to total response. It clearly shows that first 4 modes constitute 99 % of the total motion if the method is applied to the cylinder 3 dataset before $Vr_n = 9.5$, whereas when it is applied to the dataset after $Vr_n = 9.5$, first 6 modes constitute 99% of the total motion. So, there are extra two modes needed to fully reconstruct the motion with the same accuracy as in the first half. Similar to cylinder 2, Figure 26 (ii) represents the SOMs before $Vr_n = 9.5$, and illustrates that first two dominant modes in cross-flow is similar to first mode then there is very small contribution of second mode in the third SOM. Figure 26 represents the SOMs after $Vr_n = 9.5$, and illustrates that first two dominant modes constitute 90% of the total oscillation, and these modes are similar first modes in both directions. In this case,

cross-flow motion response is much larger than the in-line response. Second mode in cross-flow appears in the third SOM, but similar to cylinder 2, this additional third mode only adds 1% to total motion, therefore it is not significant. Second mode in in-line appears in the fourth SOM where in-line response is stronger than cross-flow response, therefore small 5% jump in the energy fraction at the fourth mode level is thought to be due to this in-line response.

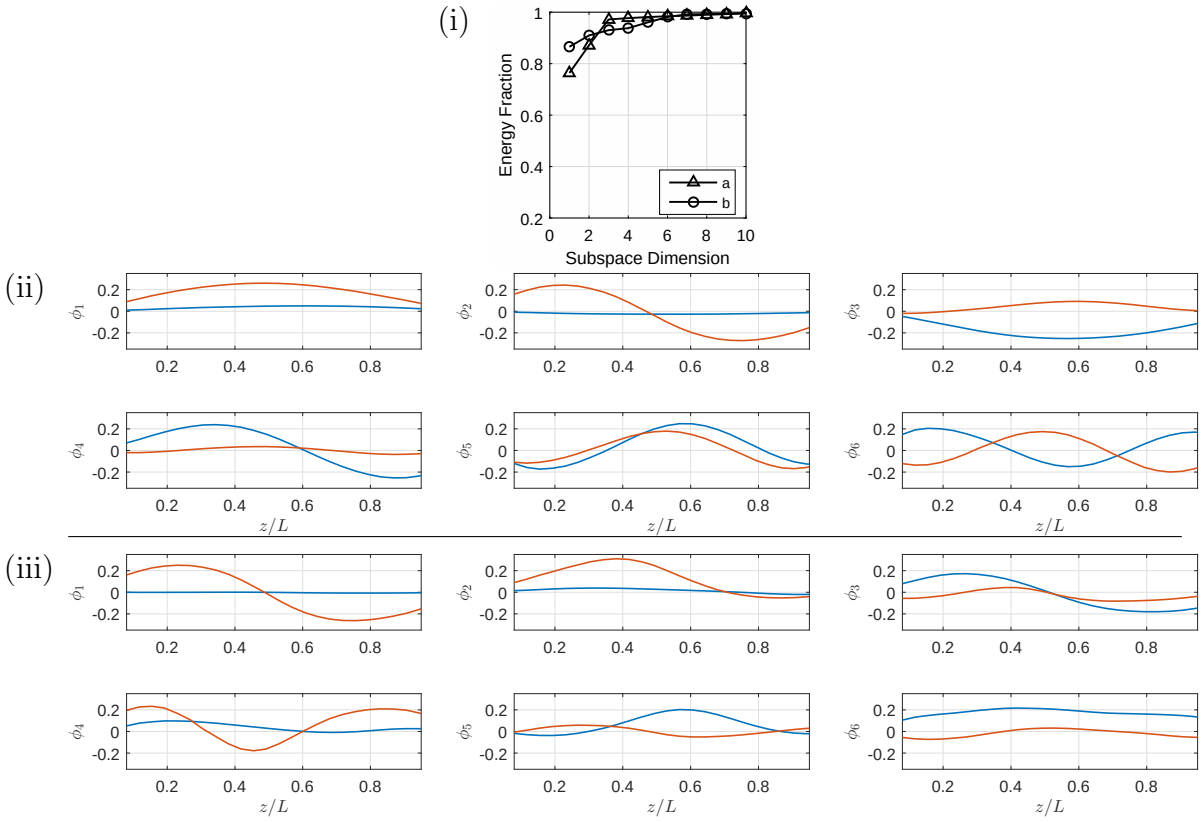

Figure 27: (i) Energy fraction in first 10 subspace dimension, (ii) First 6 SOMs for cylinder 4 where input data matrix includes the dataset up to $Vr_n = 15$. (iii) First 6 SOMs for cylinder 4 where input data matrix includes dataset after $Vr_n = 15$. Red is cross-flow, blue is in-line.

Figure 27 shows the energy fraction and first 6 SOMs of test cylinder 4. In the Figure 27 (i), it is clear that in the first 10 SOMs contribution to total response, first three SOMs before $Vr_n = 15$ (Fig. 27 (i, a)) consitute 99% of the total motion and first 6 SOMs after $Vr_n = 15$ consitute 99% of the total motion. Previously,

similar results were shown using the local POD method [20]. In the current study, SOD method is applied to the dataset before and after $Vr_n = 15$. Figure 27 (ii) illustrates the first 6 SOMs for the dataset before $Vr_n = 15$. It shows that first SOM is similar to first mode shape and is the most dominant SOM among first three SOMs in both directions constituting 78% of the total motion; then, second dominant SOM is similar to second mode shape in cross-flow and first mode in in-line constituting 7% of the total motion. Third SOM is some first-third mode combination in cross-flow and pure first mode in in-line. Figure 27 (iii) illustrates the first 6 SOMs for the dataset after $Vr_n = 15$. It shows that first SOM is similar to second mode shape in cross-flow with no in-line motion, second SOM is some combination of first-second mode in cross-flow with very small in-line; third SOM is large second mode in-line response with small third mode cross-flow, and fourth mode is large third mode in cross-flow with second mode in-line. Other higher modes constitute only 4% of the total motion.

In summary, this study shows that SOD based vibration mode identification is a possible statistical toolbox in vortex-induced vibration dynamic response analysis. This method enables one to decompose the signal to best possible and smooth fits with lowest possible dimension in comparison with traditional POD method. This comparison is also discussed in quite detail in Gedikli et al. [23]. For example, when POD method is used, one will need at least first 8 sub-dimensions in a 25 dimensional space (which represents the number of points along cylinder's span) to fully reconstruct the original motion with 99% accuracy, but with SOD one can achieve the same goal using only the first 6 sub-dimensions or less.

4.6 Euler-bernoulli elastic beam response under uniform load and limited asymmetric response

General equation of motion for the steady-state transverse response of a pinned-pinned viscously damped euler elastic Bernoulli beam subjected to a time varying load can be written as;

$$EIy'''' + \mu\ddot{y} + c\dot{y} = f(x,t) \tag{23}$$

where y is the transverse displacement of the beam, EI is the flexural rigidity of the beam, μ is the mass per unit length of the beam, and c is the coefficient of external damping of the beam. Right side of the equation represents the forcing function in time.

By solving the eigenvalue problem for a pinned-pinned uniform beam with a uniformly distributed sinusoidal loading varying with time, one can easily find the natural modes of the Euler beam (see Appendix 4.9).

In this section, we test three different cases solving Eq. 28 where a symmetric loading is applied to the Euler beam equation. Since there is n^2 relationship between mode shapes, we test the frequency ratios of $f/f_n = 1, 4, 9$ where up to third mode is allowed. In the simulations, damping ratio is kept constant at 0.04 and resulting mode shapes are compared.

Left image in Figure 28 shows uniform sinusoidal loading on a beam and the corresponding spatial response. As clearly seen, when the oscillation frequency is equal to first mode natural frequency, the resulting shape resembles a symmetric first mode. The center image shows the second mode excitation where the oscillation frequency is four times the first mode natural frequency. The resulting shape still resembles to the first mode shape, only bended close to the end points. Right image shows the response of a beam where frequency of oscillation is 9 times the natural frequency. The resulting shape resembles to third mode as predicted. As

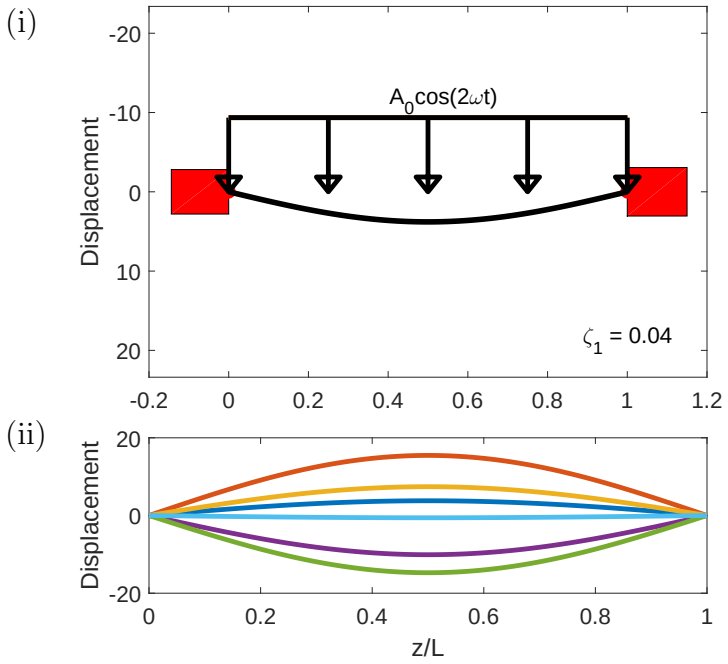

Figure 28: Top image (i): Symmetrically distributed uniform loading with frequency ratio ($f/f_n = 1$) where cylinder oscillates one time the natural frequency. Bottom image (ii): Resulting motion shape at different time traces.

a result, analytic solution to Euler Bernoulli beam illustrates that a beam under symmetric loading is not capable of oscillating with even modes (second, fourth, and so on) and only oscillates with odd modes (first, third, fifth, and so on).

Idealized cylinder 2 oscillation is modeled so that cylinder‘s oscillation is four times the first mode natural frequency. In other words, loading is symmetric but desired spanwise response is asymmetric. As a result, center image in Figure 30 shows that even though cylinder has second mode frequency, the spatial response still resembles to a first mode shape; however, different than idealized cylinder 1 response, the shape is bended at the quarter locations and resembles to a first mode shape.

In Cylinder 3 model, oscillation frequency of the system is nine times the first mode natural frequency. As shown in right image in Figure 30, when the cylinder is exposed to the same uniform loading, the system this time allows cylinder to

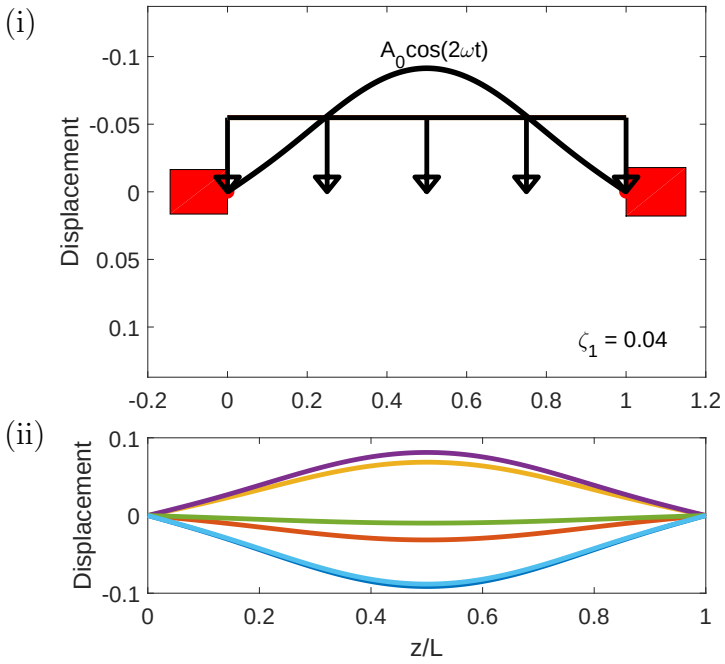

Figure 29: Top image (i): Symmetrically distributed uniform loading with frequency ratio ($f/f_n = 4$) where cylinder oscillates four times the natural frequency. Bottom image (ii): Resulting motion shape at different time traces.

oscillate with the desired third mode shape which is also symmetric.

4.7 Discussion

In comparison, the tension-dominated and bending-dominated systems in this study demonstrate one common behavior: despite frequency excitation in cross-flow that is twice the frequency in the in-line direction and tuning natural frequencies to have specific mode shapes, it is difficult or not possible to significantly excite an asymmetric second mode shape in the in-line direction. There are a couple important aspects of this phenomenon that always should be remembered: 1) This phenomenon is thought to be possible only under symmetric loading conditions (i.e. uniform loading). 2) Cylinder has to have a symmetric mass distribution i.e. has to be as smooth as possible with no dimples on it. 3) Mass ratio should be small (close to 1) therefore the gravity effect (i.e natural sagging of the cylinder) on the cylinder becomes minimum. 4) These results were only observed when the

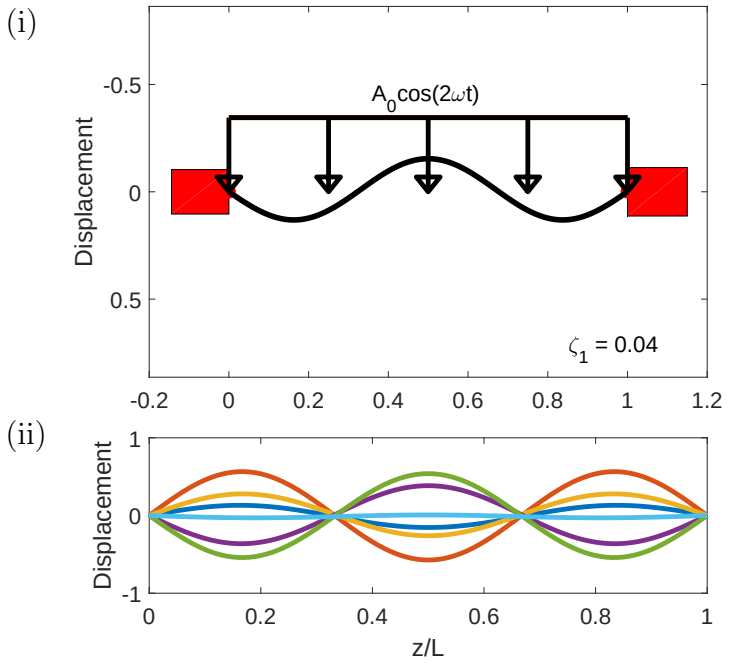

Figure 30: Top image (i): Symmetrically distributed uniform loading with frequency ratio ($f/f_n = 9$) where cylinder oscillates nine times the natural frequency. Bottom image (ii): Resulting motion shape at different time traces.

cylinder was totally submerged underwater and placed horizontal in the in-line direction. However, it is thought that if the cylinder is placed vertical (perpendicular to incoming fluid flow), and intersects the water level at the top, then this condition might create an asymmetry in the response. If this is the case, even mode excitation becomes possible.

Vandiver and Jong [14] observed a similar behavior in field experiments, attributing this behavior to the symmetric distribution of the drag force over the cylinder in a uniform flow. Later, Gedikli and Dahl [20] observed this phenomenon in tensioned cylinder experiments that were conducted in a uniform recirculating flow channel. If one considers a uniform distribution of force over the span of a simply-supported beam, where the amplitude of the force is a harmonic function applied with a frequency equal to the second mode natural frequency, one finds that the structure will have a symmetric shape similar to the first mode shape

(see Fig. 29). In fact, for any frequency associated with an even mode, the spanwise shape will be similar to the next lowest odd mode shape. Even modes could certainly be excited in the case of sheared flow, where an asymmetry of the flow speed would result in an asymmetry to the distributed drag load. This is also significant to the flexible cylinder studies conducted vertically in a towing tank or water tunnel. In conditions where a flexible cylinder pierces the water surface, a slight asymmetry may occur in the loading of the structure, which would demonstrate asymmetric mode excitation that would not typically occur if the loading was purely symmetric (for example if the cylinder is oriented horizontally in the water column). This has general relevance in understanding responses observed in field or lab experiments studying the response of flexible cylinders.

In the particular experiments mentioned, additional interesting behaviors are observed. For example, cylinder 3 is tuned so that the first mode in-line will correspond with the forcing frequency from vortex shedding in the transverse direction, while the third structural mode will correspond with the vortex shedding frequency in the in-line direction. Despite this tuning, the in-line direction undergoes resonant response with dominant first mode shape (due to the loading distribution as described above). This is interesting, however, since in order to oscillate with the observed frequency and mode, a linear treatment of the frequency response and adjustment of the effective natural frequency would require an extremely large negative added mass, since the frequency of oscillation in the in-line direction is so far from the natural frequency associated with the first mode. This is highly unlikely and the frequency transitions observed for cylinder 3 are more likely to stem from non-linear resonant conditions from the coupling of vortex shedding effects on the cross-flow and in-line response. It is necessary to investigate forces and wake structures on these flexible structures in order to understand this relationship.

Finally, the transition between 1:1 mode shape response and 2:3 mode shape response seen in the tensioned cylinder is not necessarily unique to the tensioned cylinder, since the natural frequency relation for the bending-dominated cylinder requires the natural frequencies to be further spaced from one another. Due to the limitations of the flow channel, higher speeds could not be tested to see if the transition to higher modes would follow a similar behavior for the bending-dominated systems.

4.8 Conclusion

The main objective of the current study was to study the cylinder's mode effects on the total response. Previously, Vandiver and Jong [14] in field experiments, and Gedikli and Dahl [20] in laboratory experiments showed that a flexible cylinder is not capable of oscillating with even modes if the fluid loading on the body is distributed uniformly along its span. This study also allows us to test this hypothesis, since we systematically control the cylinder oscillations by molding rectangular shaped plastic beams through the center of the cylinder. Each of these test cylinders have unique characteristics so that varying the in-line mode shape from one to three and keeping the cross-flow mode shape constant would allow the in-line response effect to total coupled response.

This systematic study has showed that even though a flexible cylinder is tuned to oscillate with an asymmetric mode shape (i.e. second mode) in in-line, it is not possible to have an asymmetric mode shape due to symmetric loading. However, asymmetric mode shape is possible if drag force distribution is not symmetric as discussed above. Multivariate analysis approach is used to analyze the contribution of higher order VIV empirical modes. Especially, apart from POD, SOD method is showed to be an effective method in this study to analyze the non-linear modes. An effort is given to understand if it is possible to match the higher order SOMs

with the designed mode shapes (i.e. cylinder 2 does not oscillate with second mode in in-line but at what sub-dimension it oscillates if SOD method is used?). It is found that even though cylinder primarily oscillates with odd mode shapes, there are even modes that are present in the first 6 SOMs if multivariate analysis approach is applied. If one needs to model this fluid-structure phenomenon, instead of ignoring the even modes in in-line, higher order SOMs approach can be used to fully reconstruct the real motion with substantially lower dimensions.

4.9 Appendix A. Euler-Bernoulli elastic beam response under uniform load

This appendix explains how the euler-bernoulli beam theory is applied in the current study. Extensive studies clearly explain how the Euler-Bernoulli beam can be solved for different boundary conditions [24, 25, 26, 27] and this appendix is a simple summary for the current problem.

Let consider the equation of motion for the current problem be Equation 23.

Assuming the forcing function can be written in the form of separating variables;

$$f(x,t) = A_0 F(x) G(t) \tag{24}$$

where A_0 is the initial response amplitude, $F(x)$ is the spatial portion of the forcing function, and $G(t)$ is time dependent portion of the forcing function. A_0 will have different values depending on different combinations of spatial and time dependent portion of the forcing functions.

The normal mode functions for this end conditions (pinned-pinned) can be written as;

$$Y_n(x) = \sqrt{2}\sin(\beta_n x) \tag{25}$$

where the eigenvalues are $\beta_n x = n\pi$. Equation 17 shows the relationship between the eigenvalues and the natural frequencies for Euler-Bernoulli beam. Damping ratio may be introduced as $\zeta_1 = \dfrac{c}{2\mu\omega_1}$ where $\omega_n = 2\pi f_n$. Since we are interested in different combination of mode shapes, damping ratios in the higher modes can be described as ;

$$\zeta_i \omega_i = \zeta_1 \omega_1 \qquad \text{where} \qquad i = 2, 3, 4, ... \tag{26}$$

which shows that as the system excites higher modes, damping ratios decrease.

Introducing a new variable $u(x,t)$ for the displacement, the exact solution for Eq. 23 becomes;

$$u(x,t) = \sum_{n=1}^{\infty} q_n(t) Y_n(x) \tag{27}$$

where $Y(x)$ are the normal modes of an undamped/unforced beam and $q(t)$ is time dependent coordinate of the beam. After substitution of equations 25 and 27 into the general equation of motion 23 and applying the orthogonal conditions to Eq. 23, one can get the final equation of motion of a beam subjected to an external loading as;

$$\ddot{q}_n + 2\zeta_n \omega_n \dot{q}_n + \omega_n^2 q_n = \frac{A_0 F_n}{\mu} G(t) \qquad n = 1, 2, ... \tag{28}$$

Let $G(t)$ be a harmonic forcing function that is described by;

$$G(t) = \cos\omega t \tag{29}$$

where ω is the forcing frequency. Then, the steady-state response of the Eq. 28 can be written in the complex plane as;

$$q_n(t) = \frac{A_0 F_n}{\mu \omega_n^2} |H_n(j\omega)| \cos(\omega t + H_n \angle(j\omega)) \tag{30}$$

where

$$H_n(j\omega) = \frac{1}{1 - (\omega/\omega_n)^2 + 2j\zeta_n(\omega/\omega_n)} \qquad n = 1, 2, ... \tag{31}$$

which represents the imaginary part of the complex frequency response. Therefore, Eq.27 can easily be solved by substituting Equations 30, 31 to the equation.

List of References

[1] T. Sarpkaya, "A critical review of the intrinsic nature of vortex-induced vibrations," *Journal of Fluids and Structures*, vol. 19, no. 4, pp. 389–447, 2004.

[2] P. W. Bearman, "Vortex shedding from oscillating bluff bodies," *Annual review of fluid mechanics*, vol. 16, no. 1, pp. 195–222, 1984.

[3] C. Williamson and R. Govardhan, "Vortex-induced vibrations," *Annu. Rev. Fluid Mech.*, vol. 36, pp. 413–455, 2004.

[4] P. Bearman, "Circular cylinder wakes and vortex-induced vibrations," *Journal of Fluids and Structures*, vol. 27, no. 5, pp. 648–658, 2011.

[5] H. Marcollo, A. Eassom, E. Fontaine, M. Tognarelli, P. Beynet, Y. Constantinides, and O. H. Oakley, "Traveling wave response in full-scale drilling riser viv measurements," in *ASME 2011 30th International Conference on Ocean, Offshore and Arctic Engineering*. American Society of Mechanical Engineers, 2011, pp. 523–537.

[6] Y. Modarres-Sadeghi, F. Chasparis, M. Triantafyllou, M. Tognarelli, and P. Beynet, "Chaotic response is a generic feature of vortex-induced vibrations of flexible risers," *Journal of Sound and Vibration*, vol. 330, no. 11, pp. 2565–2579, 2011.

[7] T. S. Sarpkaya, *Wave Forces on Offshore Structures*. Cambridge University Press, 2010.

[8] H. Lie and K. Kaasen, "Modal analysis of measurements from a large-scale {VIV} model test of a riser in linearly sheared flow," *Journal of Fluids and Structures*, vol. 22, no. 4, pp. 557 – 575, 2006. [Online]. Available: http://www.sciencedirect.com/science/article/pii/S0889974606000077

[9] J. Chaplin, P. Bearman, F. H. Huarte, and R. Pattenden, "Laboratory measurements of vortex-induced vibrations of a vertical tension riser in a stepped current," *Journal of Fluids and Structures*, vol. 21, no. 1, pp. 3–24, 2005.

[10] A. Trim, H. Braaten, H. Lie, and M. Tognarelli, "Experimental investigation of vortex-induced vibration of long marine risers," *Journal of fluids and structures*, vol. 21, no. 3, pp. 335–361, 2005.

[11] J. Vandiver, H. Marcollo, S. Swithenbank, V. Jhingran, *et al.*, "High mode number vortex-induced vibration field experiments," in *Offshore Technology Conference*. Offshore Technology Conference, 2005.

[12] E. Passano, C. M. Larsen, and J. Wu, "Viv of free spanning pipelines: Comparison of response from semi-empirical code to model tests," in *ASME 2010*

29th International Conference on Ocean, Offshore and Arctic Engineering. American Society of Mechanical Engineers, 2010, pp. 567–577.

[13] F. Huera-Huarte, Z. Bangash, and L. González, "Towing tank experiments on the vortex-induced vibrations of low mass ratio long flexible cylinders," *Journal of Fluids and Structures*, vol. 48, pp. 81–92, 2014.

[14] J. Vandiver and J.-Y. Jong, "The relationship between in-line and cross-flow vortex-induced vibration of cylinders," *Journal of Fluids and Structures*, vol. 1, no. 4, pp. 381–399, 1987.

[15] J. Dahl, F. Hover, and M. Triantafyllou, "Two-degree-of-freedom vortex-induced vibrations using a force assisted apparatus," *Journal of Fluids and Structures*, vol. 22, no. 6, pp. 807–818, 2006.

[16] J. Dahl, F. Hover, M. Triantafyllou, S. Dong, and G. Karniadakis, "Resonant vibrations of bluff bodies cause multi-vortex shedding," *Physical Review Letters*, vol. 99, no. 144503, 2007.

[17] N. Srinil, H. Zanganeh, and A. Day, "Two-degree-of-freedom viv of circular cylinder with variable natural frequency ratio: Experimental and numerical investigations," *Ocean Engineering*, vol. 73, pp. 179–194, 2013.

[18] Z. Kang and L. Jia, "An experiment study of a cylinder's two degree of freedom viv trajectories," *Ocean Engineering*, vol. 70, pp. 129–140, 2013.

[19] J. Dahl, F. Hover, M. Triantafyllou, and O. Oakley, "Dual resonance in vortex-induced vibrations at subcritical and supercritical reynolds numbers," *Journal of Fluid Mechanics*, vol. 643, pp. 395–424, 2010.

[20] E. D. Gedikli and J. M. Dahl, "Mode excitation hysteresis of a flexible cylinder undergoing vortex-induced vibrations," *Journal of Fluids and Structures*, vol. 69, pp. 308 – 322, 2017. [Online]. Available: http://www.sciencedirect.com/science/article/pii/S0889974616303188

[21] B. Feeny and R. Kappagantu, "On the physical interpretation of proper orthogonal modes in vibrations," *Journal of Sound and Vibration*, vol. 211, no. 4, pp. 607 – 616, 1998. [Online]. Available: http://www.sciencedirect.com/science/article/pii/S0022460X97913869

[22] D. Chelidze and W. Zhou, "Smooth orthogonal decomposition-based vibration mode identification," *Journal of Sound and Vibration*, vol. 292, no. 35, pp. 461 – 473, 2006. [Online]. Available: http://www.sciencedirect.com/science/article/pii/S0022460X05005948

[23] E. D. Gedikli, J. M. Dahl, and D. Chelidze, "Multivariate analysis of vortex-induced vibrations in a tensioned cylinder reveal nonlinear modal interactions," in *10th International Conference on Structural Dynamics*. Eurodyn, 2017.

[24] H. Benaroya, *Mechanical Vibration: Analysis, Uncertainties, and Control*, 2nd ed. Marcel Dekker, New York, 2004.

[25] J. Ginsberg, *Mechanical and Structural Vibrations: Theory and Applications*. John Wiley and Sons, 2001.

[26] W. Thomson and M. Dahleh, *Theory of Vibration with Applications*, 5th ed. Prentice Hall, Englewood Cliffs, 1998.

[27] L. Meirovitch, *Fundamentals of Vibrations*. McGraw-Hill, New York, NY., 2001.

CHAPTER 5

Underwater vibration control of flexible cylinders using piezo stripe actuators

by

Ersegun Deniz Gedikli*, David Chelidze** and Jason Dahl*

*Department of Ocean Engineering, University of Rhode Island, Narragansett, RI 02882, USA

**Department of Mechanical, Industrial and Systems Engineering, University of Rhode Island, Kingston, RI, 02881, USA

To be submitted to the Journal of Sound and Vibration

Abstract

In this study, piezo stripe actuators were used to control the vibrations of flexible cylinders underwater. In the tests, piezo stripes were attached at the anti-nodes of a rectangular plastic beam in the in-line direction (in the direction of fluid flow) and then molded using urethane rubber material to give the test beam a circular shape. In-line direction was chosen simply because the resulting motions are generally lower than cross-flow motions in vortex-induced vibrations (VIV) and therefore require lower energy input to control. Through the use of high voltage signal generator, two separate cases were investigated. In the first case, piezo stripe actuators were activated right before spatial mode change, thus tripping the frequency and forcing the cylinder to excite with a higher mode (vibration suppression). In the second case, piezo actuators were activated right before an apparent amplitude increase, forcing cylinder to jump to the higher amplitude response regime (vibration enhancement). In the tests, the beam was designed to oscillate up to third mode in in-line keeping the cross-flow response constant at first mode. Experiments were first carried out in air to characterize the piezo responses, and then similar experiments were carried out in the recirculating flow channel that is located at the Narragansett Bay campus of the University of Rhode Island. This study presents two important observations: 1) piezo actuators can possibly trip the response frequency and force cylinder to oscillate with a different mode, thus reducing the total response amplitude significantly, 2) it is also possible to increase the response amplitude if piezos are activated right before an apparent jump in the response amplitudes.

5.1 Introduction

Vortex-induced vibration is an inherent problem in engineered structures that are subject to a fluid flow. Especially slender structures in water such as offshore

risers, offshore wind turbines, underwater cables, horizontal pipeline span, etc. are prone to such motions. When a bluff body is subjected to an incoming flow, it creates vortices shedding downstream. These vortices have a particular frequency associated with them, i.e. vortex shedding frequency. When the vortex shedding frequency gets close to one of the natural frequencies of a long structure (lock-in), large vibrations might occur. These vibrations can be very dangerous; they may affect the fatigue life or may even give significant damages to the structure if not carefully monitored.

Previously, high harmonic forcing has been demonstrated to be associated with large amplitude figure-eight type of motion of cylinders undergoing VIV [1]. This high harmonic forcing can potentially reduce fatigue life estimates on flexible structures undergoing VIV by orders of magnitude [2]. Recent studies on flexible cylinders have demonstrated that specific mode combinations on a flexible cylinder are more or less likely to produce figure eight-type motions [3, 4]. Therefore, predicting and suppressing these undesirable motions of such systems is of utmost importance to the offshore industry for many years.

Different control techniques have been developed in the past to control vortex-induced vibrations. One of them is the passive control mechanism where the main goal is to give a disturbance to the flow downstream through changing the geometry of the structure. In this method, there is no external energy input to the structure, and can be a very effective tool to cancel the vibration [5, 6, 7, 8]. Popular systems for suppressing the VIV of subsea tubulars may include helical strakes, strouts, or fairings that are fitted along the span of the structures. Such systems disturb the flow around the structure, break up the correlation of vortices along the tubular, and cause random forces. Therefore, they can be very effective at reducing vortex-induced vibrations for a wide range of applications. On the

other hand, addition of such systems usually increases the drag force acting on the structure. Another control technique that is widely mentioned in the literature suppressing the vibration includes active control mechanisms. In this case, an energy input is required to give a disturbance to fluid-structure interaction through use of open-loop or closed-loop control techniques. In an open-loop system, an actuator (i.e., piezo stripe actuator) driven by an external energy source can be used to disturb the motion [9], or in a closed loop system, a feedback mechanism can be used [10, 11]. Both of these methods have been proven to be successful to reduce the vibration amplitudes in a fluid-structure interaction. In addition to above menioned active control mechanisms, there are vortex-shedding suppression and wake control methods that are considered as active flow control mechanisms with regards to vortex-induced vibration oscillation control. Some of these methods have been recently reviewed and discussed more in detail in Rashidi et al. [12]. Active and passive control mechanisms can also be used to enhance the vibration [13, 14].

The main purposes of this study are: first, to develop an experimental system and test if it is possible to change the mode shape of a flexible cylinder through the use of piezo stripe actuators (i.e. trip the oscillation frequency and cause mode switch), which is vibration suppression; second, to test if it is possible to increase the amplitude, hence vibration enhancement. This study: includes 1) the use of piezo stripe actuators for energy input to perturb the motion and consequently active control mechanism, 2) in-air measurements, 3) in-water measurements. In air a shaker-rail mechanism is designed to find out at what input signal frequencies, piezo stripe results in the highest amplitude. Also, this system helps to find out if it is possible to trip the frequency to one above energy level (one above mode shape) and thus decrease the motion amplitude. Second part of the study includes

the experiments in water where the designed experimental apparatus allows one to attach the cylinder vertically in the flow direction. In the tests, cylinder's moving part is completely submerged and symmetrically attached at the top and bottom of the tank. This configuration reduces the asymmetry in the water column due to wave formation after a certain flow speed and allows cylinder to have uniform loading across its span.

In this paper, a through introduction is given in section 5.1, experimental apparatus in air is described in section 5.2, then experimental apparatus in water is described in section 5.3. The major findings are introduced in section 5.4. A brief summary and conclusion is given in section 4.5.

5.2 Test cylinder and experiments in air using shaker-rail apparatus

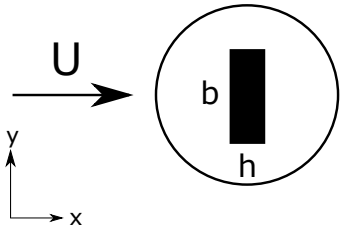

Figure 31: Cross section of the test cylinder with beam. Water flows from left to right. x represents in-line, y represents cross-flow

In the experiments a rectangular beam was placed through the center of a circular cylinder as sketched in Figure 31 where b represents the width of the beam, h represents the height of the beam, U represents the flow speed. Test beam was designed to oscillate up to third mode in in-line keeping the cross-flow mode shape constant. To find the correct size of beam, the natural frequency equation for a fixed-fixed beam was used:

$$f_n = \frac{\lambda_n^2}{2\pi}\sqrt{\frac{EI}{ML^4}} \tag{32}$$

where $\lambda_n = (2n+1)\frac{\pi}{2}$, E is the elasticity of modulus, I is the area moment of inertia, n is the mode number, M is the mass per unit length, L is the beam length.

Table 6 gives the detailed information about the beam characteristics and experimental parameters where D is the cylinder diameter, f_n is the natural fre-

quency of the cylinder in air in the in-line direction, m^* is the mass ratio and AR is the aspect ratio of the test cylinder.

Shaker experiments were conducted using a basic shaker-rail apparatus (see Fig. 33). Tests were performed: 1) using the base excitation only over a range of frequencies to characterize the base system response, 2) using the piezo actuation only to characterize the forced input from piezos over a range of frequencies, 3) using the shaker excitation and piezo excitation simultaneously.

Table 6: Test cylinder and experimental parameters

Variable	Values	Units
h	0.635	mm
b	3	mm
D	9.525	mm
f_n	5	Hz
m^*	1.15	–
AR	40	–

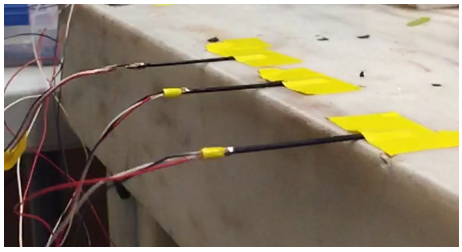

Figure 32: Multiple piezo stripes actuated by high voltage signal generator.

In the experiments, piezo stripes were bonded at the anti-nodes of the test beam in in-line and molded using flexible urethene rubber material from Smooth-on to give a circular shape. In-line direction was chosen simply because the resulting motions are generally lower than cross-flow motions in vortex-induced vibrations (VIV) and therefore require lower energy input from piezo actuators to control. Each piezo stripe actuator has a total length of 49 mm, width of 2 mm, and thickness of 0.80 mm. The manufacture lists the maximum deflection of the stripe actuator to be larger than 1.6 mm and resonance frequency to be around $110Hz$. Figure 32 illustrates the example image of piezo stripes that are connected with cables to a high voltage signal generator.

Left image in Figure 33 shows the picture of the experimental setup which includes a shaker (VTS- Vibration Test Systems) for base excitation, a function generator (Wavetek) to control the shaker, laser displacement sensors (Keyence) to measure the displacement of the beam at certain locations, a high voltage signal generator to control the piezo stripe actuators, and a National Instruments DAQ card for signal analysis. Right image in Figure 33 illustrates the detailed sketch of the experimental setup to emphasize the main equipment used in the experiments. AC power supply is a Compact Power Titan MAC-02 with MOS-01 plug-in. The plug-in is a manual oscillator with knobs, but it also accepts input from an external function generator.

In the experiments, sinusoidal external base excitation was provided by the shaker and the test cylinder was attached to the moving part (rail) of the test system with fixed-fixed end conditions. Shaker was controlled using the function generator for a specific range of amplitudes and frequencies. Laser displacement sensor was used to measure the displacement of the beam at the center and at $L/4$ from the top where L is the cylinder length. Table 7 shows the experimental test matrix for the shaker-rail system where A is the shaker amplitude, f_{shaker} is the shaker frequency, f_{piezo} is the piezo frequency. Two set of experiments were conducted to characterize the response of the cylinder. First, cylinder was excited using the shaker only for the range shown in Table 7 keeping the piezo frequency off. By doing that, natural response of the cylinder to the given base excitation was identified. Secondly, only piezo excitation was recorded with no base excitation within the frequency range

Table 7: Experimental test matrix for the shaker-rail system

Parameters	Range	Spacing	Units
A	Constant	2	mm
f_{shaker}	6 - 24	1	Hz
f_{piezo}	14 - 110	2	Hz

given in Table 7. Therefore, natural response of the cylinder to the piezo was also identified. Last, previously identified maximum response of the cylinder to base excitation was controlled using the maximum piezo response identified in the second step.

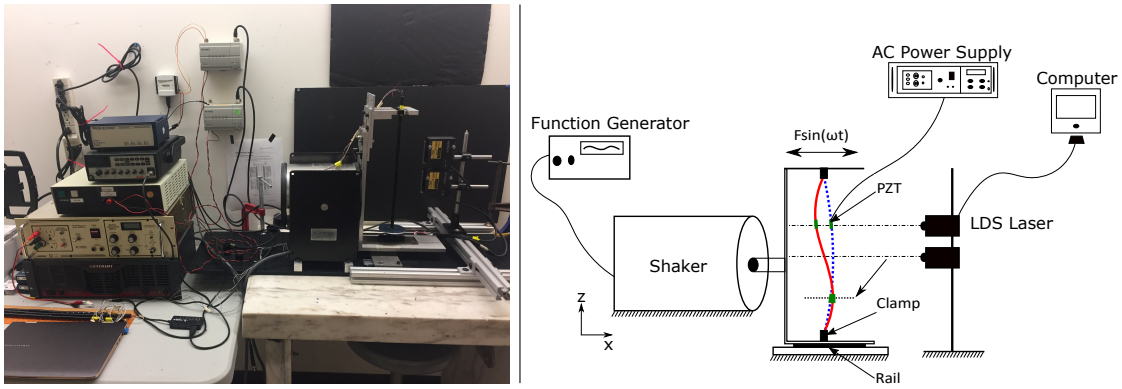

Figure 33: Left image: Picture of the shaker table. Right image: Detailed sketch of the shaker-rail apparatus.

5.3 Water tunnel experiments

Experiments were conducted in a flow visualization water tunnel that is located at the Narragansett Bay campus of University of Rhode Island. The water tunnel is a closed circuit system that has 38 cm wide by 51 cm high by 152 cm long test section. The test section has three viewing windows at the sides and at the bottom of the tank, and there is an extra window in the downstream with a section of 38 cm by 38 cm for axial viewing. Flow tunnel is capable of operating flow speeds between 0.1 m/s to 1.3 m/s whereas current experiments were limited upto 0.6 m/s to decrease the effect of water level drop. Test apparatus includes a free surface suppression wall which perfectly eliminates the formation of the water waves for the tested flow speed range and provides similar end conditions at the top and bottom of the cylinder. Figure 34 shows the experimental apparatus (left image) with sketch of the downstream view of the test cylinder (right image).

In the experiments, two Phantom V10 high speed cameras with two Nikon

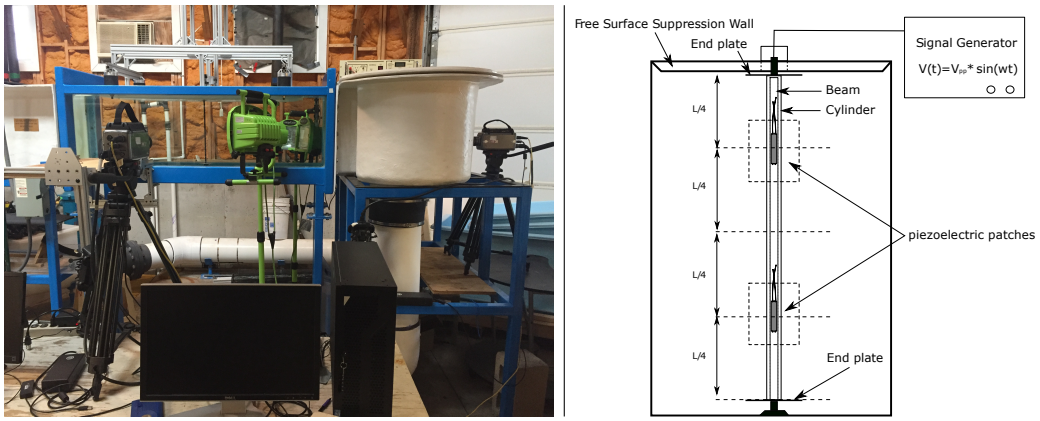

Figure 34: Left image: Experimental apparatus in flow channel. Cameras are orthogonal with respect to each other. Flow is from left to right. Right image: Sketch of the downstream view of the test cylinder.

Nikkor 50 mm f/1.2 lenses were used for motion tracking. One of the cameras was placed at the side of the tank to capture the motion of the cylinder in the flow direction (in-line), and the other was placed downstream side of the tank to capture the motion of the cylinder perpendicular to flow direction (cross-flow). Test cylinder was marked with 21 circular equally spaced (1.6 cm apart) white dots along its span. Two lights were placed at the sides of the tank to increase the visibility of the markers on the cylinders. Each circular dot had a diameter of 2 mm which was identified to be sufficient enough to be captured by the motion tracking for the entire set of experiments.

Motion tracking software used in the experiments works based on subpixel accuracy and identifies the location of the dots with less than 1% error similar to those in Gedikli and Dahl [4]. For detailed information about the software (with error analysis) and how the process is performed, the reader is encouraged to read Gedikli [15] and Gedikli and Dahl [4].

Table 8 shows the experimental parameters for water tunnel experiments where f_{n_w} represents the natural frequency of the test cylinder in water in in-line, U represents the flow speed range, Re represents the Reynolds number range

and St represents the Strouhal number. As expected, natural frequency obtained from the decay tests in water was lower than the ones in air.

Table 8: Experimental parameters

Variable	Values	Units
f_{n_w}	4.2	Hz
U	0.1–0.54	m/s
Re	900–5200	–
St	0.19	–

There are two main objectives of this study. First objective is to see if it is possible to trip the frequency of oscillation thus force cylinder to change its modal response and decrease the response amplitude (vibration suppression). Second objective is to see if it is possible to actuate the piezo stripes right before an apparent amplitude jump, thus force cylinder to increase the vibration amplitude earlier than the natural response (vibration enhancement).

5.4 Results

In-air experiments were concentrated on the response of the test cylinder in the in-line direction, and cross-flow motion (motion perpendicular to shaker direction) was not captured. Therefore, two laser displacement sensors were located in front of the shaker apparatus and measured the response in the direction of the shaker (see Fig. 33). Displacement of the cylinder was sampled at 1000 Hz and experiments were contained minimum of 8-10 *seconds* of data.

5.4.1 Piezo characterization using shaker-rail apparatus and proof of concept

To measure the natural response of the test cylinder, pluck tests were performed and resulting motion was captured using laser displacement sensors. Figure 35 shows the time history of the response of the test cylinder in in-line (left image) and the corresponding frequency plot (right image) obtained from pluck-tests. According to the frequency analysis, natural frequency of the test cylinder

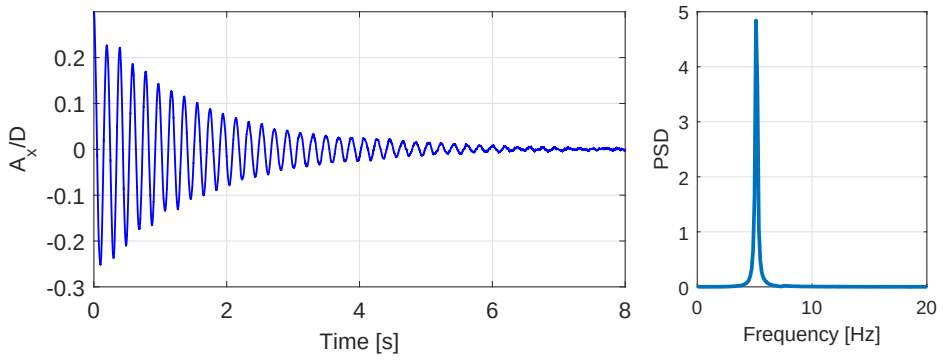

Figure 35: Left image: Time history of the center point cylinder motion obtained from decay tests. Right image: Frequency plot of the center point cylinder motion obtained from decay tests.

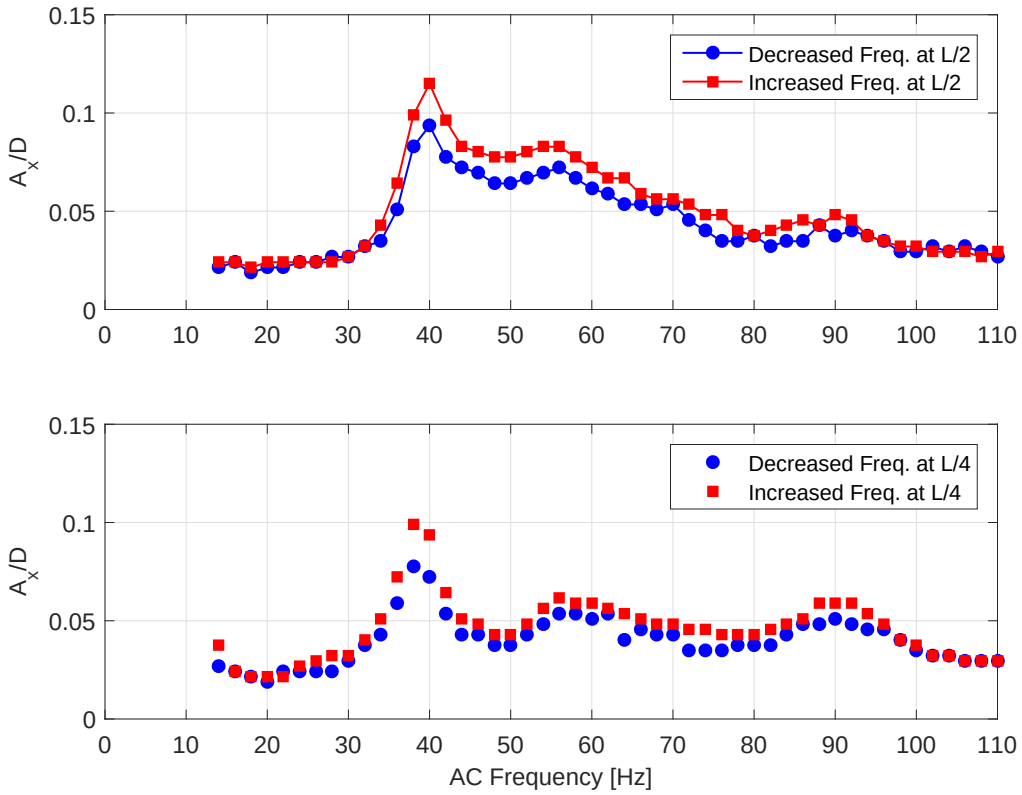

Figure 36: Top image: Piezo only response of the test cylinder at center. Bottom image: Piezo only response of the test cylinder at L/4 from the top of the cylinder. Red represents the increased high voltage signal (abbreviated as AC) frequency. Blue represents the decreased AC frequency.

was around 5 Hz. In the tests, test cylinder was molded with urethene rubber to give a circular shape.

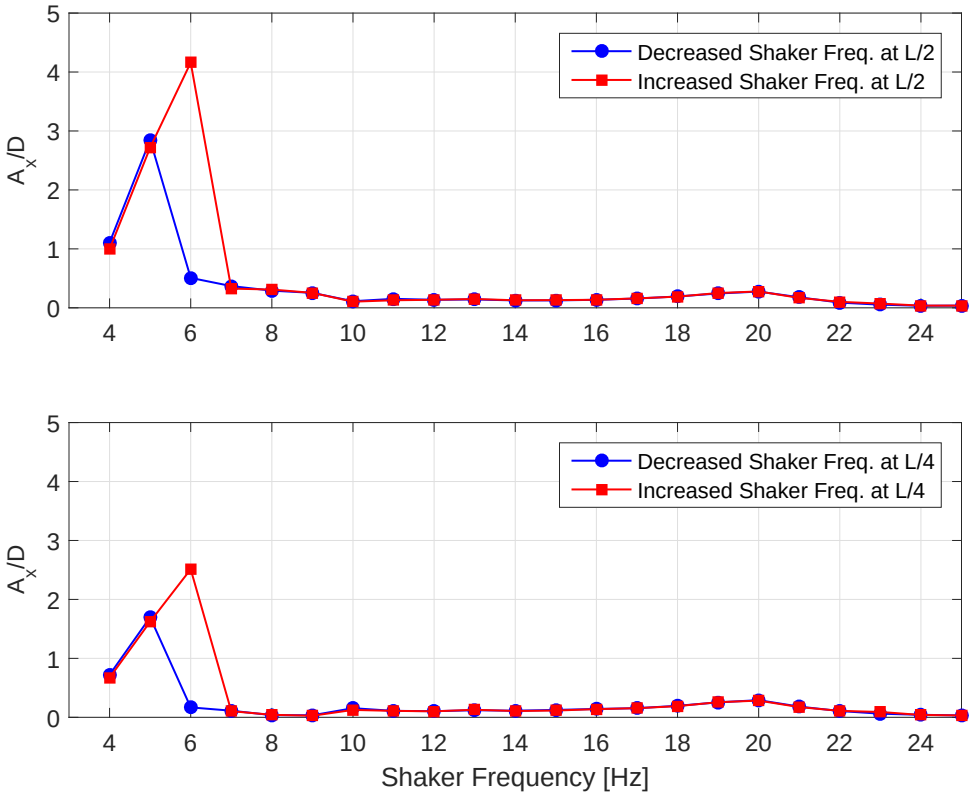

Figure 37: Top image: Shaker only response of the test cylinder at center. Bottom image: Shaker only response of the test cylinder at L/4 from the top of the cylinder.

Figure 36 illustrates the response of the test cylinder when only piezo was activated without moving the shaker. Top image in Fig. 36 shows the piezo-only-response at center point of the test cylinder for increased and decreased shaker frequency values and bottom image in Fig. 36 shows the similar response at $L/4$ from the top. This analysis clearly shows that around shaker frequency of 38-40 Hz, cylinder reached to maximum non-dimensional amplitude in in-line with a value of 0.12 at the center and 0.1 at $L/4$, and fluctuated at a lower amplitude pace as the shaker frequency increased. Hysteretic behavior in the response was observed in between the amplitude responses (i.e. cylinder oscillated with higher amplitudes when the AC frequency increased, and oscillated with lower amplitudes

when the AC frequency decreased).

Figure 37 shows the shaker-only-response as a function of non-dimensional response amplitude in in-line direction without piezo actuation. This response is important, because it actually shows at what shaker frequency cylinder reaches the maximum response amplitude and then decreases again. Similar to Figure 36, experiments were conducted for increased and decreased shaker frequency values. Since these experiments were carried out as a proof of concept, shaker amplitude kept constant, and only shaker frequency was varied within the range of 4 - 25 Hz.

Figure 37 shows that cylinder's maximum non-dimensional amplitude response at center point location reached the value of 4.1 at shaker frequency of 6 Hz for increased shaker frequencies, and reached maximum non-dimensional amplitude response of 3 at shaker frequency of 5 Hz when it was decreased. Experiments were conducted three times to see if this result represents a pure and stable response of the test cylinder to the base excitation. Interestingly, in all cases two different responses were observed for increased and decreased shaker frequencies hence hysteresis. Similar results were also obtained at location $L/4$ from the top (see bottom image in Fig. 37).

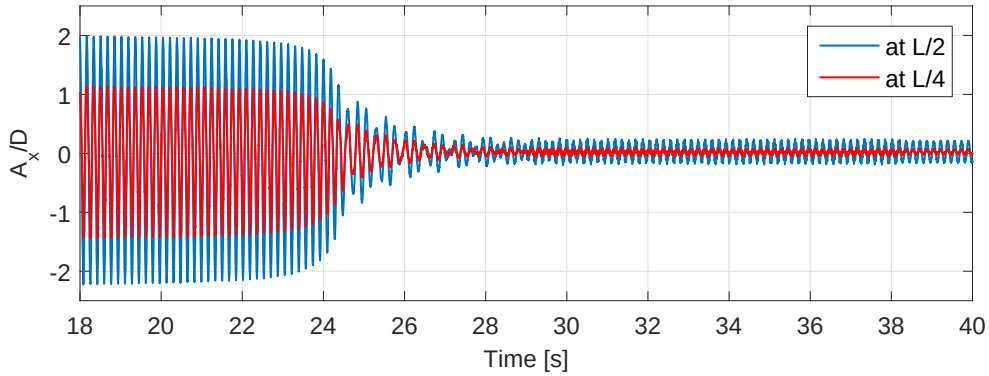

Figure 38: Piezo controlled response with piezo frequency 40 Hz at shaker frequency of 6 Hz. Blue represents the response at cylinder location $L/2$. Red represents the response at cylinder location $L/4$ from the top.

After identifying the maximum shaker response and piezo responses sepa-

rately, additional tests were performed to see if it was possible to trip the frequency of oscillation and decrease the amplitude response. Since cylinder reached the maximum response amplitude at shaker frequency of 6 Hz (increased frequency case), this particular response was chosen to control with the piezo stripes. In the test, cylinder first oscillated at non-dimensional amplitude of 4.1 with shaker frequency of 6 Hz, and then piezo stripe actuators were actuated with a frequency of 40 Hz.

Figure 38 illustrates the cylinder's response at $L/2$ and at $L/4$ after piezo stripes were actuated with frequency of 40 Hz. Initially, the cylinder oscillated with 6 Hz of shaker frequency and maximum non-dimensional amplitude of 4.1, however after the piezo stripes were activated, significant reduction (up to 90 %) in the amplitude was observed.

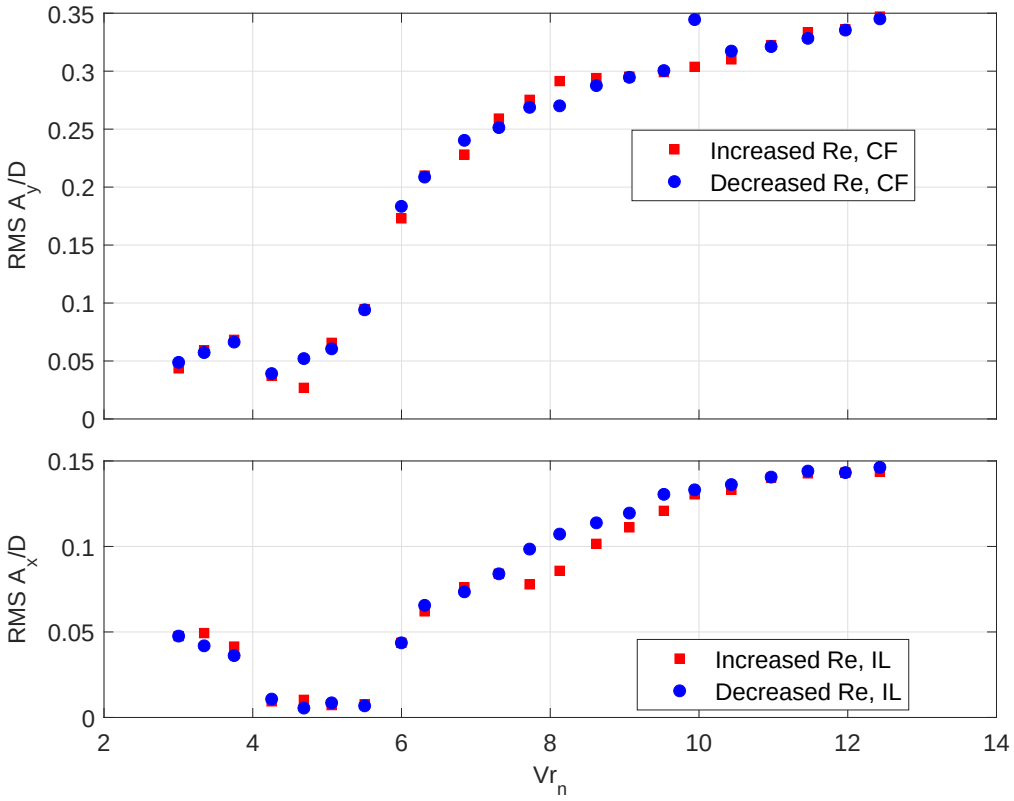

Figure 39: Top image: RMS amplitude response in cross-flow. Bottom image: RMS amplitude response in in-line. Red square represents increased Reynolds number values. Blue circle represents decreased Reynolds number values.

5.4.2 Flow channel experiments

Similar to shaker-rail experiments in air, experiments in re-circulating flow channel were conducted for increased and decreased flow speeds between the Reynolds number values of 900 - 5200.

RMS Amplitude response

Figure 39 shows the rms amplitude response of the test cylinder for increased and decreased Reynolds number values. Top image of Fig. 39 illustrates the cross-flow response amplitudes, and bottom image illustrates the in-line response amplitudes.

According to this amplitude response analysis, three different amplitude responses (or three different response amplitude regimes) were observed. Until the reduced velocity of 4.25, large in-line and cross-flow, between the reduced velocities of 4.25 and 6 very small in-line and cross-flow, and after the reduced velocity of 6, gradually increasing large in-line and cross-flow amplitude responses for all the reduced velocities were tested.

In this set of experiments, mode hysteresis as in Gedikli and Dahl [4] was not observed. However, different amplitude responses were observed at different reduced velocities.

Spanwise motion response

Different rms amplitude response regimes shown in Fig. 39 correspond different spanwise responses. Experiments showed that until the reduced velocity of 4.25 (first rms amplitude response regime), cylinder oscillated similar to first mode (half sinusoidal shape) in both in-line and cross-flow directions. In the second rms amplitude response regime ($Vr_n = 4 - 5.9$), cylinder oscillated similar to second mode (full sinusoidal shape) in in-line with very small amplitude, and first mode

in cross-flow. After the reduced velocity of 6 (at $Vr_n = 6, 6.3, 6.5$), multi-mode (combination of first, second and third mode) with some traveling wave was observed in in-line and similar to first mode shape was observed in cross-flow. Lastly, dominant first mode only response was observed in both in-line and cross-flow directions between the reduced velocities of 7 and 12.5.

Figures 40,41 and 42 show example dynamic responses of the test cylinder in in-line and cross-flow directions at $Vr_n = 3.75, 4.25, 5.5, 6, 6.3$ and 9.53.

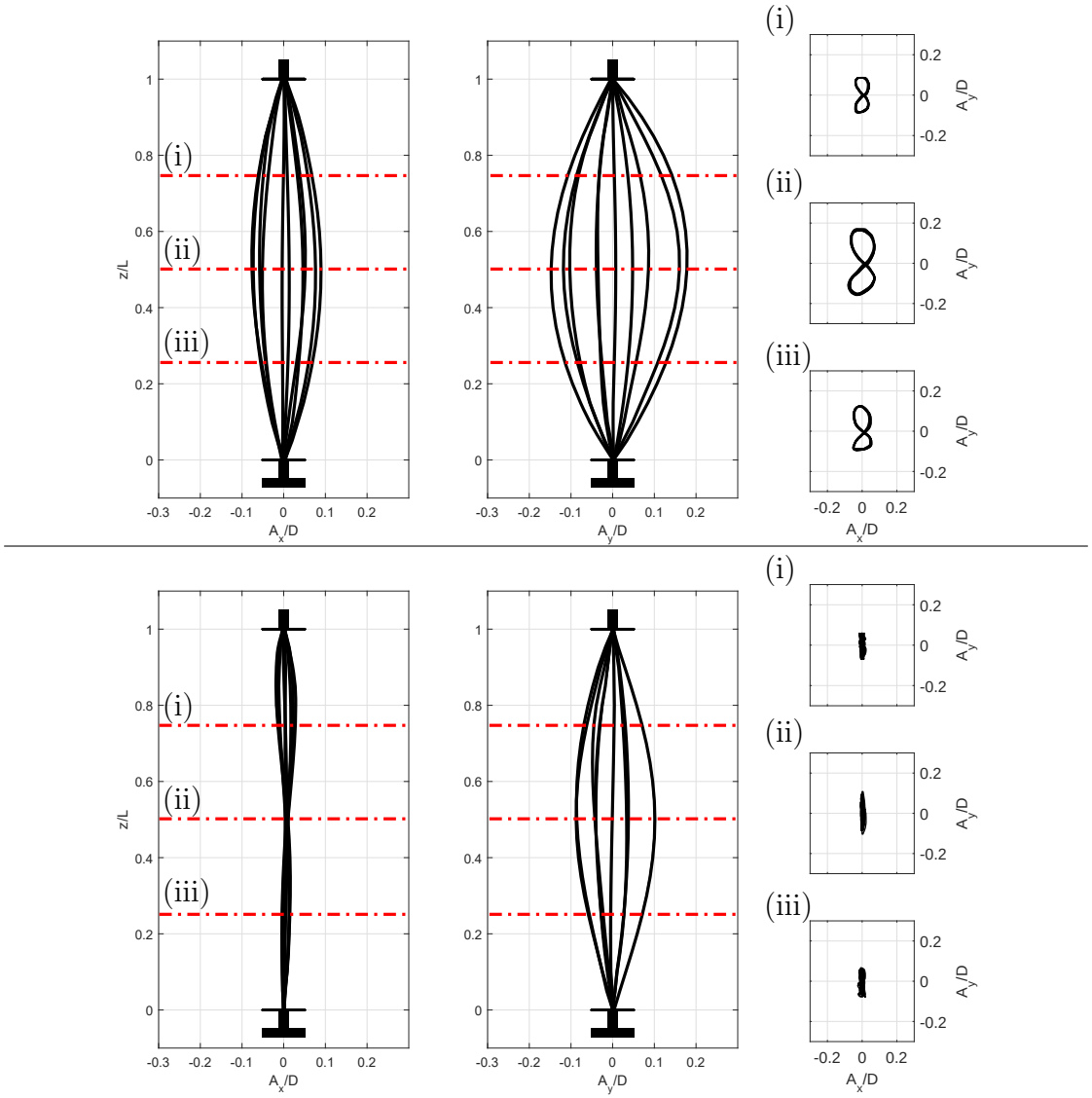

Figure 40: Top image: Maximum motion amplitude at $Vr_n = 3.75$. Bottom image: Maximum motion amplitude at $Vr_n = 4.25$

Top image in Figure 40 displays the dynamic response of the test cylinder at $Vr_n = 3.75$ and corresponding Lissajous shapes at three different locations $(L/4, L/2, 3L/4)$ along the span. At this reduced velocity, maximum amplitude in in-line reached the non-dimensional diameter of 0.2, and maximum amplitude in cross-flow reached the non-dimensional diameter of 0.4. Observed response was similar to first mode in both directions and motion resembled figure eight type of motion across its span. Bottom image in Figure 40 displays the dynamic response of the test cylinder at $Vr_n = 4.25$ and corresponding Lissajous shapes at three different locations along the span. This time, maximum amplitude in in-line switched its spatial mode shape and displayed a mode similar to second mode with smaller maximum amplitude. Cross-flow response displayed a mode shape similar to first mode as the previous case with smaller amplitude. Motion resembled to a line shaped response in cross-flow with very small in-line response.

Top image in Figure 41 shows the dynamic response of the test cylinder at $Vr_n = 5.5$ and corresponding Lissajous shapes at three different locations along the span. At this reduced velocity, very small in-line motion was observed, and maximum cross-flow response reached the non-dimensional diameter of 0.4. Observed response was similar to first mode in cross-flow and total motion resembled to a line shaped response in cross-flow with very small in-line response as in at $Vr_n = 4.25$. Bottom image in Figure 41 displays the dynamic response of the test cylinder at $Vr_n = 6$ and corresponding Lissajous shapes at three different locations along the span. This time, maximum amplitude in in-line switched its spatial mode shape and displayed a mode similar to second mode with traveling wave. Cross-flow response displayed a mode shape similar to first mode as the previous case with larger amplitude. In the experiments, cylinder reached maximum non-dimensional response amplitude of 0.4 in in-line and 0.8 in cross-flow.

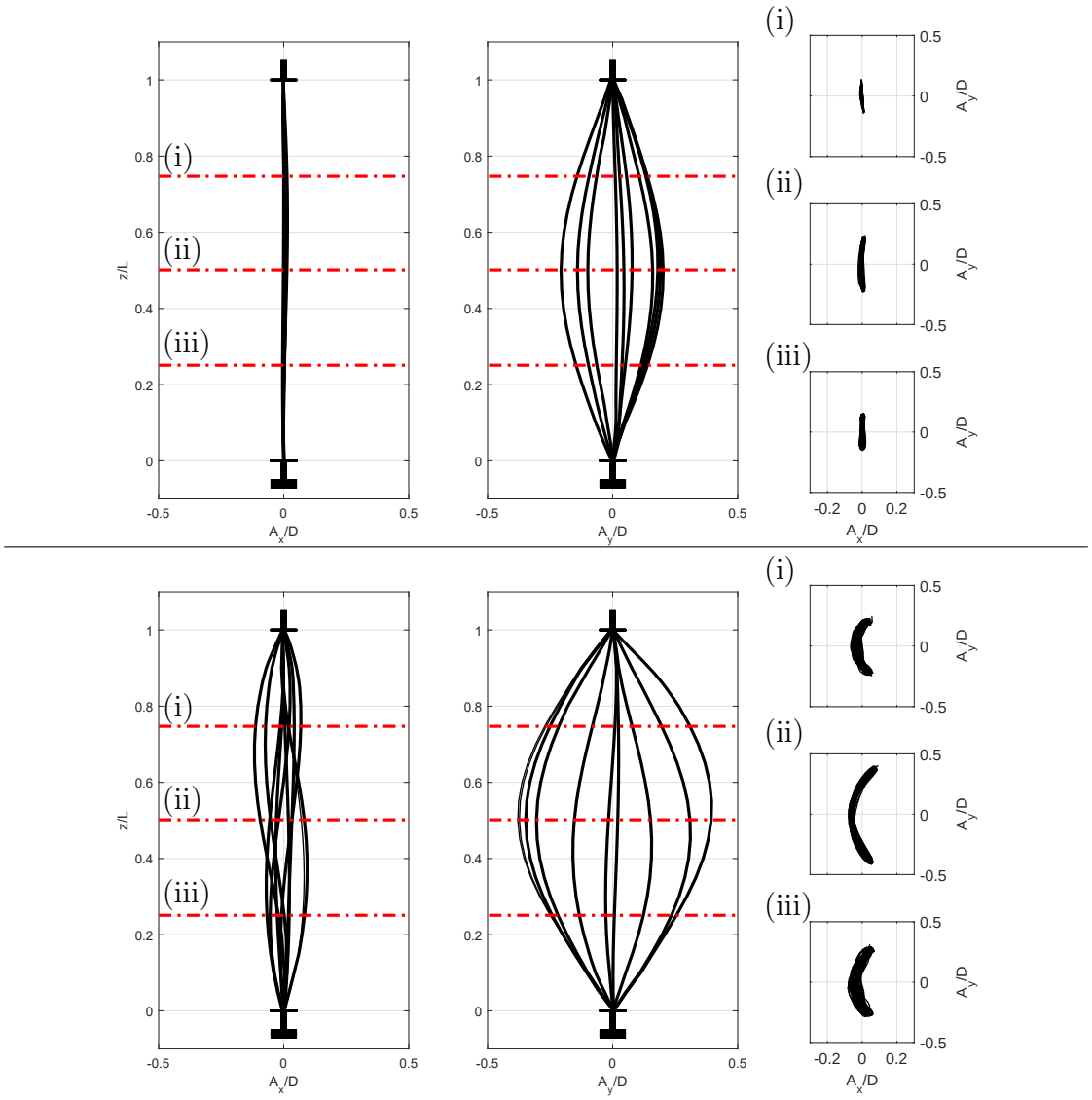

Figure 41: Top image: Maximum motion amplitude at $Vr_n = 5.5$. Bottom image: Maximum motion amplitude at $Vr_n = 6$

Resulting motion resembled to crescent shaped response across the cylinder's span.

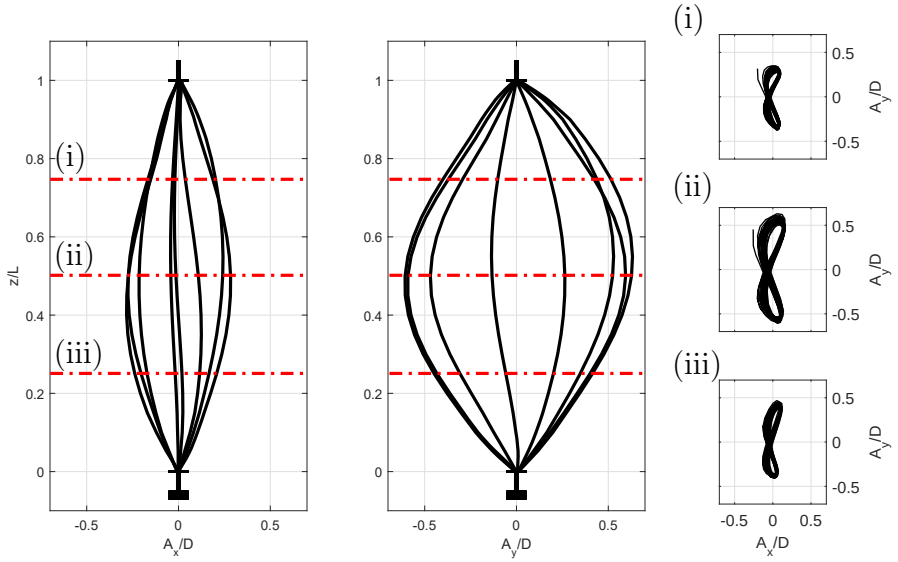

Figure 42: Dynamic response of the test cylinder at $Vr_n = 9.53$ and resulting Lissajous shapes at three different locations across it's span.

Figure 42 shows the dynamic response of the cylinder in in-line and cross-flow at $Vr_n = 9.53$. As mentioned earlier, this motion falls into the regime where first mode is dominant in both directions. At this flow speed, cylinder reached maximum non-dimensional response amplitude of 0.6 in in-line and 1.3 in cross-flow, and response shape resembles to first mode in both directions, resulting in a figure eight type of response.

Frequency analysis

Frequency analysis was carried across the cylinder's span for all the flow speeds tested. In this paper, focus was given to the individual reduced velocities that have been introduced in the previous section.

Left image in Figure 43 illustrates the spanwise frequency response of the cylinder in in-line and right image illustrates the spanwise frequency response in cross-flow at $Vr_n = 3.75$. In both images, frequency response was distributed similar to modal response (first mode) with frequency ratio of 2:1 (in-line:cross-

flow).

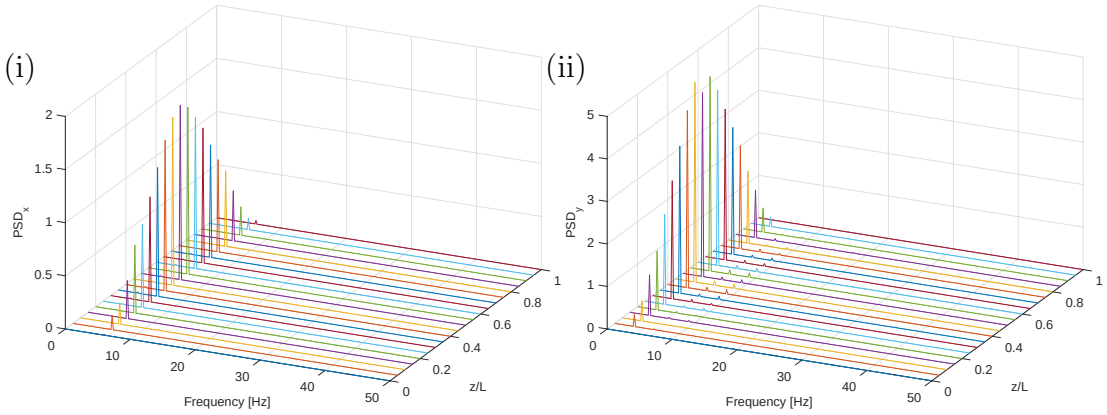

Figure 43: Frequency response along the span at $Vr_n = 3.75$. (i) In-line frequency response. (ii) Cross-flow frequency response.

Left image in Figure 44 illustrates the spanwise frequency response of the cylinder in in-line, and right image illustrates the spanwise frequency response in cross-flow at $Vr_n = 4.25$. As mentioned earlier, cylinder displayed a motion similar to second mode in in-line and first mode in cross-flow at this reduced velocity. Spanwise frequency plot at this flow speed demonstrates a similar behavior; the amplitude of the frequency distribution in in-line resembles to second mode with a constant frequency of 10.4 Hz. Again, cross-flow frequency distribution is similar to first mode with frequency of 3.5 Hz. So, different than the previous case, in-line to cross-flow frequency ratio is constant with a value 3:1. It should be noted that, this motion at $Vr_n = 4.25$ comes right after the cylinder's motion at $Vr_n = 3.75$, which means that when cylinder changes its spanwise response from first mode to second mode in in-line, in-line to cross-flow frequency ratio suddenly changes from 2:1 to 3:1.

Left image in Figure 45 illustrates the spanwise frequency response of the cylinder in in-line and right image illustrates the spanwise frequency response in cross-flow at $Vr_n = 5.5$. As shown in the top image of Figure 41, cylinder displayed very small motion in-line and first mode type of behavior in cross-flow. In-line

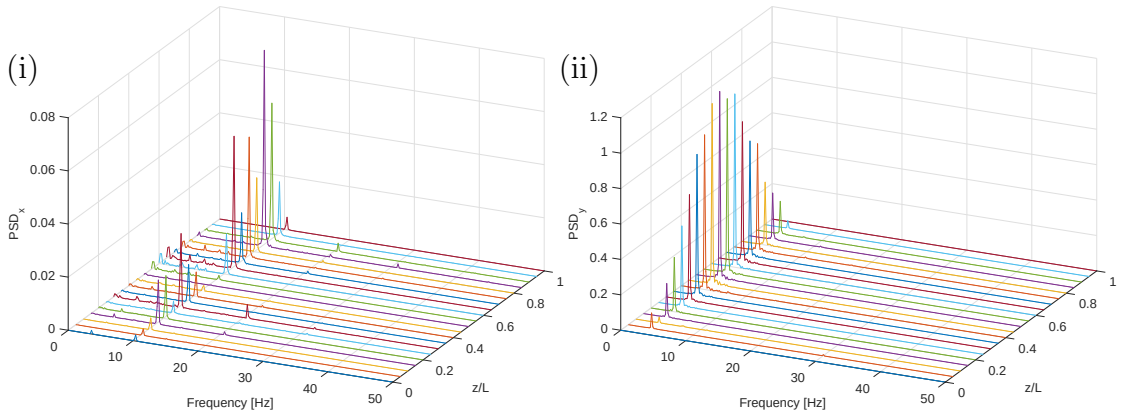

Figure 44: Frequency response along the span at $Vr_n = 4.25$. (i) In-line frequency response. (ii) Cross-flow frequency response.

spanwise frequency plot at this flow speed produces a noisy response due to very small in-line motion, but frequencies are distributed along the span at reduced velocities of 4.5, 8.9, and 11.3, respectively. Cross-flow frequency distribution across the span is constant with a value of 4.5 Hz.

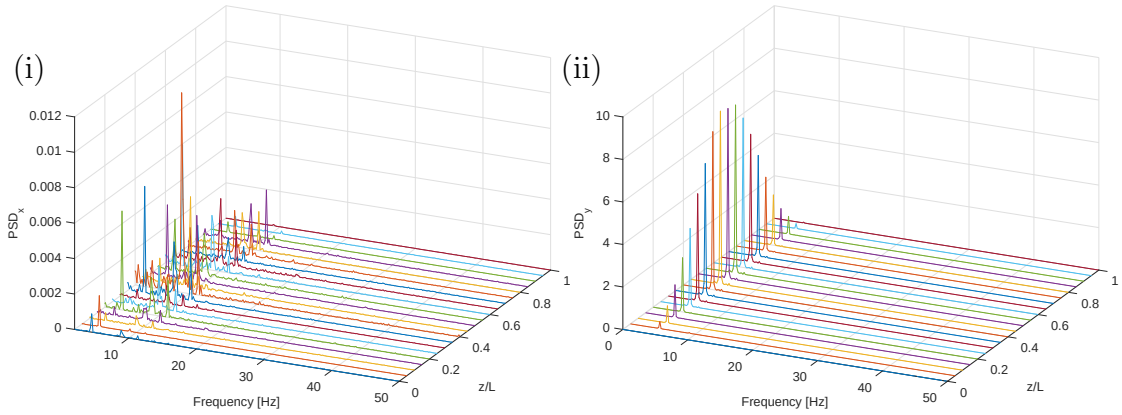

Figure 45: Frequency response along the span at $Vr_n = 5.5$. (i) In-line frequency response. (ii) Cross-flow frequency response.

Left image in Figure 46 illustrates the spanwise frequency response of the cylinder in in-line and right image illustrates the spanwise frequency response in cross-flow at $Vr_n = 6$. As shown in the bottom image of Figure 41, the cylinder displayed multi-mode type of behavior in in-line with some traveling wave and first mode type of behavior in cross-flow. In-line spanwise frequency plot at this

flow speed has a frequency distribution similar to first mode with larger frequency amplitudes at frequency of 8.7 Hz, and there is also contribution of higher order frequency content at 12.3 Hz with a frequency distribution similar to second mode. However, at 12.3 Hz, the amplitudes of the frequency distribution are much smaller than the ones at 8.7 Hz. Cross-flow frequency distribution across the span is constant with a value of 4.35 Hz which again yields a 2:1 (in-line:cross-flow) frequency ratio if dominant frequencies are taken into consideration.

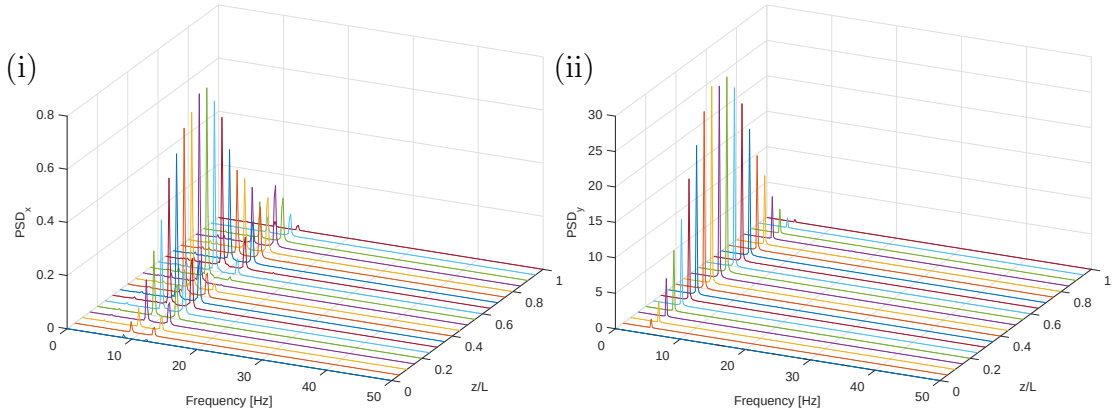

Figure 46: Frequency response along the span at $Vr_n = 6$. (i) In-line frequency response. (ii) Cross-flow frequency response.

Left image in Figure 47 illustrates the spanwise frequency response of the cylinder in in-line and right image illustrates the spanwise frequency response in cross-flow at $Vr_n = 9.53$. At this particular flow speed, cylinder oscillated similar to first mode in both in-line and cross-flow directions (see Fig. 42). Spanwise frequency response distribution displays a similar behavior; it has a large amplitude frequency at the center and small amplitude responses at the edges with a constant frequency of 13.4 Hz in in-line and 6.6 Hz in cross-flow.

5.4.3 Active control with piezo actuator
Vibration suppression

In the tests, in-line mode shapes were varied significantly within the flow speed range tested whereas no significant mode shape variation was observed in

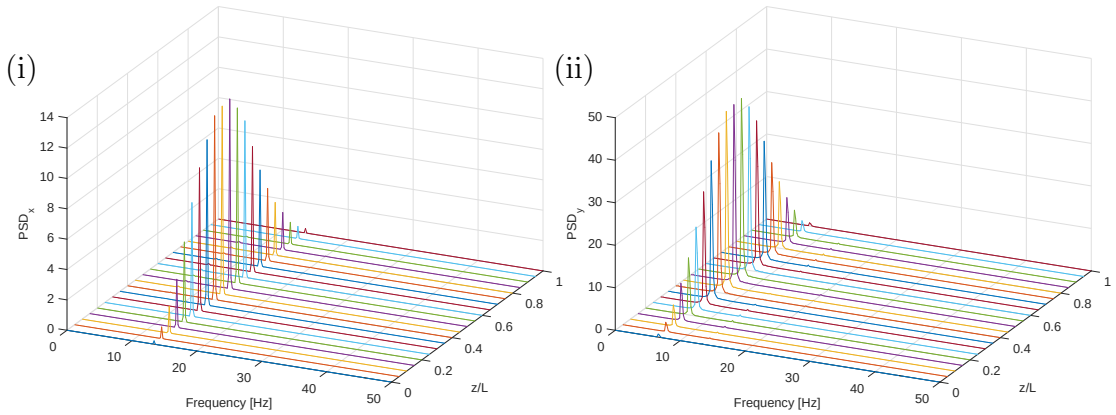

Figure 47: Frequency response along the span at $Vr_n = 9.53$. (i) In-line frequency response. (ii) Cross-flow frequency response.

the cross-flow direction. Different dominant in-line mode responses were observed at low reduced velocity values up to 6.5 where cylinder oscillated with first mode, second mode and some combination of first and second mode with a traveling wave. Then at higher flow speeds, modal response was settled having a first mode shape. On the contrary, spatial cross-flow response was always similar to dominant first mode within the same flow speed range.

Since the apparent mode switch was occurred in the in-line direction between the reduced velocity of 3.75 and 4.25, we chose the motion at $Vr_n = 3.75$ as an example illustration. At this flow speed, cylinder has large in-line and cross-flow oscillations.

Figure 48 shows the original (black) and piezo activated (red) response plots at the reduced velocity of 3.75 and corresponding Lissajous shapes at locations $L/4, L/2$ and $3L/4$. In the tests, piezo frequency was actuated at 40 Hz since the maximum response had occurred at this frequency as shown in shaker-rail experiments (see Fig. 37). Experiments showed that after the piezo activated, it resulted in a dramatic mode change and significant reduction in both in-line and cross-flow motion of the body (75% in cross-flow only). Also, natural figure eight type of response changed to very small cross-flow response across the span.

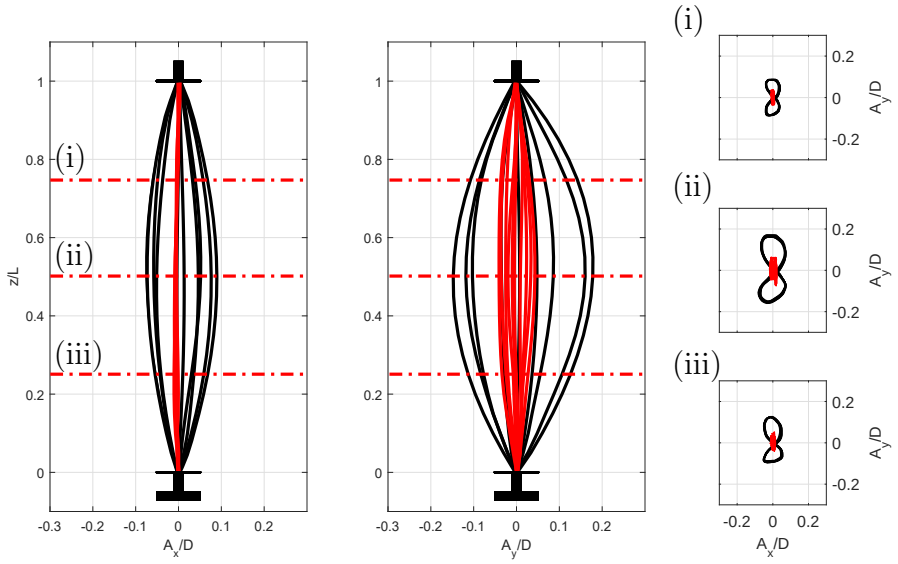

Figure 48: Piezo activated dynamic response of the test cylinder at $Vr_n = 3.75$ and resulting Lissajous shapes at three different locations across it's span. Black motion response indicates the motion before the piezo actuation, and red motion response indicates the motion after the piezo actuation.

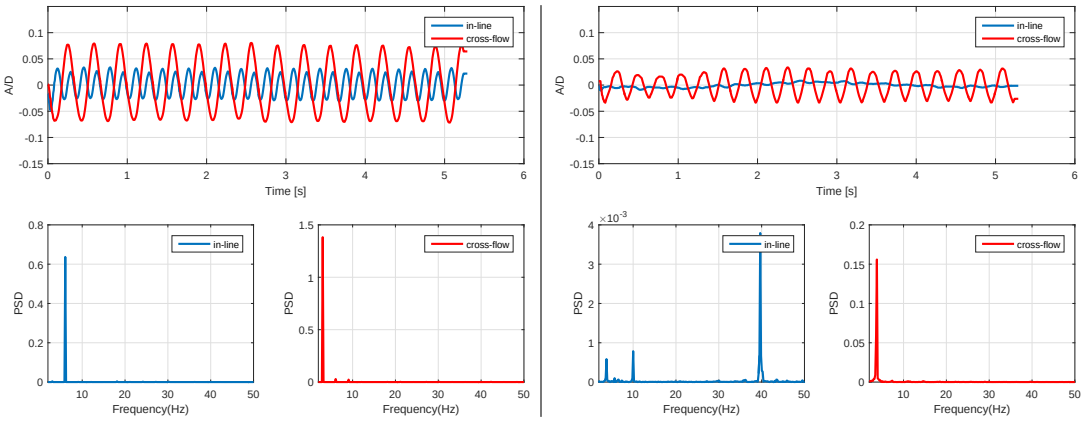

Figure 49: Left image: Time history and frequency response at $Vr_n = 3.75$. Right image: Time history and frequency response at $Vr_n = 4.25$. Data represents the point at $L/4$ from the top.

Left image in Figure 49 shows the time history and frequency response of the original motion of the cylinder at $Vr_n = 3.75$. As seen, cylinder oscillates with frequency of 3 Hz in cross-flow, and with 6 Hz in in-line causing cylinder to have 2:1 (in-line:cross-flow) frequency ratio. Right image in Figure 49 shows the time history and frequency response of the piezo activated cylinder's response. Resulting dominant in-line frequency was 40 Hz which was the piezo frequency, but cross-flow frequency was 3.8 Hz. In these plots, the motion data represents the point at $L/4$ from the top.

Vibration enhancement

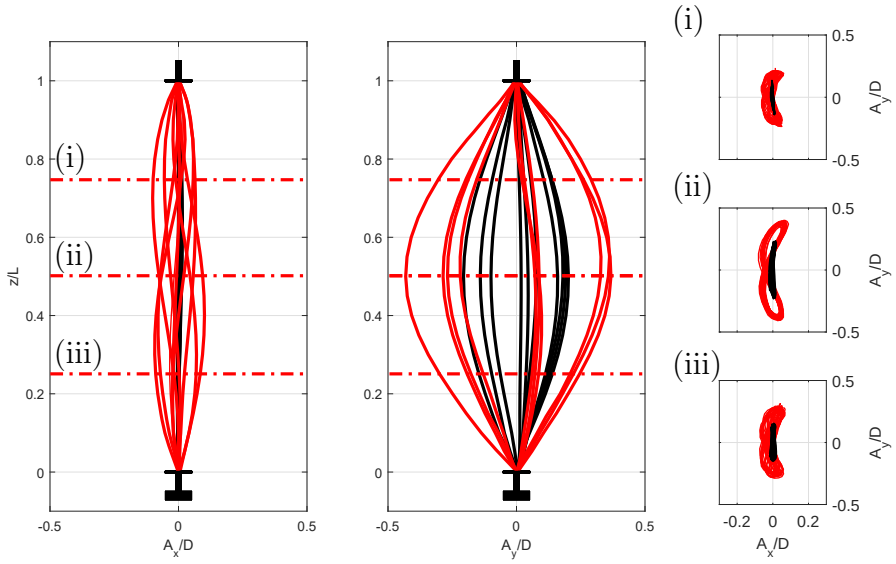

Figure 50: Piezo activated dynamic response of the test cylinder at $Vr_n = 5.5$ and resulting Lissajous shapes at three different locations across it's span. Black motion response indicates the motion before the piezo actuation, and red motion response indicates the motion after the piezo actuation.

Figure 39 showed that there is an apparent amplitude jump after $Vr_n = 5.5$ from low RMS amplitude of 0.1 to large amplitude of 0.17 in cross-flow and from very little motion of 0.01 to 0.05 in in-line. Since the apparent mode increase was occurred between the reduced velocity values of 5.5 and 6, we chose the motion at $Vr_n = 5.5$ as an example illustration. At this flow speed, cylinder has very small

in-line motion and large cross-flow motion.

Figure 50 shows the original (black) and piezo activated (red) response plots at the reduced velocity of 5.5, and corresponding Lissajous shapes at locations $L/4, L/2$ and $3L/4$. Similar to previous vibration suppression method, piezo frequency was actuated at 40 Hz since the maximum response had occurred at this frequency (see Fig.37). Experiments showed that, after piezo activated, it resulted in a dramatic amplitude increase in both in-line and cross-flow motion of the body (100% in cross-flow). Also, the natural response of the body switched from small only cross-flow response to large tilted figure eight type of response.

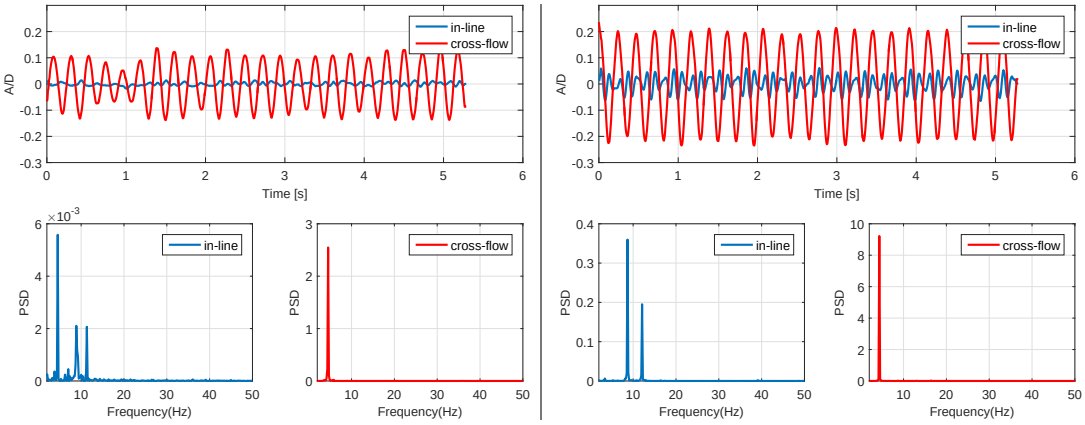

Figure 51: Left image: Original time history and frequency response at $Vr_n = 5.5$. Right image: Piezo actuated time history and frequency response at $Vr_n = 5.5$. Data represents the point at $L/4$ from the top.

Left image in Figure 51 shows the time history and frequency response of the original motion of the cylinder at $Vr_n = 5.5$. As seen, cylinder oscillates with frequency of 4.35 Hz in cross-flow, and with frequencies 4.5, 8.9, and 11.3 Hz in in-line. Right image in Figure 51 shows the time history and frequency response of the piezo activated cylinder's response. Resulting dominant in-line frequency was 8.7 with an additional frequency contribution at 12.1 Hz, and cross-flow frequency was 4.5 Hz. In these plots, the motion data represents the point at $L/4$ from the top.

5.5 Discussion

Current study can be discussed based on two different aspects: first, the cylinder's dynamic response without piezo actuation, and second, active control of flexible cylinder through the use of piezo actuators.

5.5.1 Multimode in-line and traveling wave response

Dynamic response of the beam-dominated cylinder experiments showed that an asymmetric response (even mode excitations) is possible in in-line at low Reynolds number values despite the earlier findings of [4, 3, 16]. However, it is important to remember that even though cylinder is attached symmetrically at the top and bottom of the cylinder, piezo attachment and cable connections within the cylinder provide an asymmetric mass distribution which in turn breaks the total symmetric fluid loading on the cylinder. Therefore, natural symmetric loading provided by the recirculating uniform flow channel does not exist in this set-up.

In the tests, at low reduced velocity values, cylinder oscillated with different in-line motions while keeping the cross-flow response constant at first mode. Frequency of these low reduced velocity motions showed that despite the fact that cylinder oscillated with 2:1 (in-line:cross-flow) mode shape, motion settled with 3:1 (in-line:cross-flow) frequency ratio at all the 2:1 modal responses. This observation is significant, because it shows that multi-mode in-line oscillations may be associated with a different frequency ratio which in the current tests is 3:1. This is a common result of highly non-linear flexible cylinder responses in VIV.

To explain such relationship, interaction of in-line and cross-flow responses can be investigated. Figure 52 shows the relationship between normalized vortex shedding frequency and the normalized reduced velocity in the current tests. Generally, a cylinder undergoing VIV oscillates with the shedding frequency in cross-flow and

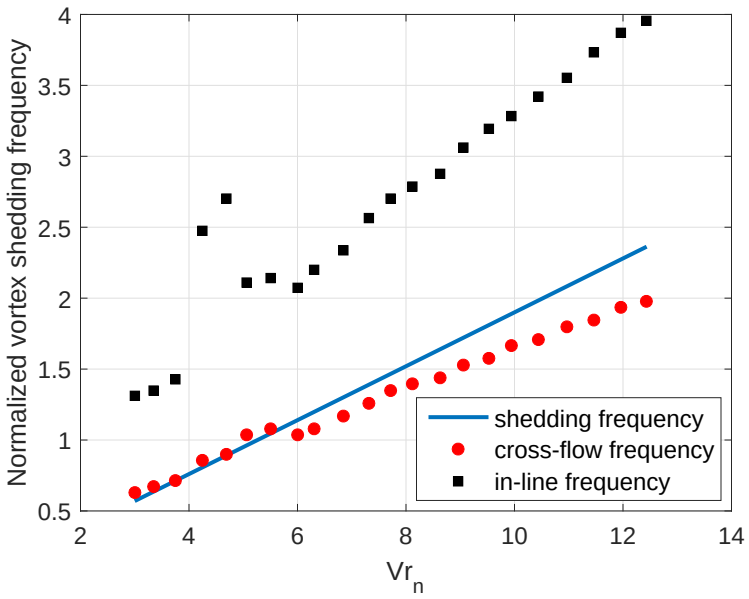

Figure 52: Plot of normalized vortex shedding frequency versus normalized reduced velocity (Vr_n). Vortex shedding frequency (StU/D) is normalized with the first natural frequency in water where shedding frequency is the assumed shedding frequency based on cylinder St.

twice the shedding frequency in in-line. However, non-linear interactions between in-line and cross-flow may produce an excitation in in-line which is the sum of the in-line excitation (twice shedding frequency) and cross-flow (shedding frequency) excitation; namely, three times the shedding frequency. In the current tests, this result has been observed for the reduced velocity values of 4.25 and 4.7 and caused cylinder to have large cross-flow response with very small in-line response (i.e., motion resembles to a line motion in cross-flow with very small in-line motion). Traveling wave is another result of such interaction. Between the normalized reduced velocities of 6 and 7, cylinder oscillated with one dominant frequency in cross-flow which is close to the shedding frequency (see Fig. 52), and two frequencies in in-line, in which case one of them is twice the shedding frequency hence excitation frequency (see Fig.46), and another one is three times the shedding frequency which is caused by the non-linear interaction between in-line and cross-

flow. Figure 53 shows such example traveling wave at $Vr_n = 6$ that is bouncing at the top and bottom of the cylinder in in-line direction and cross-flow response is similar to standing wave response. Resulting motion is similar to crescent shape across cylinder's span (see Fig. 41).

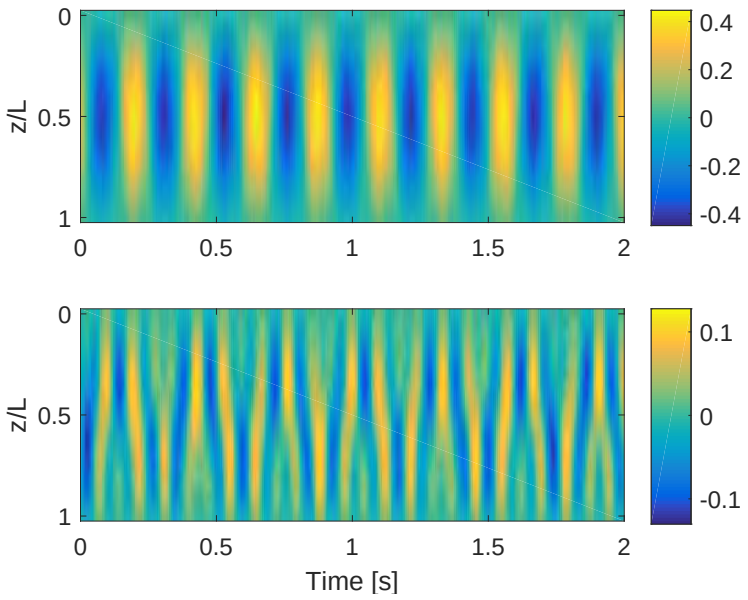

Figure 53: Time history of the spanwise response at $Vr_n = 6$. Top image: First mode standing wave in cross-flow. Bottom image: Second mode with traveling wave in in-line.

5.5.2 Active control in VIV

Understanding the motion of flexible cylinders undergoing vortex-induced vibrations and being able to control them are of utmost importance to the offshore industry. In terms of controlling the motion, different methods were explained in Section 5.1. In the current study, focus was given to understanding the modal interactions and controlling the motion through controlling the mode variations.

The main observation from the present experiments is that in uniform flow conditions, cylinder could excite with different modes in in-line direction keeping the cross-flow motion constant at first mode, and these mode variations in in-line

may be controlled through the use of piezo stripe actuators.

Previously, Baz and Kim [10] used a flexible cylinder with clamped-free boundary condition in air and bonded the piezo actuators at the bottom of the cylinder to control the dominant mode of vibration. Later, Cheng et al. [9] used piezo actuators as an external energy source on a rigid square cylinder which was allowed to move only in cross-flow direction in air. In the current study, the experimental approach to control the VIV response was carried out in two ways: 1) piezo stripe actuators were activated before a spatial mode change thus tripping the frequency and forcing the cylinder to excite with a higher mode hence vibration suppression, 2) piezo actuators were activated right before and apparent amplitude increase, thus forcing the cylinder to jump to higher amplitude response regime hence vibration enhancement.

Results of this study show that a flexible cylinder vibration in VIV can be significantly reduced through spatial mode change. In the experiments, piezo excitation provided additional energy input in in-line and forced cylinder to change it's spatial mode shape. Since the cylinder's response was coupled both in in-line and cross-flow, this approach resulted a large amplitude decrease in cross-flow as well. However, it should be emphasized that in-line response was selected to control the motion since controlling the in-line response is easier than cross-flow. It is easier because mode variations appears at low flow speeds and therefore there is less drag contribution in the direction of fluid flow. In addition to vibration suppression, similar analogy was used for vibration enhancement so that piezo actuators were activated before an apparent amplitude jump, thus forcing the cylinder to jump to higher amplitude response regime.

5.6 Acknowledgment

The authors gratefully acknowledge support for this work from the Office of Naval Research (grant N00014-16-1-2968, PM Kelly Cooper)

List of References

[1] J. Dahl, F. Hover, M. Triantafyllou, S. Dong, and G. Karniadakis, "Resonant vibrations of bluff bodies cause multi-vortex shedding," *Physical Review Letters*, vol. 99, no. 144503, 2007.

[2] Y. Modarres-Sadeghi, H. Mukundan, J. Dahl, F. Hover, and M. Triantafyllou, "The effect of higher harmonic forces on fatigue life of marine risers," *Journal of Sound and Vibration*, vol. 329, no. 1, pp. 43–55, 2010.

[3] E. D. Gedikli, J. M. Dahl, and D. Chelidze, "Multivariate analysis of vortex-induced vibrations in a tensioned cylinder reveal nonlinear modal interactions," in *10th International Conference on Structural Dynamics*. Eurodyn, 2017.

[4] E. D. Gedikli and J. M. Dahl, "Mode excitation hysteresis of a flexible cylinder undergoing vortex-induced vibrations," *Journal of Fluids and Structures*, vol. 69, pp. 308 – 322, 2017. [Online]. Available: http://www.sciencedirect.com/science/article/pii/S0889974616303188

[5] R. D. Blevins, *Flow Induced Vibrations*, 2nd ed. Van Nostrand Reinhold Company, New York, NY, 1990.

[6] M. Zdravkovich, "Review and classification of various aerodynamic and hydrodynamic means for suppressing vortex shedding," *Journal of Wind Engineering and Industrial Aerodynamics*, vol. 7, no. 2, pp. 145 – 189, 1981. [Online]. Available: http://www.sciencedirect.com/science/article/pii/0167610581900362

[7] M. F. Unal and D. Rockwell, "On vortex formation from a cylinder. part 2. control by splitter-plate interference," *Journal of Fluid Mechanics*, vol. 190, p. 513 529, 1988.

[8] J. F. Wilson and J. C. Tinsley, "Vortex load reduction : Experiments in optimal helical strake geometry for rigid cylinders," *Journal of Energy Resources Technology*, vol. 111, p. 72 76, 1989.

[9] L. Cheng, Y. Zhou, and M. Zhang, "Perturbed interaction between vortex shedding and induced vibration," *Journal of Fluids and Structures*, vol. 17, no. 7, pp. 887 – 901, 2003. [Online]. Available: http://www.sciencedirect.com/science/article/pii/S0889974603000422

[10] A. Baz and M. Kim, "Active modal control of vortex-induced vibrations of a flexible cylinder," *Journal of Sound and Vibration*, vol. 165, no. 1, pp. 69 – 84, 1993. [Online]. Available: http://www.sciencedirect.com/science/article/pii/S0022460X83712435

[11] J. F. Williams and B. Zhao, "The active control of vortex shedding," *Journal of Fluids and Structures*, vol. 3, no. 2, pp. 115 – 122, 1989. [Online]. Available: http://www.sciencedirect.com/science/article/pii/S0889974689900261

[12] S. Rashidi, M. Hayatdavoodi, and J. A. Esfahani, "Vortex shedding suppression and wake control: A review," *Ocean Engineering*, vol. 126, pp. 57 – 80, 2016. [Online]. Available: http://www.sciencedirect.com/science/article/pii/S0029801816303675

[13] M. M. Bernitsas, K. Raghavan, Y. Ben-Simon, and E. Garcia, "Vivace (vortex induced vibration aquatic clean energy): A new concept in generation of clean and renewable energy from fluid flow," *Journal of offshore mechanics and Arctic engineering*, vol. 130, no. 4, p. 041101, 2008.

[14] A. Mehmood, A. Abdelkefi, M. Hajj, A. Nayfeh, I. Akhtar, and A. Nuhait, "Piezoelectric energy harvesting from vortex-induced vibrations of circular cylinder," *Journal of Sound and Vibration*, vol. 332, no. 19, pp. 4656 – 4667, 2013. [Online]. Available: http://www.sciencedirect.com/science/article/pii/S0022460X13003192

[15] E. D. Gedikli, "Experimental invastigation of low mode number cylinders subjected to vortex-induced vibrations," Master's thesis, University of Rhode Island, USA, 2014.

[16] J. Vandiver and J.-Y. Jong, "The relationship between in-line and cross-flow vortex-induced vibration of cylinders," *Journal of Fluids and Structures*, vol. 1, no. 4, pp. 381–399, 1987.

CHAPTER 6

Concluding remarks

6.1 Dynamic and wake response analysis of vortex-induced vibration of flexible cylinders

Motivation: A large majority of past research on VIV has characterized the behavior of rigid cylinder undergoing VIV to classify fundamental characteristics of this phenomenon. However, there are not many studies characterizing the behavior of a flexible cylinder in ocean, which is a more realistic representation of an offshore structure. This study focuses on this nonlinear fluid structure interaction, with emphasis on understanding the physics underlying VIV, nonlinear dynamics and their applications towards developing mathematical tools for VIV prediction.

Methodology: Focus is given to understand the dynamic response of tensioned and bending dominated flexible cylinders. Flexible cylinder fluid-structure interactions are analyzed using high-speed cameras. This approach allow to characterize spatial mode shapes, and show how they change depending on the flow speeds. In addition, a novel experimental system is designed to connect wake and structural responses in an attempt to understand complex coupled fluid-structure interactions (see Appendix A).

Major contributions:

- Dynamic response of flexible cylinder experiments showed that, a flexible cylinder can have different amplitude and modal responses at the same Reynolds number values depending on increased and decreased flow speeds. More importantly, it is found that there is a hysteretic region, which is governed by both the wake and the structural characteristics, affects the mode shape (the idea of mode hysteresis), frequency characteristics and amplitude response. This result is significant, because previously proposed prediction

methods and computational approaches to the problem indicated that there should not be any hysteretic response in the same parametric region. This indicates that the problem is very complicated and fluid-structure interaction depends on many variables; simplified predictions are not always a reliable source and need to be updated with the current findings.

- It is observed that if a cylinder is attached horizontal to the incoming flow under uniform flow conditions such that drag load is distributed symmetrically across cylinder's span, cylinder is unable to sustain an asymmetric excitation (even mode excitation) in in-line direction.

- A carriage mechanism is developed and an experimental procedure is introduced to create a three-dimensional reconstruction of cylinder's wake. Using this system, stereoscopic PIV measurement of velocity field at various two-dimensional slices along the cylinder length was obtained. Then, applying phase averaging method, three-dimensional wake response is reconstructed (see Appendix A).

- It is shown that a flexible cylinder can have different responses than expected in VIV due to nonlinear fluid-structure interactions. To build off of previous research, multivariate analysis methods are applied to identify nonlinear mode interactions in the flexible cylinder's response. It is found that specific mode combinations on a flexible cylinder are likely to produce figure eight type of motions.

- The idea of being unable to sustain asymmetric modes in a uniform flow is investigated through molding beams into the cylinders. In the tests, three bending-dominated cylinders are tested with varying stiffness in the cross-flow and in-line directions of the cylinder in order to produce varying struc-

tural mode shapes associated with a fixed 2:1 (in-line:cross-flow) natural frequency. Both analytic and experimental results confirm that cylinder is unlikely to oscillate with an even mode shape if the loading is distributed symmetrically across the cylinder's length.

6.2 Active control of flexible cylinders undergoing vortex-induced vibrations using piezo stripe actuators

Motivation: To build off of the previous work, active control of flexible cylinders is considered.

Suppression of the VIV is a major concern for the offshore industry since large VIV motions may give significant damage to the structures. These structures include but not limited to deep water offshore risers, long underwater cables or offshore wind turbines. The scientific question we are trying to answer is "Can we apply control strategy to avoid high fatigue conditions from vibrations by altering which mode is being excited?".

Methodology: This research includes active control of flexible cylinders undergoing VIV using piezo-stripe actuators that are bonded at the anti-nodes of a flexible cylinder to control low vibration modes (i.e. first, second and third) in the in-line direction. The goal is to change the spatial mode shape of a cylinder through the activation of piezo-stripe actuators which may result either an increase (vibration enhancement) or decrease (vibration suppression) in the amplitude response.

Major contributions:

- Using multiple actively controlled piezo actuators has been demonstrated to be effective at both changing the excited mode and reducing the response undergoing flow-induced vibrations (vibration suppression). Experiments show that upto 75% amplitude reduction is possible in cross-flow direction using

this method.

- It is observed that significant vibration enhancement in the amplitude is also possible if there is an apparent jump in the amplitude response within the tested flow speed range.

- Control method is observed to work for both high (air) and low (water) mass ratio systems. Therefore, the application of this method can be extended to be used in different industries such as defense industry or renewable energy industry.

6.3 Future work

In this dissertation, vortex-induced vibration of flexible cylindrical structures was studied. Focus was given to understand the dynamic response of flexible structures, non-linear modal interactions and how to control them to prevent and/or suppress large VIV motions. While this dissertation has provided valuable insights on the response of flexible structures, and active control methods, many opportunities for extending the scope of this dissertation remain. This section presents some of these directions.

- To have a broader understanding of the modal interactions, higher order modes should be studied. Investigating the additional modes will certainly help to understand the effect of mode shape to the total oscillation since real structures have very high mode numbers.

- Wake measurements should be done across the cylinder's span along with the dynamic response measurements. This will help to characterize the wake and help to understand complex coupled fluid-structure interactions.

- When using the optical methods for dynamic response analysis, additional

sensors (i.e., accelerometers, strain gauges) can be embedded into the structures for comparison, and these sensors can provide a direct measurement of the fluid forces at that sensor location. Therefore, fluid force estimations across the cylinder can be updated using these results.

- Multivariate methods were shown to be very effective identifying non-linear modal interactions in VIV. These methods can be applied to the wake to create a mapping of the non-linear empirical modes of the wake. Resulting motions can be used to construct a non-linear fluid force model for vortex-induced vibration prediction.

- Piezo stripe actuators used for active mode control is not the best stripe actuators, and does not provide a lot of energy to the structure due to low amplitude response. However, using a strip actuator that have a larger amplitude response can provide more energy to the structural response, and may cause a mode change for a broader range of reduced velocity values.

- In this study, piezoelectric patches were attached to a beam in the in-line direction. However, piezo control orientation can be altered and be applied in cross-flow direction or both in in-line and cross-flow directions. Therefore, one can have flexibility to change a mode in the desired direction.

- A computational model can be developed based on the active-control-experiments to predict VIV.

- Flow visualization of the wake can be done along with the piezo control experiments to fully characterize the fluid-structure-piezo interaction.

- Passive control can be applied using an electrical circuit to damp the oscillations through electro-mechanical coupling.

- In a broad range of reduced velocities, cross-flow amplitude is the largest amplitude for a cylinder response, and recently, the addition of in-line is found to increase the total response amplitudes. Therefore, one can extract more energy from vibrations of flexible structures and convert it to electrical power. Therefore, similar to the proposed method in Chapter 4 for active control, piezoelectric patches can be used for energy harvesting from flexible cylinders.

APPENDIX A

3D flow visualization of the wake of a flexible cylinder undergoing vortex-induced vibrations using digital particle image velocimetry

by

Ersegun Deniz Gedikli* and Emma Thomas ** and Jason Dahl*

*Department of Ocean Engineering, University of Rhode Island, Narragansett, RI 02882, USA

**Department of Physics, University of Massachusetts, Amherst, MA 01003, USA

Published in SURFO Technical Report No. 15-01 (2015)

This appendix includes an updated version of the above report that introduces a novel experimental system to connect the wake and the structure.

Abstract

Vortex-induced vibrations (VIV) have been studied for years due to problems they pose for marine structures that make use of long, cylindrical cables such as oil rigs and offshore wind energy systems. Due to the high cost and difficult implementation of obtaining 3D datasets, the wake of a cylinder undergoing VIV has typically been visualized using seperate 2D slices oriented perpendicular to the vibrating cylinder. This method is limited to detecting vorticity within the sampled plane, and only provides data representing a single location along its length. In order to create a 3D reconstruction of such a cylinder's wake, we used Stereoscopic Digital Particle Image Velocimetry (DPIV) to obtain 2D vorticity fields of the flow at several different locations. Since the slices were recorded at different times, motion tracking of the cylinder was used to find the periodicity of the vibrations, allowing both the cylinder's motion and the shape of the water flow to be averaged across many cycles (or phase-averaged). Slices of the wake are recorded at 20 locations, spaced 1 cm apart along a cylinder with a diameter of 0.635 cm. Currently, a phase-averaged wake representing a typical cycle has been assembled using the z-component of vorticity, as in previous 2D experiments. The methods developed here, however, may be used to find vortices in other directions, and will ultimately allow for more accurate analysis of a range of similar experiments aimed at characterizing the shape of the wake of a flexible cylinder undergoing VIV.

A.1 Introduction

Both the durability and cost-effectiveness of marine structures including offshore oil rigs and wind energy systems, tow lines, and mooring lines stand to be improved by a more comprehensive understanding of Vortex-Induced Vibrations. The problem of VIV includes many different interrelated issues, including the mode shape and frequency of the cylinder, the pattern of the wake it creates, the forces

acting between the cylinder and the fluid, and how all of these are connected to one another. The shape of the 2D wake, specifically, has been studied extensively, resulting in the classification of vortex shedding modes [1]. Many different methods have been explored, from smoke visualizations [2] to DPIV. Other experiments such as [3] have used motion tracking software to visually track features on the cylinder, while yet others, e.g. [4], make use of accelerometers and load meters to simultaneously track the cylinder and its wake. What the majority of experimental studies have in common is that they only present 2D information on the wake at any moment in time, and as such mostly deal with vorticity in only one direction (usually parallel to the cylinder).

There are multiple techniques used to obtain similar data in three dimensions, such as Volumetric 3D Velocimetry [5], which requires a specialized triple-aperture camera, and the hydrogen bubble method [6], which uses bubbles generated by the cylinder itself. Stereoscopic DPIV, a technique already widely used to obtain data within a 2D plane, has the potential to provide a 3D visualization across larger volumes and without extra equipment.

DPIV is a technique that uses neutrally buoyant particles to track water movement; before DPIV there were much slower PIV methods used for similar purposes [7]. Neutrally buoyant particles are mixed into the water, at a concentration that will allow accurate particle tracking; a laser, converted into a laser sheet with a cylindrical lens, illuminates the particles within its plane. Two high-speed cameras with slightly differing perspectives (making the process stereoscopic) take images as the experiment is carried out. The positions of particles in consecutive images are compared using cross correlation to obtain velocities for each of the interrogation windows the images are divided into, producing a velocity field of the illuminated plane. The differing perspectives of the two cameras allow velocities perpendic-

ular to the plane to be calculated, as well. DPIV, if stereoscopic, yields velocity fields with components in three spatial directions, but is limited to providing 2D vorticity fields.

This work uses phase-averaging techniques on Stereoscopic DPIV produced velocity and vorticity fields to construct a 3D visualization of a flexible cylinder's wake over a typical cycle. By tracking the motions of the cylinder simultaneously, these methods will provide 3D vorticity data that may be visualized to better understand how the shape of such a cylinder's wake corresponds to its behavior. Additionally, continuous 3D velocity fields will potentially reveal vorticity components in multiple directions, creating a more accurate complex picture of a VIV associated wake.

A.2 Methods

A.2.1 Setup and initial testing

Data were collected using a recirculating open water flow channel with glass viewing walls providing side, bottom, and head-on views such that both in-line and cross-flow movements could be observed. A black 30A neoprene rubber cylinder, diameter 0.635 cm with 25 round white dots at 1 cm intervals along its length was stretched horizontally across the channel and affixed to the side of the flow channel with suction cups. In order to allow motion perpendicular to the cylinder's orientation (but not along the cylinder), the suction cups are joined to the cylinder at either end with U-joints. Round plastic plates, with a diameter ten times that of the cylinder, were situated between the U-joints and suction cups to provide a flat surface for vortices to end on. All trials were conducted with the flow set at 0.17 m/s, and images of the cylinder and wake were recorded at a speed of 250 Hz by two high-speed Vision Research Phantom V10 cameras.

Given that DPIV requires both cameras capturing images of the same plane,

preliminary tests were conducted using one camera to capture the cross-flow motion of the cylinder and the other to capture in-line motion. The white markers were placed on the surface of the cylinder at right angles (2 at each distance), so that the footage of both the in-line and cross-flow motion would include features that can be used for motion analysis. Footage was captured for a period of 8 s, and then exported from LaVision software as *.avi* files. The motion of the cylinder was tracked using ProAnalyst to obtain a typical cycle of motion.

A.2.2 Stereoscopic DPIV

DPIV uses a time-series of images to calculate the velocity field of a 2D plane. Stereoscopic DPIV, as is used in these experiments, uses the differing perspectives of two cameras to obtain velocity components within this plane as well as components perpendicular to it, though the locations of data points are still confined to the plane. In order to obtain these components for the entire 3D volume of the cylinder's wake, stereoscopic DPIV was carried out for multiple planes lining up with the 20 marked locations along the cylinder's length.

A class 4 laser with a wavelength of 532 nm was situated underneath the flow tank, illuminating the seeded particles at an angle so as to minimize the cylinder's shadow across the wake. Additionally, changing either the distance between the laser sheet and the cameras or the ratio of water to air between them renders the software's calibration inaccurate. To deal with this, the laser and both cameras were held at a constant distance from one another on a structure that allowed the position of the entire system to be adjusted. To solve the problem of the water-to-air ratio, the cameras were directed not at the tank's viewing window but at an angled, underwater mirror in a smaller, adjacent tank. The picture of the entire setup is shown in Fig. A.1 and detailed description of the setup is diagrammed in Fig. A.2. Images were again recorded for a duration of 8 s at each plane with a

frame rate of 250 Hz. Due to the angle of the cameras and the size of the suction cups, the last 5 dots were not visible, so there are only data on the first 20 points, starting on the far side of the tank.

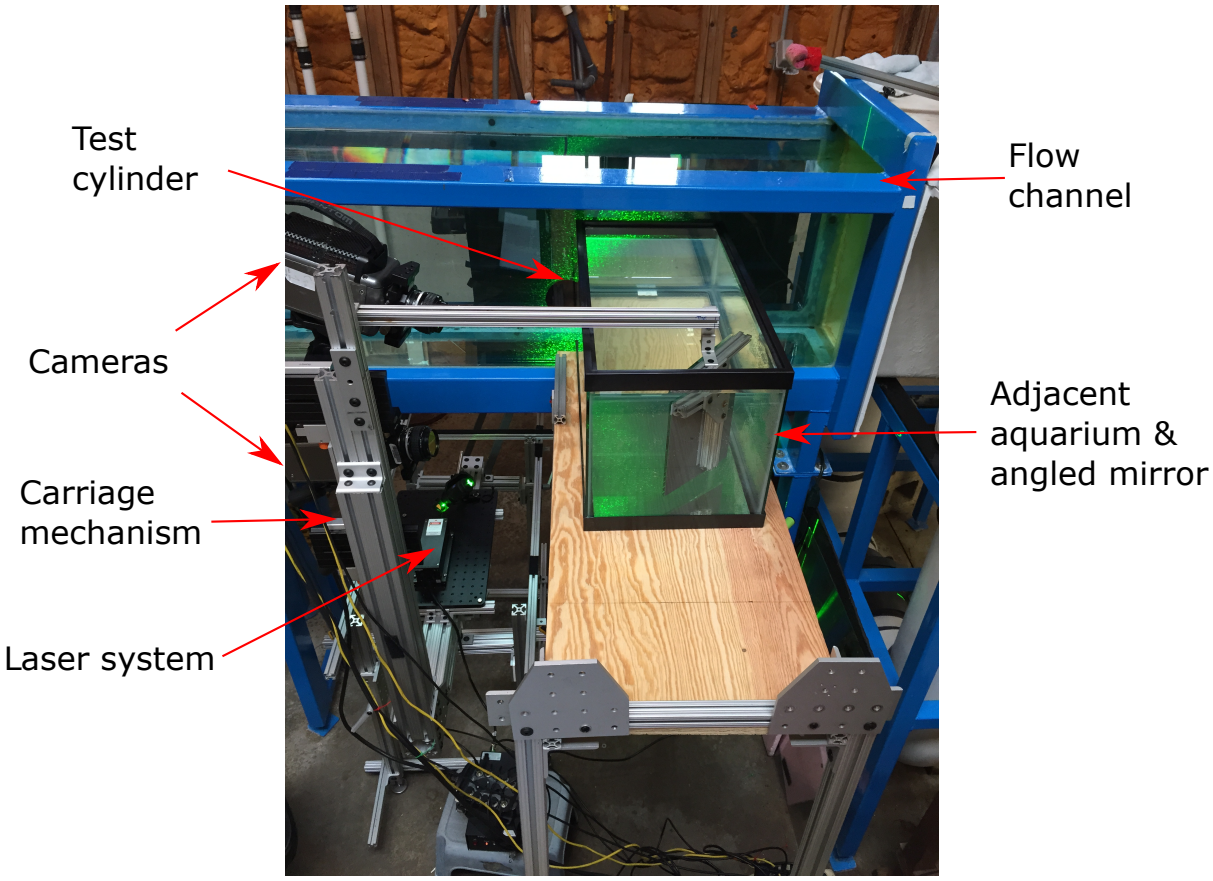

Figure A.1: Image of the experimental setup.

A.2.3 Data analysis and visualization

LaVision DPIV software was used to obtain a 2D vorticity field for each of the 20 slices; this only included the vorticity's z-components since a spatial derivative in the z-direction (across multiple slices) is required for x- or y-components. In order to compile planes of data taken at different times into a single representative cycle of motion, they must be phase-averaged using known characteristics of the cycle.

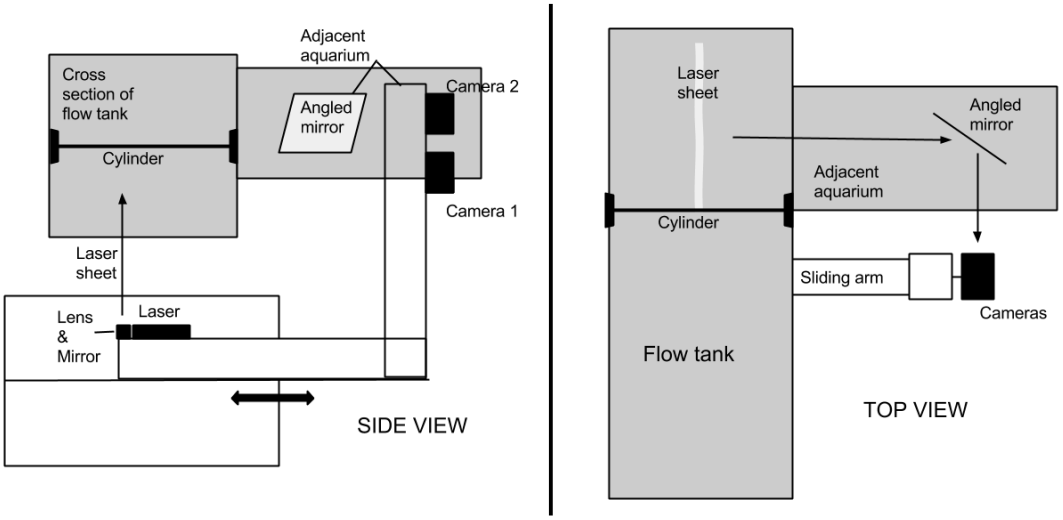

Figure A.2: Left image: Sketch of the stereoscopic DPIV setup, viewed from the side with the water flowing into the paper. Right image: Sketch viewed from the top, with the water flowing from bottom to the top of the diagram.

A.2.4 Obtaining phase and phase averaging

Fig. A.4 depicts an example image taken as part of the time-series for each slice. The smaller white dots are the seeding particles; the laser reflecting off the edge of the cylinder results in the larger white smudge. Whereas PIV software uses particle-tracking of the seeding particles to produce velocity and vorticity fields, using the simpler ProAnalyst to track the cylinders crescent in a time series of PNG images exported from LaVision can provide information about the periodicity of the whole process. To this end, filters were applied to the original image, making the crescent more distinct and therefore more easily tracked (right image in Fig. A.4). A calibration was also applied that set the origin of the tracking data in the same location as in the PIV data, using the axes included in the exported image series as a guide. This tracking process was repeated for each of the twenty 2000-frame time series corresponding with their respective planes.

The resulting tracking data were then used to assign a phase value between

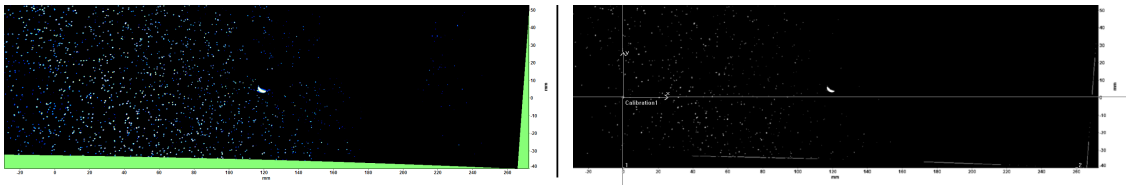

Figure A.3: Left image: An example frame taken during the DPIV process. The white crescent indicates where the laser is reflecting off the edge of the cylinder. The edges of the image are skewed because the frame is calibrated to provide a head-on perspective (as opposed to the original, angled view of the camera) Right image: The same frame, with filters applied so the crescent is more easily tracked.

$-\pi$ and π to each frame of the corresponding time-series. These phase values were converted to degrees (from 0° to 360°) and divided into 10° sections, resulting in 36 phase bins. The vorticity data from every frame assigned a phase within a given bin were averaged with all of the other data falling within that phase bin. For instance, 75 out of the 2000 images might fall within the first bin for a given slice's time series, and the average of their data provides a single representative beginning to the cycle. Due to time constraints, only every tenth data point was included and this was carried out just for slices 7 to 17.

A.2.5 Visualization

The cylinder tracking data for each slice were similarly phase-averaged and assembled to provide the cylinder's shape and position at each phase of the averaged cycle. As with vorticity, slices were phase-averaged separately from one another and all of the data for a given phase combined into a 3D representation of the cylinder's position at that phase. This revealed which positions in the cylinder's cycle correspond with specific stages of its wake.

Due to small variations in the cylinder's position at each slice, however, the combined segments did not produce a coherent mode shape without significant adjustments. Rather than use absolute position coordinates, it proved more practical to instead visualize how each segment oscillated around a given center point

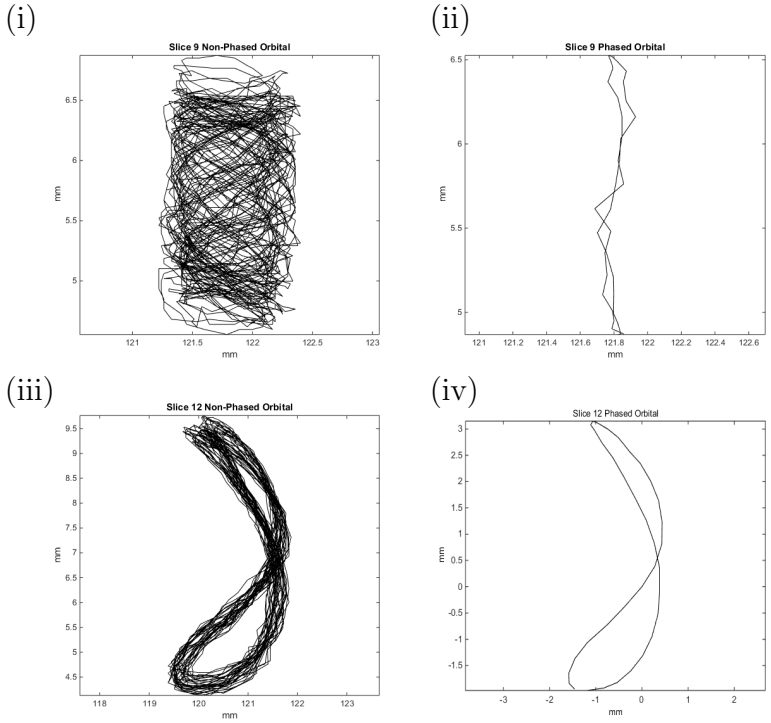

Figure A.4: (i) The path traced by the cylinder's $9th$ cross section's movement in the $xy-$plane, over the entire recording. This contrasts to the figure-eight crescent shape seen in other slices' orbitals. (ii) The result of attempting to phase-average this orbital. (iii) The path traced by the $12th$ cross section's movement, which has a much more recognizable pattern and is more representative of the rest of the cylinder. (iv) The phase-averaged orbital of the $12th$ slice.

at which the whole cylinder presumably takes the shape of a straight, completely horizontal line. The preliminary tests in which the full cylinder's motion was tracked allowed for this position, and the phase at which it occurs, to be found, then, phases were assigned to each of the 2000 positions of the cylinder. The phase values with the lowest standard deviation of point positions along the cylinder were recorded.

Finally, the position of each segment at the bin in which most of these phase values fall was subtracted from all of that segment's data. For instance, if most of the phase values with low standard deviations fell between 70-80 phase degrees, each segment was normalized according to its position during the 8th bin. In order to make sure the relative positions of the cylinder and the wake were correct, the coordinates of the vorticity field data are given the same offsets as the cylinder segments.

Additionally, the position given by the tracking data was shifted for each cylinder upwards by a distance of the radius of the cylinder and at an angle of $\pi/4$. While assuming the tracked point was located exactly on the bottom left edge of the cylinder was not very precise, fitting a circle of the correct radius to some of the crescents and finding their coordinates confirmed that this method caused no major anomalies.

The final, adjusted cylinder and wake data were written into 36 VTK unstructured grid and structured grid files, respectively (one for each phase), and loaded into Paraview software, where the averaged cycle of both may be viewed either as individual images or animated.

A.3 Results

All phase-averaged cylinder orbitals except for slice 9 confirm that this procedure can give reasonable and synchronized data. Whereas most other points

had distinctive, expected curved figure-8 shapes, the motion occurring when the data at slice 9 were taken appears to have been much more erratic (Fig. A.4a). This results in a nearly meaningless average cycle (Fig. A.4b). In contrast, slice 12, a typical representation of the rest of the data, traces a slightly varying but consistent orbital (Fig. A.4c). This results in a reasonable looking and more useful average cycle (Fig. A.4d). Therefore, the actions of the ninth cylinder segment in the positions of segments 8 and 10. When the orbitals for all slices are compared (Fig. A.5), including this virtual 9th point, it is easy to see that they all represent similar behavior.

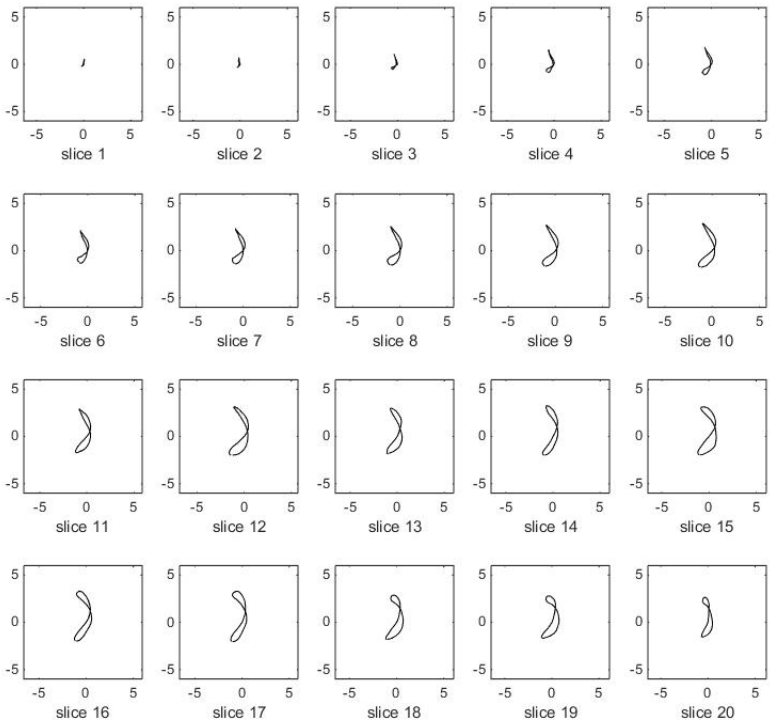

Figure A.5: Phase-averaged orbitals for every recorded slice, with slice 9 adjusted to be the average of slices 8 and 10.

The entire cross-flow motion as recorded in the initial tests is depicted in gray in Fig. A.6, with the length of the cylinder on the horizontal axis and its

oscillation amplitudes on the vertical. The 20 frames with the lowest standard deviation of amplitude are highlighted in black, demonstrating the center position of a typical cross-flow oscillation. The phases of these 20 frames are plotted against all phases (Fig. 8) and are shown to all occur roughly at the same point in the cycle, supporting this as an accurate strategy to normalize the cylinder's position data.

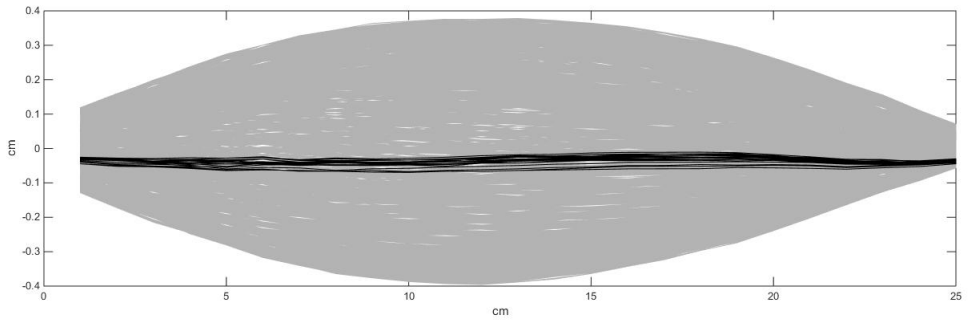

Figure A.6: The transverse movements of the cylinder are plotted, with the distance along the cylinder on the horizontal axis and its displacement perpendicular to the flow on the vertical. Each line represents the cylinder's position in one frame; the highlighted black lines are those with the lowers standard deviation in vertical positions across the length of the cylinder.

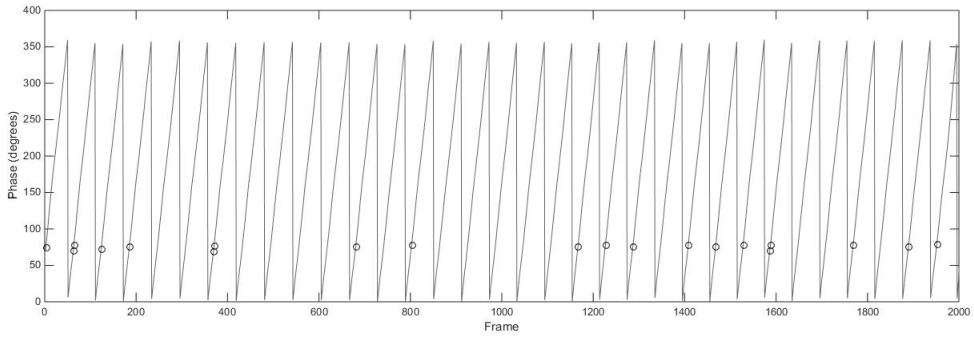

Figure A.7: Each frame is assigned a phase-value between 1 and 360, so at the end of each cycle the phase value returns to 1, producing this saw-tooth pattern. The phases of the frames with the highlighted center positions (Fig. A.6) are indicated on the graph with circles, showing they all occur at the same stage in the cycle.

When the 36-frame time series of the cylinder is loaded into Paraview software, the cylinder's motion appears exactly as expected; the first mode is observed in

both the cross-flow and in-line directions, as was observed visually and in the preliminary motion tracking data, and the frequency in the in-line direction is roughly twice that in the cross-flow direction.

The wake data was reconstructed based on the time series of the original motion using the Paraview. Fig. A.8 shows the resulting wake motion in time.

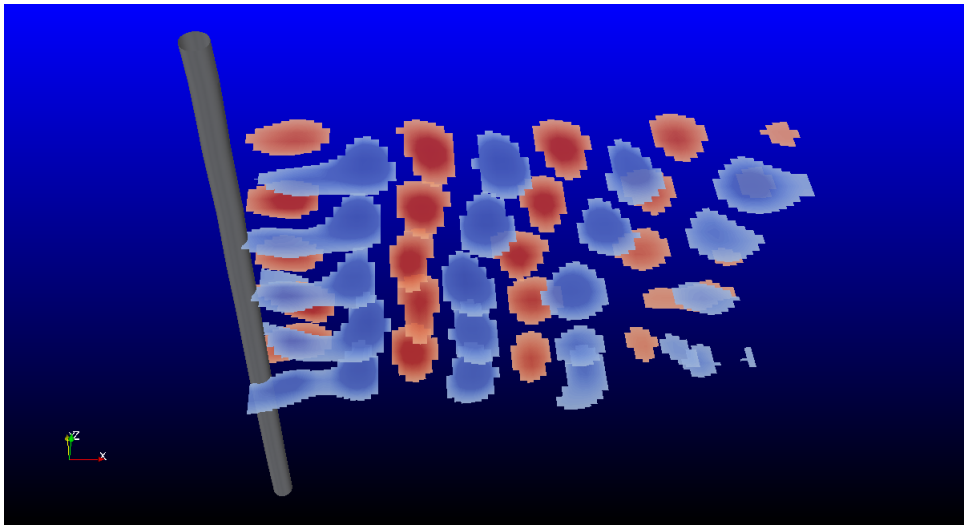

Figure A.8: 3D reconstructed wake based on the cylinder's motion. Colors show vorticity.

A.4 Discussion

For future visualizations, experiments should be conducted to ensure that the behavior of the cylinder during the data collection at each plane remains the same. Slice 9 in these experiments, for instance, presented an entirely different cycle of motion than other slices, and even the more similar orbitals had some differences. Many papers on VIV discuss the effects of hysteresis, in which changing or disturbing the flow speed between trials can result in certain non-reversible cycles [8, 9]. Additionally, these methods should be tested with different flow speeds to determine whether the observed irregular motion is a result of 0.17 m/s being a transition point between cylinder modes or frequencies.

Future projects should also focus on calculating a 3D vorticity field from similarly assembled velocity fields, since this is one of the most important potential products of attempting such a visualization in the first place.

This project has confirmed that tracking the illuminated crescent provides accurate information on the motion of the cylinder, although a better method for finding the necessary shift to apply to the tracked point is a worthwhile goal. It is possible that this method could be used to track, in addition to the crescent, a virtual point created in ProAnalyst at the location of the cylinder's center. If an additional high-speed camera is available, however, it may be more fruitful to simply take images of the cylinder's cross-flow motion and analyze these separately. One setback to this last suggestion, and the main reason this was not attempted here, is that all cameras would need to be completely synchronized so that the motion tracking and wake data line up with each other correctly. Finally, the structure of the VTK file format caused some difficulties in making MATLAB analysis more efficient. A potentially faster approach than the one used here would be to write in the data of each slice to the file as it is calculated; given the VTK organization, it was instead necessary to save all data points for every slice and every phase before writing the files for visualization in Paraview.

Overall, the phase-averaging techniques attempted here have potential to be extremely useful in studying the properties of vortex-induced vibrations, though many important details will need to be worked through before a viable procedure is produced.

List of References

[1] C. Williamson and A. Roshko, "Vortex formation in the wake of an oscillating cylinder," *Journal of fluids and structures*, vol. 2, no. 4, pp. 355–381, 1988.

[2] O. M. Griffin and S. E. Ramberg, "The vortex-street wakes of vibrating cylinders," *Journal of Fluid Mechanics*, vol. 66, no. 3, p. 553576, 1974.

[3] E. D. Gedikli and J. M. Dahl, "Mode shape variation for a low-mode number flexible cylinder subject to vortex-induced vibrations," in *ASME 2014 33rd International Conference on Ocean, Offshore and Arctic Engineering*. American Society of Mechanical Engineers, 2014, pp. V002T08A071–V002T08A071.

[4] J. Xu, M. He, and N. Bose, "Vortex modes and vortex-induced vibration of a long, flexible riser," *Ocean Engineering*, vol. 36, no. 6, pp. 456 – 467, 2009. [Online]. Available: http://www.sciencedirect.com/science/article/pii/S0029801809000146

[5] K. Peterson, B. Regaard, S. Heinemann, and V. Sick, "Single-camera, three-dimensional particle tracking velocimetry," *Opt. Express*, vol. 20, no. 8, pp. 9031–9037, Apr 2012. [Online]. Available: http://www.opticsexpress.org/abstract.cfm?URI=oe-20-8-9031

[6] K. Matsuzaki, M. Shingai, Y. Haramoto, M. Munekata, and H. Ohba, "Visualization of three-dimensional flow structures in the wake of an inclined circular cylinder," *Journal of Visualization*, vol. 7, no. 4, p. 309316, 2004.

[7] C. Willert and M. Gharib, "Digital particle image velocimetry," *Experiments in Fluids*, vol. 10, p. 181193, 1991.

[8] T. Sarpkaya, "A critical review of the intrinsic nature of vortex-induced vibrations," *Journal of Fluids and Structures*, vol. 19, no. 4, pp. 389–447, 2004.

[9] E. D. Gedikli and J. M. Dahl, "Mode excitation hysteresis of a flexible cylinder undergoing vortex-induced vibrations," *Journal of Fluids and Structures*, vol. 69, pp. 308 – 322, 2017. [Online]. Available: http://www.sciencedirect.com/science/article/pii/S0889974616303188

APPENDIX B

Recirculating flow channel flow velocities

Measured Flow Velocities	
Motor Speed [Hz]	Velocity [m/s]
1	0.01
2	0.0275
3	0.05
4	0.06625
5	0.08
6	0.1
7	0.12
8	0.13375
9	0.15
10	0.17
11	0.1875
12	0.2025
13	0.22
14	0.24
15	0.2525
16	0.27375
17	0.2925
18	0.30875
19	0.325
20	0.345
21	0.3625
22	0.38125
23	0.3975
24	0.4175
25	0.43875
26	0.45875
27	0.47875
28	0.4975
29	0.51625
30	0.53625

APPENDIX C

Equipment used in the experiments

C.1 High-speed cameras

Two phantom V10 type high speed cameras were used for motion tracking. Cameras are capable of recording continues images up to 480 frames per second using the full resolution of 2400 × 1800 pixel CMOS imaging sensor array. User can specify other aspect ratios to increase the speed or extend recording times [1].

Figure C.1: Example image of phantom V10 high-speed camera [1].

C.2 Test cylinder molding

Test cylinders were molded using clear flex - urethane rubber material from Smooth-On. To give the cylinder black outlook, black tints were used. After molding, cylinder was marked with white dots equally spaced across it's span.

Left image in Figure C.2 shows an example image of the test cylinder that was molded inside an acrylic tube, and right image in Figure C.2 shows circular white markers placed across cylinder's span.

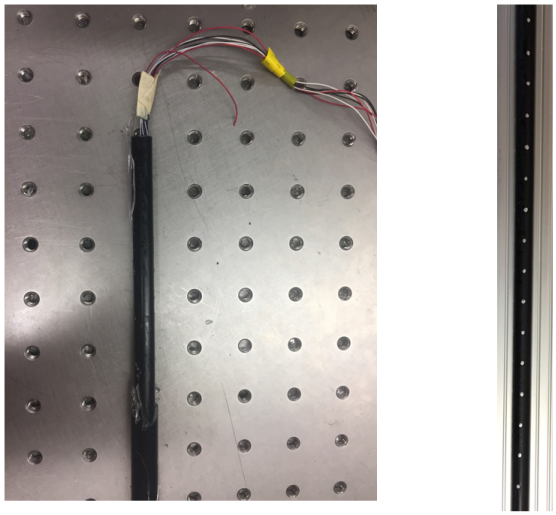

Figure C.2: Cylinder molding process.

C.3 Motion tracking

Motion tracking was done using ProAnalyst software which works based on sub-pixel accuracy. The software is capable of tracking a specified marker (in this case dots) in 1-Dimension (line tracking) and/or in 2-Dimensions (feature tracking). Software takes .avi files as an input and continuously track the location of a specific marker that is identified in the video.

In the tests, cylinders were marked with white dots for tracking. Therefore, the quality of the tracking depends on the resolution of the dots after traditional filtering methods are being applied. These methods are available in the interface of the software and were discussed in more detail in [2]. In order to enhance the quality of the tracking, additional lights can be used to brighten the camera view.

Figure C.3 shows an example image of the filtered cylinder. It should be remembered that if the filtering is clean (i.e. white dots are distinct and background is completely black), the processing is more successful; otherwise, user manually need to track the dots for high accuracy tracking. This was not a problem in the current experiments. However, in the earlier experiments of [2], wave formation at

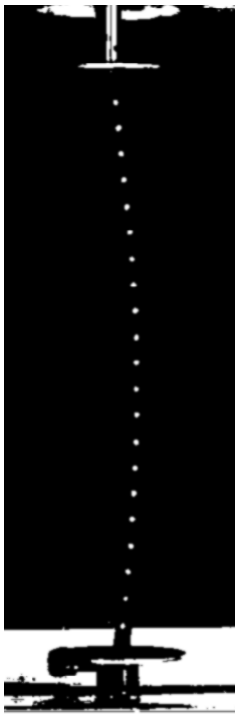

Figure C.3: Example image of the filtered cylinder using the ProAnalyst.

high flow speeds resulted generating bubbles at the surface of the water, and that required manual tracking (because this makes filtering very hard and results the software not to be able to separate the white dots and the water particles). This problem is prevented in this work by either not doing the experiments at high flow speeds, or making an experimental apparatus that allow no wave formation for certain flow speed range.

Figure C.4 shows the example image of the ProAnalyst window. Each dot is tracked in two dimensions (in-line (x) and cross-flow (y)). Boxes around the dot represents the search window specified within the software and it should cover the total displacement of that point in both directions. In addition to motion tracking, software also allows one to monitor the frequency and time history in real time for the desired point across the cylinder's span.

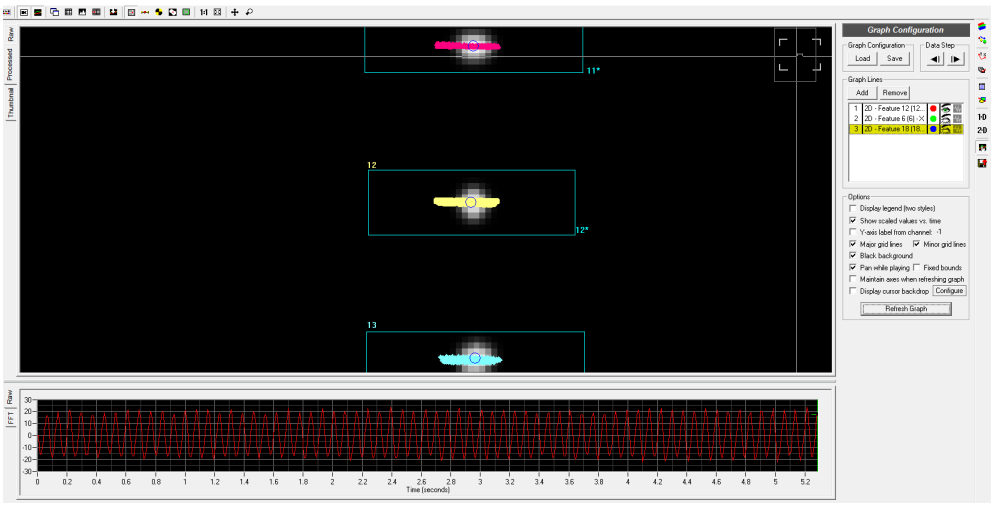

Figure C.4: Example image of the ProAnalyst window in 2D tracking.

C.4 Lased displacement sensor

Laser displacement sensor (LDS) was used to characterize the motion of the test cylinders in air. LDS used in the experiments is a Class 2 laser Keyence LK-081, and works with a 24 VDC power supply. The sensor measures the displacement of a desired location within the range of 80 mm and measures the maximum displacement of 30 mm [3]. Figure C.5shows the image of the LDS head and laser controller.

Figure C.5: Keyence LK-081 laser displacement sensor head with laser controller.

C.5 Shaker and function generator

Figure C.6 shows the function generator (top image) and shaker (bottom image) used in-air experiments for the manuscript 4. Function generator is a Wavetek FG3C, and is capable of generating sinusoidal motions within the frequency range of 0.3 Hz to 7 MHz with a distortion rate less than 1%. Shaker is a Vibration Test Systems (VTS) single vibrator VTS 100 system. Rated force for this shaker is 100 lbf and is capable of oscillating within the frequency range of 2-6500Hz.

(i)

(ii)

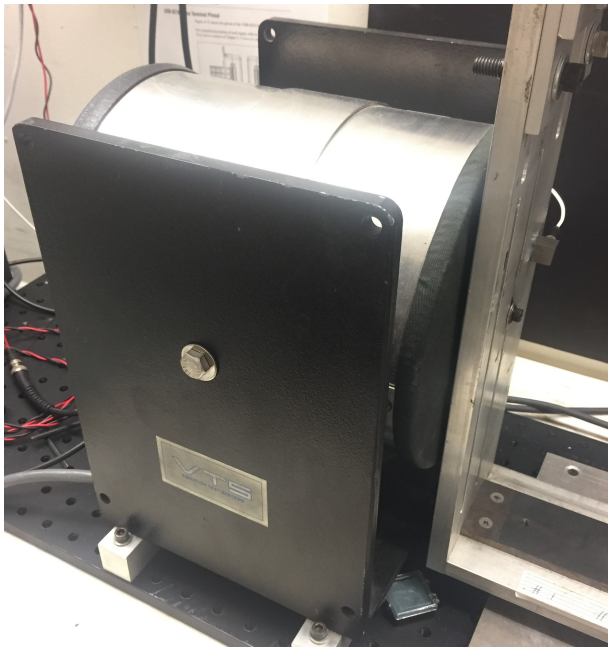

Figure C.6: (i) Function generator from Wavetek. (ii) Shaker from VTS.

List of References

[1] V. Research, "Phantom v10 user manual," 2008.

[2] E. D. Gedikli, "Experimental invastigation of low mode number cylinders subjected to vortex-induced vibrations," Master's thesis, University of Rhode Island, USA, 2014.

[3] Keyence, "Lk series ccd laser displacement sensor instruction manual," 1997.

BIBLIOGRAPHY

Baz, A. and Kim, M., "Active modal control of vortex-induced vibrations of a flexible cylinder," *Journal of Sound and Vibration*, vol. 165, no. 1, pp. 69 – 84, 1993. [Online]. Available: http://www.sciencedirect.com/science/article/pii/S0022460X83712435

Bearman, P. W., "Vortex shedding from oscillating bluff bodies," *Annual review of fluid mechanics*, vol. 16, no. 1, pp. 195–222, 1984.

Bearman, P., "Circular cylinder wakes and vortex-induced vibrations," *Journal of Fluids and Structures*, vol. 27, no. 5, pp. 648–658, 2011.

Benaroya, H., *Mechanical Vibration: Analysis, Uncertainties, and Control*, 2nd ed. Marcel Dekker, New York, 2004.

Bernitsas, M. M., Raghavan, K., Ben-Simon, Y., and Garcia, E., "Vivace (vortex induced vibration aquatic clean energy): A new concept in generation of clean and renewable energy from fluid flow," *Journal of offshore mechanics and Arctic engineering*, vol. 130, no. 4, p. 041101, 2008.

Bishop, R. and Hassan, A., "The lift and drag forces on a circular cylinder oscillating in a flowing fluid," *Proceedings of the Royal Society of London A*, vol. 277, pp. 51–75, 1964.

Blevins, R. D., *Flow Induced Vibrations*, 2nd ed. Van Nostrand Reinhold Company, New York, NY, 1990.

Bourguet, R., Karniadakis, G., and Triantafyllou, M., "Vortex-induced vibrations of a long flexible cylinder in shear flow," *Journal of Fluid Mechanics*, vol. 677, pp. 342–382, 2011.

Brika, D. and Laneville, A., "Vortex-induced vibrations of a long flexible circular cylinder," *Journal of Fluid Mechanics*, vol. 250, pp. 481–508, 1993.

Chaplin, J., Bearman, P., Huarte, F. H., and Pattenden, R., "Laboratory measurements of vortex-induced vibrations of a vertical tension riser in a stepped current," *Journal of Fluids and Structures*, vol. 21, no. 1, pp. 3–24, 2005.

Chelidze, D. and Zhou, W., "Smooth orthogonal decomposition-based vibration mode identification," *Journal of Sound and Vibration*, vol. 292, no. 35, pp. 461 – 473, 2006. [Online]. Available: http://www.sciencedirect.com/science/article/pii/S0022460X05005948

Cheng, L., Zhou, Y., and Zhang, M., "Perturbed interaction between vortex shedding and induced vibration," *Journal of Fluids and Structures*, vol. 17, no. 7, pp. 887 – 901, 2003. [Online]. Available: http://www.sciencedirect.com/science/article/pii/S0889974603000422

Dahl, J., Hover, F., and Triantafyllou, M., "Two-degree-of-freedom vortex-induced vibrations using a force assisted apparatus," *Journal of Fluids and Structures*, vol. 22, no. 6, pp. 807–818, 2006.

Dahl, J., Hover, F., Triantafyllou, M., Dong, S., and Karniadakis, G., "Resonant vibrations of bluff bodies cause multi-vortex shedding," *Physical Review Letters*, vol. 99, no. 144503, 2007.

Dahl, J., Hover, F., Triantafyllou, M., and Oakley, O., "Dual resonance in vortex-induced vibrations at subcritical and supercritical reynolds numbers," *Journal of Fluid Mechanics*, vol. 643, pp. 395–424, 2010.

Feeny, B. and Kappagantu, R., "On the physical interpretation of proper orthogonal modes in vibrations," *Journal of Sound and Vibration*, vol. 211, no. 4, pp. 607 – 616, 1998. [Online]. Available: http://www.sciencedirect.com/science/article/pii/S0022460X97913869

Gedikli, E. D., "Experimental invastigation of low mode number cylinders subjected to vortex-induced vibrations," Master's thesis, University of Rhode Island, USA, 2014.

Gedikli, E. D. and Dahl, J. M., "Mode shape variation for a low-mode number flexible cylinder subject to vortex-induced vibrations," in *ASME 2014 33rd International Conference on Ocean, Offshore and Arctic Engineering*. American Society of Mechanical Engineers, 2014, pp. V002T08A071–V002T08A071.

Gedikli, E. D. and Dahl, J. M., "Mode excitation hysteresis of a flexible cylinder undergoing vortex-induced vibrations," *Journal of Fluids and Structures*, vol. 69, pp. 308 – 322, 2017. [Online]. Available: http://www.sciencedirect.com/science/article/pii/S0889974616303188

Gedikli, E. D., Dahl, J. M., and Chelidze, D., "Multivariate analysis of vortex-induced vibrations in a tensioned cylinder reveal nonlinear modal interactions," in *10th International Conference on Structural Dynamics*. Eurodyn, 2017.

Ginsberg, J., *Mechanical and Structural Vibrations: Theory and Applications*. John Wiley and Sons, 2001.

Griffin, O. M. and Ramberg, S. E., "The vortex-street wakes of vibrating cylinders," *Journal of Fluid Mechanics*, vol. 66, no. 3, p. 553576, 1974.

Huera-Huarte, F., "Multi-mode vortex-induced vibrations of a flexible circular cylinder," PhD, Imperial College London, London, April 2006.

Huera-Huarte, F., Bangash, Z., and González, L., "Towing tank experiments on the vortex-induced vibrations of low mass ratio long flexible cylinders," *Journal of Fluids and Structures*, vol. 48, pp. 81–92, 2014.

Huera-Huarte, F. and Bearman, P., "Wake structures and vortex-induced vibrations of a long flexible cylinderâ"part 1: Dynamic response," *Journal of Fluids and Structures*, vol. 25, no. 6, pp. 969 – 990, 2009. [Online]. Available: http://www.sciencedirect.com/science/article/pii/S0889974609000449

Jauvtis, N. and Williamson, C., "The effect of two degrees of freedom on vortex-induced vibration at low mass and damping," *Journal of Fluid Mechanics*, vol. 509, pp. 23–62, 2004.

Kang, Z. and Jia, L., "An experiment study of a cylinder's two degree of freedom viv trajectories," *Ocean Engineering*, vol. 70, pp. 129–140, 2013.

Keyence, "Lk series ccd laser displacement sensor instruction manual," 1997.

Khalak, A. and Williamson, C., "Motions, forces and mode transitions in vortex-induced vibrations at low mass-damping," *Journal of fluids and Structures*, vol. 13, no. 7, pp. 813–851, 1999.

Klamo, J., Leonard, A., and Roshko, A., "The effects of damping on the amplitude and frequency response of a freely vibrating cylinder in cross-flow," *Journal of Fluids and Structures*, vol. 22, pp. 845–856, 2006.

Lie, H. and Kaasen, K., "Modal analysis of measurements from a large-scale {VIV} model test of a riser in linearly sheared flow," *Journal of Fluids and Structures*, vol. 22, no. 4, pp. 557 – 575, 2006. [Online]. Available: http://www.sciencedirect.com/science/article/pii/S0889974606000077

Marcollo, H., Eassom, A., Fontaine, E., Tognarelli, M., Beynet, P., Constantinides, Y., and Oakley, O. H., "Traveling wave response in full-scale drilling riser viv measurements," in *ASME 2011 30th International Conference on Ocean, Offshore and Arctic Engineering*. American Society of Mechanical Engineers, 2011, pp. 523–537.

Matsuzaki, K., Shingai, M., Haramoto, Y., Munekata, M., and Ohba, H., "Visualization of three-dimensional flow structures in the wake of an inclined circular cylinder," *Journal of Visualization*, vol. 7, no. 4, p. 309316, 2004.

Mehmood, A., Abdelkefi, A., Hajj, M., Nayfeh, A., Akhtar, I., and Nuhait, A., "Piezoelectric energy harvesting from vortex-induced vibrations of circular cylinder," *Journal of Sound and Vibration*, vol. 332, no. 19, pp. 4656 – 4667,

2013. [Online]. Available: http://www.sciencedirect.com/science/article/pii/S0022460X13003192

Meirovitch, L., *Fundamentals of Vibrations*. McGraw-Hill, New York, NY., 2001.

Modarres-Sadeghi, Y., Chasparis, F., Triantafyllou, M., Tognarelli, M., and Beynet, P., "Chaotic response is a generic feature of vortex-induced vibrations of flexible risers," *Journal of Sound and Vibration*, vol. 330, no. 11, pp. 2565–2579, 2011.

Modarres-Sadeghi, Y., Mukundan, H., Dahl, J., Hover, F., and Triantafyllou, M., "The effect of higher harmonic forces on fatigue life of marine risers," *Journal of Sound and Vibration*, vol. 329, no. 1, pp. 43–55, 2010.

Passano, E., Larsen, C. M., and Wu, J., "Viv of free spanning pipelines: Comparison of response from semi-empirical code to model tests," in *ASME 2010 29th International Conference on Ocean, Offshore and Arctic Engineering*. American Society of Mechanical Engineers, 2010, pp. 567–577.

Peterson, K., Regaard, B., Heinemann, S., and Sick, V., "Single-camera, three-dimensional particle tracking velocimetry," *Opt. Express*, vol. 20, no. 8, pp. 9031–9037, Apr 2012. [Online]. Available: http://www.opticsexpress.org/abstract.cfm?URI=oe-20-8-9031

Prasanth, T., Premchandran, V., and Mittal, S., "Hysteresis in vortex-induced vibrations: critical blockage and effect of m*," *Journal of Fluid Mechanics*, vol. 671, pp. 207–225, 2011.

Rashidi, S., Hayatdavoodi, M., and Esfahani, J. A., "Vortex shedding suppression and wake control: A review," *Ocean Engineering*, vol. 126, pp. 57 – 80, 2016. [Online]. Available: http://www.sciencedirect.com/science/article/pii/S0029801816303675

Research, V., "Phantom v10 user manual," 2008.

Sanaati, B. and Kato, N., "Vortex-induced vibration (viv) dynamics of a tensioned flexible cylinder subjected to uniform cross-flow," *Journal of Marine Science and Technology*, vol. 18, pp. 247–261, 2013.

Sarpkaya, T., "A critical review of the intrinsic nature of vortex-induced vibrations," *Journal of Fluids and Structures*, vol. 19, no. 4, pp. 389–447, 2004.

Sarpkaya, T. S., *Wave Forces on Offshore Structures*. Cambridge University Press, 2010.

Seyed-Aghazadeh, B. and Modarres-Sadeghi, Y., "Reconstructing the vortex-induced-vibration response of flexible cylinders using limited localized measurement points," *Journal of Fluids and Structures*, vol. 65, pp. 433–446, 2016.

Smogeli, O. N., Hover, F. S., and Triantafyllou, M. S., "Force-feedback control in viv experiments," in *ASME 2003 22nd International Conference on Offshore Mechanics and Arctic Engineering*. American Society of Mechanical Engineers, 2003, pp. 685–695.

Srinil, N., Zanganeh, H., and Day, A., "Two-degree-of-freedom viv of circular cylinder with variable natural frequency ratio: Experimental and numerical investigations," *Ocean Engineering*, vol. 73, pp. 179–194, 2013.

Stansby, P. K., "The locking-on of vortex shedding due to the cross-stream vibration of circular cylinders in uniform and shear flows," *Journal of Fluid Mechanics*, vol. 74, pp. 641–665, 1976.

Strang, G., *Introduction to applied mathematics*. Wellesley-Cambridge Press Wellesley, MA, 1986.

Swithenbank, S. and Vandiver, J., "Identifying the power-in region for vortex-induced vibrations of long flexible cylinders," in *26th International Conference on Offshore Mechanics and Arctic Engineering (OMAE 2007)*, vol. 3, 2007, pp. 723–730.

Thomson, W. and Dahleh, M., *Theory of Vibration with Applications*, 5th ed. Prentice Hall, Englewood Cliffs, 1998.

Triantafyllou, M., Techet, A., Hover, F., and Yue, D.-P., "Viv of slender structures in shear flow," in *IUTAM Symposium on Flow-Structure Interaction*, Rutgers State University, New Brunswick, NJ, 2003.

Trim, A., Braaten, H., Lie, H., and Tognarelli, M., "Experimental investigation of vortex-induced vibration of long marine risers," *Journal of fluids and structures*, vol. 21, no. 3, pp. 335–361, 2005.

Unal, M. F. and Rockwell, D., "On vortex formation from a cylinder. part 2. control by splitter-plate interference," *Journal of Fluid Mechanics*, vol. 190, p. 513 529, 1988.

Vandiver, J. K., Jaiswal, V., and Jhingran, V., "Insights on vortex-induced, traveling waves on long risers," *Journal of Fluids and Structures*, vol. 25, no. 4, pp. 641–653, 2009.

Vandiver, J. and Jong, J.-Y., "The relationship between in-line and cross-flow vortex-induced vibration of cylinders," *Journal of Fluids and Structures*, vol. 1, no. 4, pp. 381–399, 1987.

Vandiver, J., Marcollo, H., Swithenbank, S., Jhingran, V., *et al.*, "High mode number vortex-induced vibration field experiments," in *Offshore Technology Conference*. Offshore Technology Conference, 2005.

Willert, C. and Gharib, M., "Digital particle image velocimetry," *Experiments in Fluids*, vol. 10, p. 181193, 1991.

Williams, J. F. and Zhao, B., "The active control of vortex shedding," *Journal of Fluids and Structures*, vol. 3, no. 2, pp. 115 – 122, 1989. [Online]. Available: http://www.sciencedirect.com/science/article/pii/S0889974689900261

Williamson, C. and Govardhan, R., "Vortex-induced vibrations," *Annu. Rev. Fluid Mech.*, vol. 36, pp. 413–455, 2004.

Williamson, C. and Roshko, A., "Vortex formation in the wake of an oscillating cylinder," *Journal of fluids and structures*, vol. 2, no. 4, pp. 355–381, 1988.

Wilson, J. F. and Tinsley, J. C., "Vortex load reduction : Experiments in optimal helical strake geometry for rigid cylinders," *Journal of Energy Resources Technology*, vol. 111, p. 72 76, 1989.

Xu, J., He, M., and Bose, N., "Vortex modes and vortex-induced vibration of a long, flexible riser," *Ocean Engineering*, vol. 36, no. 6, pp. 456 – 467, 2009. [Online]. Available: http://www.sciencedirect.com/science/article/pii/S0029801809000146

Zdravkovich, M., "Review and classification of various aerodynamic and hydrodynamic means for suppressing vortex shedding," *Journal of Wind Engineering and Industrial Aerodynamics*, vol. 7, no. 2, pp. 145 – 189, 1981. [Online]. Available: http://www.sciencedirect.com/science/article/pii/0167610581900362

Zheng, H., Price, R., Modarres-Sadeghi, Y., and Triantafyllou, M., "On fatigue damage of long flexible cylinders due to higher harmonic force components and chaotic vortex-induced vibrations," *Ocean Engineering*, vol. 49, pp. 318–329, 2014.